Development and Analysis of Hybrid Renewable Energy System for Offshore Oil and Gas Rigs

Tee Jing Zhong

Submitted in fulfilment of the requirements for the
Degree of Doctor of Philosophy

School of Engineering
College of Science and Engineering
University of Glasgow

August 2022

Abstract

Over the years, the decline of capital expenditure (CAPEX) on offshore wind turbine generation (WTG) and battery energy storage systems (BESS) has led to great interest in the electrification of offshore oil and gas (O&G) platforms with renewable sources. This will reduce the carbon footprint as the on-board gas turbine generation (GTG) can be removed. The state of the art has presented that O&G platforms integrated with BESS and an energy management system (EMS) is able to enhance output power quality to load, in the face of sequential events of dynamic loading and fluctuations in wind [11]. However, the proposed technique required a low-pass filter, which removed high frequencies in the voltage and frequency analysis, especially in the transient period. As such, it is expected that the efficiency is reduced due to power losses in the system.

The main focus of this thesis is to develop an optimised EMS for transient stability enhancement, in the presence of simultaneous changes in dynamic loads and stochasticity in wind speed, for offshore O&G platforms integrated with WTG. There are five main contributions in this thesis. First, a power stability study has demonstrated a reduction in transient deviation of output power for systems without and with BESS respectively [51]. Second, a transient stability analysis is presented for variations in BESS sizing using a commercial software, ETAP. The simulation has also shown that the proposed system, which has incorporated 2 MW of BESS, improved transient stability and met the IEC standards on maximum voltage and frequency deviations [61]. Third, an optimisation of transient stability was shown for an increased capacity in BESS from 2 MW to a total of 4 MW BESS [62]. The techno-economic feasibility of the proposed system is carried out, which shows that the BESS has the lowest operational expendture (OPEX) as compared with GTG or WTG [61], [62]. Last but not the least, an optimised transient stability solution is demonstrated with dynamic loading and stochasticity in wind speed. An EMS embedded in the BESS is developed and the simulation results for transient stability are compared against the current state of art. The superiority of the proposed EMS was demonstrated with a smaller voltage and frequency deviation, which improved the output power quality with variations in load variation and wind intermittency. In addition, it is developed with considerations to lower the overall cost of the system and provide decarbonisation for long-term continuous operation.

Contents

Publications

To promote and increase awareness of this research within the research community and marine and offshore industry, several articles were submitted and published in international peer reviewed conferences. The list of publications is provided below.

1. J.Z. Tee, K.H. Tan, I.L.H. Lim, K. Zhou, and O. Anaya-Lara, "Integration of Offshore Wind with O&G platforms with an Energy Storage System," in Proc. 2019 IEEE PES Innovative Smart Grid Technologies Europe (ISGT-Europe), 2019, pp. 1-5, doi: 10.1109/ISGTEurope.2019.8905500.

2. J.Z. Tee, I.L.H Lim, K. Zhou, and O. Anaya-Lara, "Transient Stability Analysis of Offshore Wind With O&G Platforms and an Energy Storage System," in Proc. 2020 IEEE Power & Energy Society General Meeting (PESGM), 2020, pp. 1-5, doi: 10.1109/PESGM41954.2020.9281706.

3. J.Z. Tee, I.L.H Lim, J. Yang, C.T. Choo, O. Anaya-Lara, and C.K. Chui, "Power System Stability of Offshore Wind with an Energy Storage to Electrify O&G Platform," in Proc. 2020 IEEE Region 10 Conference (TENCON), 2020, pp. 146-151, doi: 10.1109/TENCON50793.2020.9293910.

4. J.Z. Tee, I.L.H Lim, and J. Yang, "Energy Management Strategy Designed for Offshore Oil Rig with Offshore Wind," in Proc. 2022 IEEE International Conference on compatibility, Power Electronics and Power Engineering (CPE-PowerEng), 2022.

List of Tables

List of Figures

Acknowledgements

First and foremost, I would like to express my deep and sincere gratitude to both my research supervisors, Dr Idris Lim Li Hong, Dr Jin Yang and Dr Olimpo Anaya-Lara for giving me the opportunity to pursue this research at the University of Glasgow. I could not have completed this dissertation without their expertise, patience and support throughout this research. Their insightful feedback and valuable guidance have propelled me to achieve greater heights in my research journey.

In addition, I would like to extend my appreciation to all who have lent me a helping hand throughout my research process, in particular Dr. Lai Meng Tang and Ernest Sng and especially Dr Chui C.K. who used to be my mentor when I pursue Master of Engineering in National University of Singapore throughout my research process. My completion of this research could not be accomplished without their support and help rendered to me.

Last but not least, I would like to express my deepest gratitude to my family members who have provided their greatest care and love during this long and difficult journey: my supportive wife Ms Ong who is pregnant and willing to sacrifice relentlessly to provide all necessary care needed for my family and thankful to my well-behaved baby Aelius throughout my studies.

Declaration

University of Glasgow

Statement of Originality to Accompany Thesis Submission

Name: Tee Jing Zhong

Registration Number:

I certify that the thesis presented here for examination for a PhD degree of the University of Glasgow is solely my own work other than where I have clearly indicated that it is the work of others (in which case the extent of any work carried out jointly by me and anyother person is clearly identified in it) and that the thesis has not been edited by a third party beyond what is permitted by the University's PGR Code of Practice.

I declare that the thesis does not include work forming part of a thesis presented successfully for another degree [unless explicitly identified and as noted below].

I declare that this thesis has been produced in accordance with the University of Glasgow's Code of Good Practice in Research.

I acknowledge that if any issues are raised regarding good research practice based on review of the thesis, the examination may be postponed pending the outcome of any investigation of the issues.

Signature: .....

Date: 17 Aug 2022 .....

Acronyms and Symbols

BESS	Battery energy storage system
WTG	Wind turbine generation
SCGT	Simple-cycle gas turbine
SCGTs	Simple-cycle gas turbines
GHG	Green house gas
ETAP	Electrical transient analyzer program
O&G	Oil and gas
CAPEX	Capital expenditure
OPEX	Operational expenditure
EMS	Energy management system
PCC	Point of common coupling
GTG	Gas turbine generation
PMSG	Permanent magnet synchronous generator
IEC	International electrotechnical commission
NORSOK	Standards by Norwegian petroleum industry for oil and gas companies
IMO	International Maritime Organisation
MATLAB	Matrix laboratory
Simulink	MATLAB-based graphical programming environment
PSCAD	Power Systems Computer Aided Design
ULQ	Utility and living quarter
CPF	Processing and heating
WHP	Wellhead
EG	Essential generator
E.EG	Emergency essential generator
DC	Direct current
AC	Alternating current
AC/DC	Alternating current / direct current
VSC	Voltage source converter
VSCs	Voltage source converters
B2B	Back-to-back

PFC	Power factor correction
EMF	Electromotive force
PWM	Pulse Width Modulated
RSC	Rotor-side converter
GSC	Grid-side converter
TSO	Transmission system operator
Ni-MH	Nickel metal hydride
HVAC	High voltage alternating current
HVDC	High voltage direct current
O&M	Operational and maintenance
OWF	Offshore wind farm
WIS	Water injection system
SLM	Smart load management
US	United States
EUETS	European union emissions trading system
EU	European union
MSL	Mean sea level
SWL	Statoil wind limited
TCE	The crown estate
R&D	Research and development
RES	Renewable energy sources
CB	Circuit breaker
SOC	State of charge
PI	Proportional and integral
PSEMS	Proposed system with energy management system
ROI	Return on investment

Symbols used in Chapter 1

CO_2	Carbon dioxide
H_2	Hydrogen

Symbols used in Chapter 2

W	Work done per unit mass
W_{12}	Work required by compressor
W_{34}	Work output from gas turbine
W_{net}	Net-work output
h	Heat exchange
$h_2 - h_1$	Enthalpy differences between the states 2 and 1

$h_3 - h_2$	Enthalpy differences between the states 3 and 2
$h_4 - h_3$	Enthalpy differences between the states 3 and 4
C_P	Constant pressure
Q	Heat transfer per unit mass
Q_{23}	Heat addition comes from the fuel using in the combustion chamber
T	Temperature
$T_2 - T_1$	Temperature differences between states 2 and 1
$T_3 - T_2$	Temperature differences between states 3 and 2
$T_4 - T_3$	Temperature differences between states 4 and 3
TR	Temperature ratio
γ	Specific heat ratio
C_V	Heat capacity at constant temperature
C_{Pw}	Power coefficient
PR	Efficiency of the compressor
P	Power
p	Air density
ω	Rotational speed of the rotor
R	Radius to tip of the rotor
π	Constant ratio of the circumference of circle
v	Velocity
N_g	Generator efficiency
N_b	Gearbox efficiency
CF	Capacity factor
D	Diameter of rotor
RPM	Rotor speed
γ_{TSR}	Tip speed ratio
C	Minimum capacitance
t_h	Hold-up time
P_o	Output power
η	Efficiency
Y	Wye is configuration of transformer
Δ	Delta is configuration of transformer
C_{min}	Minimum battery capacity
E_d	Design energy
VAh	Autonomy time
V_{dc}	Nominal battery voltage
K_a	Battery ageing factor
K_t	Temperature correction factor

K_{dod}	Maximum depth of discharge
K_c	Capacity rating factor
E_d	Energy density,
E	Energy that the medium has
E_s	Specific energy,
V	Volume of the medium.
m	Mass
P_{net}	Net power
P_{WTG}	Power from WTG
P_{Bess}	Power from BESS

Symbols used in Chapter 4

GTG_C	Capital cost of GTG
GT_{10MW}	GT's capacity of 10,000 kW
WTG_C	Capital cost of WTG
WTG_{6MW}	WT's capacity of 6,000 kW
$BESS_C$	Capital cost of BESS
$BESS_{1MW}$	BESS's capacity of 6,000 kW
$GTG_{O\&M}$	OPEX cost of GTG
$WTG_{O\&M}$	OPEX cost of WTG
$BESS_{O\&M}$	OPEX cost of BESS

Symbols used in Chapter 5

GTG_C	Capital cost of GTG
WTG_C	Capital cost of WTG
$BESS_C$	Capital cost of BESS

Symbols used in Chapter 6

I_{d-Dev}	Control signal from frequency
I_{q-Dev}	Control signal from voltage
K_p	Proportional gain in voltage/frequency controller
f_{ref}	Reference frequency value
f_{PCC}	Measured frequency deviation value
U_{ref}	Reference voltage value
U_{PCC}	Measured voltage deviation value
K_i/T_i	Integral gain in voltage/frequency controller
Y_{max}	Maximum values in the anti-windup limiter
Y_{min}	Minimum values in the anti-windup limiter

I_{d-ref}	Reference current control signals from PCC frequency
I_{q-ref}	Reference current control signals from PCC voltage
f_{ff}	Feed forward control in term of frequency
U_{ff}	Feed forward control in term of voltage
$I_d(s)$	Output current of d-axis within inner loop of VSC
$I_q(s)$	Output current of q-axis within inner loop of VSC
$\Delta F_{PCC}(s)$	Output transient frequency deviation
$\Delta U_{PCC}(s)$	Output transient voltage deviation
$K_p(s)$	Proportional gain in EMS
K_i/s	Integral gain in EMS
$RMSD$	Root mean square deviation
X	Relates to measured voltage or measured frequency
N	Number of the samples taken
C_E	Carbon emission
P_{out}	Relates to output power rating
t	Hours
$CO_{2,em}$	Emission rate measured in metric ton

Chapter 1

Introduction

1.1 Motivation

In the developments of the last decade, offshore wind turbine generation (WTG) have been considered as an attractive source of energy for electrification of offshore oil and gas (O&G) platforms due to its proximity to load and the need for sustainability, which drives reduction in carbon emissions from O&G installations [1]. This has attracted a lot of interest on the feasibility study of such a business model. In addition, intensive research has been focused on offshore wind farm (OWF) with O&G platform for integration in a standalone micro-grid configuration to reduce carbon emission from traditional power generation of gas turbine [2], [3]. This is further driven by the fact that capital expenditure (CAPEX) of O&G platforms will be higher if subsea transmission cables are required to connect to the onshore power grid [4], [5].

This has led to a recent industry case study on the integration of offshore floating WTG with offshore O&G platforms in the off-grid configuration, which is a business model that is developing in the North Sea [6]. It has been shown to be techno-economical to power O&G platforms using offshore wind energy in deep waters based on the case studies of integrating offshore wind with O&G platforms in 2018 [7]. O&G platforms in the Beatrice oil field have also been electrified by four 5 MW wind turbine which are installed adjacent to the offshore platforms in 2012 [8]. One major challenge faced in these case studies is the intermittency of wind. In order to address this challenge, on-board simple-cycle gas turbines (SCGTs) are required to be on "stand-by" mode, which can be started up almost instantaneously, in the event of a sudden drop in wind speed. It is also illustrated in the research study in [2] that the integration of WTG with gas turbine generation (GTG) to electrify O&G platforms has resulted in frequent starts and stops of more than 500 times for the gas turbines yearly. This resulted in inefficiencies in the GTG and shorter lifespans due to wear and tear. The fuel efficiency of SCGTs reduces drastically under low loads and SCGTs in "stand-by" mode consumes at about 20% of the amount of fuel required in "full power" mode, which contributes towards increased green house gas (GHG)

emissions [8]. Another challenge faced in powering O&G platforms directly with wind energy is due to the cut in and cut out wind speeds, which results in the WTG not powering up or being yawed out of the wind. This affects the output power quality from the WTG.

The latest developments on electrification of offshore (O&G) platforms have considered the use of renewable and different mediums of energy storage such as batteries, hydrogen, and etc. Hydrogen was used for energy storage due to its higher energy density, as compared to lithium-ion batteries. In [9], it has been shown that carbon dioxide (CO_2) emissions can be reduced by up to 40% using an integrated wind and hydrogen (H_2) energy storage solution but this required a large H_2 storage capacity for full exploitation of the wind energy resource.This configuration on electrification of offshore O&G platforms have considered the use of renewables and the hydrogen energy storage system to integrate with offshore WTG and O&G platforms for energy sustainability. Comparing hydrogen energy storage systems to battery energy storage system (BESS), the BESS has a faster response, which will provide an improved transient stability.

Another user case was discussed to allow higher wind penetration without breaching grid frequency regulations [10]. However, uncertainties due to the intermittency of wind power was not covered until the research study reveals the state of the art in the smart load management (SLM) with energy storage to electrify a O &G platform for power quality enhancement in wind-powered O&G applications. In this work, a low pass filter was used which introduces additional efficiency loss, while reducing the voltage and frequency deviations. More recently, in a paper on dynamic converter capacity allocation for multi-functional energy storage systems in O&G applications [12], multiple benefits are demonstrated for a BESS with a dedicated converter, connected to an isolated offshore platform [11]. There was a significant enhancement of the local power quality through a power management strategy supported by a low pass filter, which inevitably also results in power loss. There is still a lack of improving power output quality to the load in the dynamic operation like changes in dynamic loading, as well as perturbations from stochasticity in wind. Nonetheless, these developments demonstrate the potential of energy storage system in mitigating variations in output power generation, to solve transient stability problems. In addition, it has also been shown that its integration with WTG can help to reduce carbon emissions arising from power generation through SCGTs onboard the O&G platforms. In addition, there has been a decline of CAPEX on offshore floating wind turbines and BESS, which results in a favourable business case, for in the electrification of offshore O&G platforms.

The work in this thesis seeks to improve and address the existing limitation on the techno-economic anlaysis for the integration of offshore O&G platform with WTG and BESS which is summarised as follows:

- We believe that incorporating BESS into an integrated system with offshore WTG and

O&G platforms in a standalone micro grid will improve output power quality due to disturbances. This development will be based on a power converter with a rapid response in discharging/charging output power, which will be connected to the charge controller of BESS.

- The proposed integration of the offshore WTG with the O&G platform and BESS is modelled and simulated with matrix laboratory/MATLAB-based graphical programming environment (MATLAB/Simulink). This is necessary to analyse and study the results. It is also important that the transient stability results for variations in BESS sizing are generated through a commerical software, Electrical transient analyzer program (ETAP), to demonstrate the enhancement of output power quality, which leads to an improvement in transient stability. These transient stability results will have to be compared against international electrotechnical commission (IEC) standards 61892-1, in term of the transient deviation and continuous deviation.

- Although transient stability improvement is the main focus in this thesis, the techno-economic feasibility in increasing the capacity of BESS to aid in transient stability, has to be investigated. Besides the footprint of the BESS and meeting IEC standards 61892-1, the CAPEX and operational expenditure (OPEX) has to be considered.

- Current state of art of EMS's control algorithms consisting of a low-pass filter will be demonstrated, in the presences of dynamic loading with stochastic wind speed. This reduces the efficiency as additional losses are introduced while reducing transient deviations. It is also not possible to increase the BESS capacity further due to the space constraint and weight limitation on offshore O&G platform. These considerations have motivated us to develop an improved EMS based on the production loads of a North Sea oil platform and its dimensions. The results will be compared against the state-of-the-art EMS in [11].

1.2 Aims and Objectives

The objectives of this thesis contributes to the development and analysis of a hybrid energy system for offshore O&G rigs in the following areas:

1. To develop a proposed system comprising of a BESS integrated with WTG and O&G platforms, for validation with ETAP for transient stability analysis improvement.

2. To improve transient stability in proposed system to meet the Standards by Norwegian petroleum industry for oil and gas companies (NORSOK) and IEC standards 61892-1, considering intermittency of power generation profiles.

3. To optimise the BESS for an optimal improved solution in transient stability of the proposed system, considering CAPEX and OPEX analysis.

4. To improve the development of an EMS for transient stability, in the presence of dynamic loads and stochastic wind speeds.

5. To achieve decarbonisation in the development of a techno-economic solution for the proposed system under heavy power consumption on offshore O&G platforms.

1.3 Contributions

In this thesis, new results of developing offshore hybrid renewable power generation/distribution in offshore and marine industry are presented. Key contributions in each of these areas are given as follows:

- A MATLAB/Simulink model of an integrated system comprising of WTG with O&G platforms and on-board BESS is developed with SimPowerSystems and SimElectronics.

- In load flow analysis study, an investigation has been carried out on power stability of our proposed system comprising of the integration of WTG with O&G platforms and on-board BESS. Disturbances due to the tripping of primary power generation from WTG or GTG is simulated in MATLAB/Simulink for power stability and discussed in Chapter 3. The proposed system is compared against conventional system in term of output power quality to load demand with disturbances in a standalone micro grid configuration. An improvement in transient power stability was shown.

- In a transient stability study for variations in BESS sizing, the results generated using a commercial software ETAP has demonstrated an enhancement in output power quality. This shows a transient stability improvement as maximum voltage/frequency transient deviations are reduced. These results are compared against the IEC standards 61892-1 and the NORSOK standards used by Norwegian offshore industry for maximum continuous deviation and maximum transient recovery time in Chapter 4. This has not been shown in any existing literature, to the best of our knowledge.

- Due to space constraint and weight limitation in offshore O&G platforms, the actual sizing of onboard BESS to replace the GTG is considered, in terms of its physical footprint. A further optimization in transient stability is achieved by increasing the capacity of BESS in proposed system. It is shown that there is a significant improvement in transient voltage and frequency deviations, which fulfills the requirements under IEC 61892-1 for offshore O&G platforms.

- An intensive research is conducted on cost analysis comparison between conventional system and proposed system which is required for the development of a feasible business model. Relative to the CAPEX and OPEX of the typical system, the conventional system with 2MW of BESS has a CAPEX and OPEX of 84.87% . The proposed system has a lower overall cost in term of CAPEX and OPEX. In addition, the intangible benefit of carbon emission reduction is measured and captured in Chapter 5.

- A control algorithm is proposed for our energy management strategy to mitigate uncertainties due to dynamic loading and perturbations that are introduced by stochatic wind speeds. This is embedded with the integrated offshore WTG, O&G platforms and onboard BESS to achieve optimum transient stability, even in the worst case scenario of dynamic loading and fluctuations in wind speed. The CAPEX and OPEX with an increased BESS are addressed and it is proposed to maintain the BESS sizing at $2MW$. A proportional-integral controller is designed to maintain the voltage and frequency at the desired reference values, thereby reducing the transient voltage and frequency deviations. It is shown that our proposed EMS has a lower maximum frequency deviation and a reduced maximum voltage deviation, as compared to the state of the art. Last but not the least, a cost analysis was performed to identify the breakeven point for the proposed system, as compared to the conventional system. It is shown that the proposed system will match the CAPEX and OPEX of the conventional system by the 3.75 years with a carbon reduction of 64320.48 tonnes at the end of the fifth year.

1.4 Organisation of Thesis

This thesis is organised as follows.

Chapter 1 highlights the importance of the integration of offshore O&G platform with WTG and BESS that have contributed to the motivation and scope of this thesis. It summarises the key contributions and publications achieved through this thesis.

Chapter 2 presents the necessary background and different configurations for the electrification of offshore O&G platform. The first half of this chapter presents the background on the system overview, power consumption areas, fixed and peak loads for the typical offshore O&G platforms. Subsequently, the primary power generation through the gas turbine generators is described. This is followed by the description of the secondary power generation through WTG where the system architecture of the permanent magnet synchronous generator (PMSG) and its components are explained in detail. Next, the selection and footprint of the BESS are presented. Following which, the IEC standards for the offshore O &G platform are provided. The second half of this chapter focuses on a review of the different configurations for the electrification of

offshore O &G platform integrated with offshore wind.

In Chapter 3, relevant studies and results from the integration of offshore wind with O&G platforms are discussed. This is followed by a feasibility study on our proposed system configuration, which can potentially be situated near the coast of Scotland. An illustration is provided for the integration of the WTG at the location of Hywind park and a conventional three-bridge linked O&G platform in the North Sea. This system architecture, consisting of the integration of the WTG, O &G platform and BESS, is modelled in MATLAB/Simulink according to the illustrated configuration off the coast of Scotland. In this study, the load flow analysis and power stability is analysed for a BESS of $4MW$. Four test scenarios that cover the operational sequence for electrification are described and simulated in MATLAB/Simulink with SimPower Electronics. From the test scenarios, the load flow and transient deviations for the proposed system are studied and compared to those for the conventional system, which is comprised of an O &G platform integrated with WTG. It is shown that the proposed system configuration is feasible and provides an improvement in transient power stability, as compared to the conventional system.

Chapter 4 presents the use of a commercial software, ETAP, to generate the transient stability results in terms of voltage and frequency deviations. In this chapter, the sizing of the load will be based on a North Sea oil platform on a real production day. For realistic implementation, the footprint of the BESS has been considered. In this proposed system, the BESS will occupy the space on the O&G platform, which was previously used for the backup energy generator. By removing the backup energy generator, the carbon emissions from the O&G platform will be reduced as the generator is very inefficient while on standby mode and produces carbon emissions with no production in useful energy. Four different scenarios to test the ability of the system to maintain electrical power to load when subjected to transient faults are studied. The simulation results are presented for both the conventional and proposed systems. These results are also compared against the IEC standards 61892-1 and the NORSOK standards used by Norwegian offshore industry for maximum continuous deviation and maximum transient recovery time [13].

Following on the developments in Chapter 4, Chapter 5 investigates the techno-economic feasibility of increasing the BESS capacity to further enhance the quality of the output power. This also reduces carbon emissions as one GTG will be physically replaced with an additional 2 MW BESS, which has the same footprint on the O&G platform. Through load flow analysis conducted in Chapter 4, it has been shown that the electrification of the loads based on a North Sea platform can be performed with a set of GTG with WTG and BESS in Section 4.4.4 when GTG 2 is disconnected. With an increased BESS capacity from 2 MW to 4 MW, the system performance in its transient voltage and frequency deviations is studied. It is shown that there

is a significant improvement in transient voltage and frequency deviations, which fulfills the requirements under IEC 61892-1 for offshore O&G platforms.

In our last chapter of this thesis, the dynamic operation of the proposed system is studied, considering sources of uncertainties like changes in dynamic loading, as well as perturbations from stochasticity in wind. For such scenarios, the GTG is not able to provide support in frequency response due to the larger inertia in GTG. As such, the output power quality will be severely affected [10]. This is also the main drawback of our proposed system. Hence, an EMS will be developed in Chapter 6 for the enhancement of transient stability. In order to address the increase in CAPEX and OPEX with an increased BESS, it is proposed to maintain the BESS sizing at 2 MW. From a simulation study which considers changes in load and wind profile, it is shown that our proposed EMS has a lower maximum frequency deviation and a reduced maximum voltage deviation, as compared to the state of the art. Last but not the least, a cost analysis was performed to identify the breakeven point for the proposed system, as compared to the conventional system.

Chapter 2

Background and Related Work

As discussed in the previous chapter, the development and analysis of offshore hybrid renewable energy system for O&G rigs involves two areas of research in transient stability improvement, namely the design of energy storage and energy management strategy in the integration of offshore O&G platforms. In this chapter, the background and related works involving the typical O&G platform, study of primary power generation of GTG and secondary power generation of WTG, IEC standards for designing electrification to load in offshore O&G platforms and BESS modelling will be discussed in detail.

We will start by discussing operation sequence to electrify for load in offshore O&G platforms, followed by the onboard GTG for primary power generation in the typical system architecture. This system configuration generates heavy carbon emission that motivates research and development (R&D) on the approaches to reduce carbon footprint. This is followed by a review of the WTG PMSG and its voltage source converter (VSC). A review of BESS characteristics and its application in grid-connected systems are also provided. Following this, the IEC standards used in offshore electrification will be presented, which will be used as a benchmark to compare against simulation results of our proposed system. Last but not least, the last section will provide a review of existing literature of offshore O&G platform powered with WTG, which lays the foundation for work in this thesis.

2.1 Power Flow with System Overview in Oil and Gas (O&G) platform

In this section, a study on typical O&G platforms is necessary to understand the generation sources, loads and voltage level requirements onboard the offshore O&G pplatform. O&G platforms are typically equipped with platforms consist of a utility and living quarter (ULQ)

platform, a processing and heating (CPF) platform and a wellhead (WHP) platform. These platforms are commonly powered by three sets of SCGTs, which are used as EGs and rated to meet the load demand of the platforms, as shown in Figure 2.1 [14]. In the typical O&G platforms, two EGs will always be running and one essential generator (EG) will be on standby mode. The EGs burn extracted natural gas from the field under normal operating conditions, which powers the three platforms via three main switchboards that are rated at 11 kV. The output voltage is stepped down via integral transformers in distribution panels to 3,3 kV and 400 V, to power the water injection pumps, gas compressors, drilling unit, utility loads and etc.

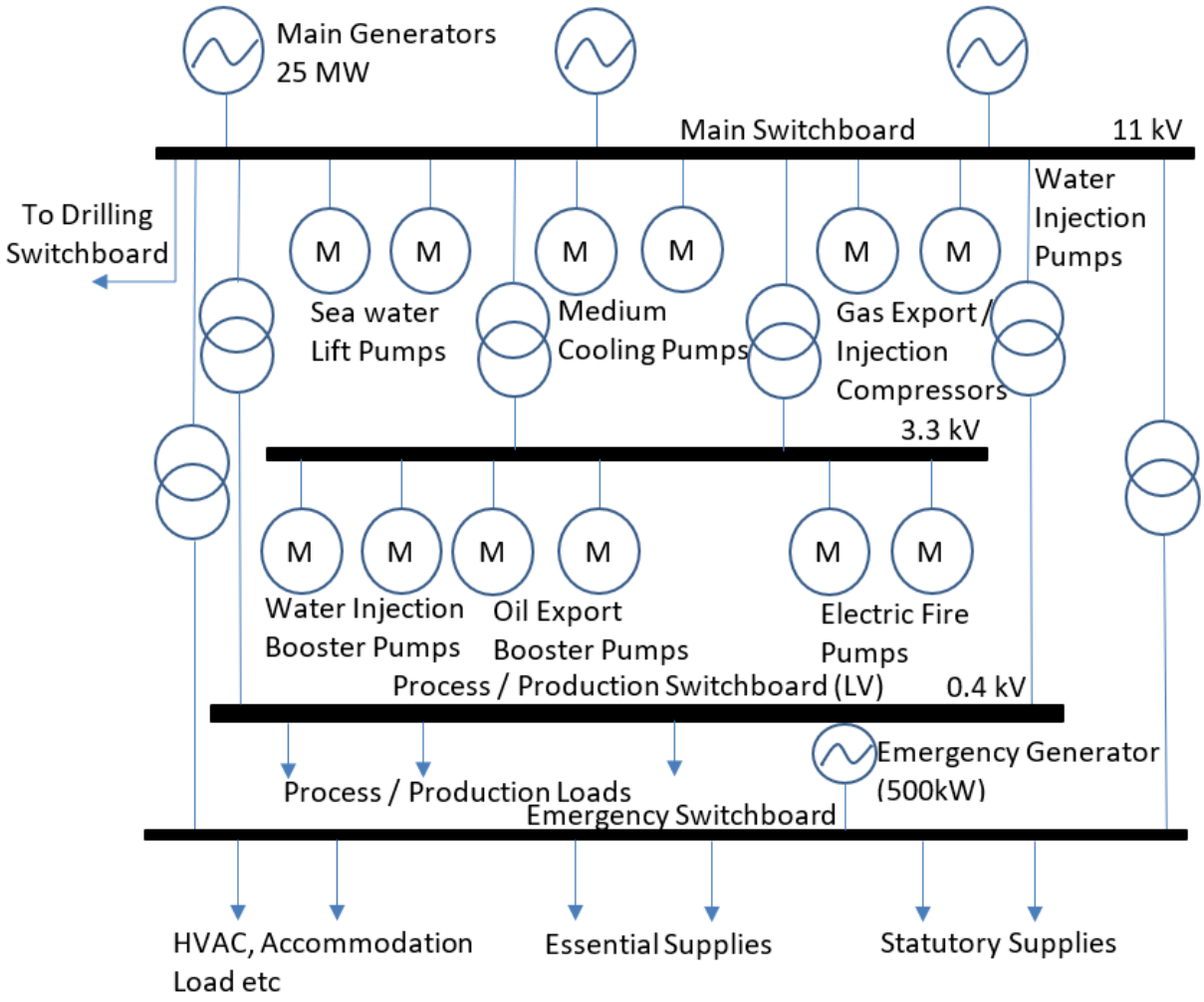

Figure 2.1: Single line diagram of typical offshore electrical system [14].

The primary power generation application in O&G platforms,as shown in Figure 2.1 [14], is the gas turbines, which are labelled as main generators. The turbine will provide direct drive to an alternator to generate power for the installation. It is normal to have at least two gas turbines on main platforms with an emergency generator as back-up. Satellite and remote or unmanned platforms are commonly provided with power from the main installation via umbilicals rather than having their own gas turbines. The typical gas turbine size in this application is 1.5 MW - 25 MW [15]. The number and configuration of turbines depends on the flexibility and redun-

dancy needed and to allow for future platform upgrades [14] .

Consumption area	Power	Type
Oil Processing Equipment	1 – 2 MW	Heating / Drives
Oil Export Systems	2 – 12 MW	Large Drives
Glycol/Methanol Regeneration Systems	0.5 – 3 MW	Heating Small Drives
Gas recompression	2-10 MW	Large Drives
Auxiliary Systems	1 – 2 MW	Small / Medium Drives
Water Injection Systems	12 – 25 MW	Large Drives
Drilling Systems	3 – 5 MW	Medium Drives
Living Quarters	0.5 – 2 MW	Lighting / Heating / Drives
Lightings, Heating and Ventilation	0.2 – 2 MW	Lighting / Heating / Drives
Heat Tracing Cable Installations	0.1 – 1 MW	Heating
Emergency Power Consumers	0.5 – 6 MW	Lighting / Heating / Drives

Figure 2.2: Main power consumption areas on an oil production platform [14].

A typical list of power consumers for an oil production platform is shown in Figure 2.2. The typical load on an offshore installation can be split into the following categories [14]:

1. Drives for process of auxiliary systems. The drives in process-system are almost exclusively powering pumps and compressors for oil, gas, water or chemicals. The required power rating can reach as high as 20 MW per unit. Traditionally units with more than 5 to 8 MW have been directly powered by turbines, while smaller units have been powered by electric motors.

2. Process heating systems of electrochemical systems. The need for process heating varies from installation to installation. When large amounts of heat are needed, these are mostly supplied by oil or gas burners, but electric boilers with ratings up to 20 MW have been installed. Additionally, electric heat tracing cables and heat elements are used for local needs with low rating, and for special applications.

3. Lighting, heating and ventilation systems. These are typically systems for the desalination of seawater, both for drinking water and for injection into the reservoir to increase the oil yield. Lighting-, heating- and ventilation systems A large platform can have a total need for lighting of 500 kW. Power for ventilation and heating of processing areas, control rooms and living quarters can reach the MegaWatts range.

2.2 Gas Turbine Generation (GTG)

Gas turbines is an equipment serve as a primary power generation in offshore O&G platforms consisting of the air compressor with the expander, driven by common shaft through a combustion chamber placed in between them. Energy generated from standalone gas turbine unit is known as an autonomous unit called simple-cycle gas turbine (SCGT). The SCGT is characterized by its lower power, light-weight and container-construction, which allows for easy transport.The SCGTs are commonly used onboard O&G platform, as compared to the combined-cycle gas turbines used at power plants on land. The highest efficiency SCGT from General Electric, LM6000 is at 42%. Conventional SCGTs have an efficiency of around 33%. A GTG can be modelled by its thermodynamic parameters and its performance characteristics. These thermodynamic parameters include the compression ratio, ambient temperature, ambient pressure, humidity, heat rate, turbine inlet temperature, specific fuel consumption, air to fuel ratio and component efficiency.

An ideal open gas turbine cycle and the T-S diagram of a typical Rankine cycle are shown in Figure 2.3.

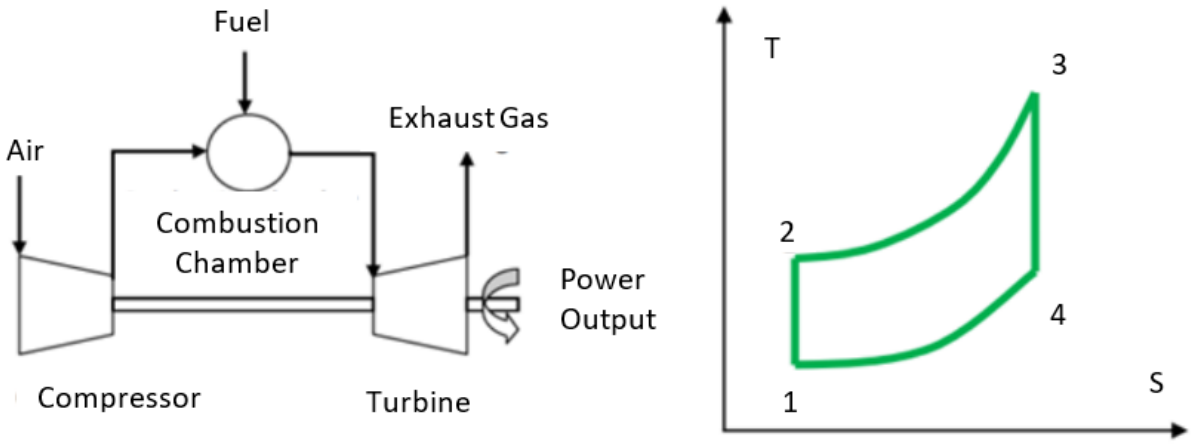

Figure 2.3: Open GT and T-S diagram [16].

There are a series of four processes from pressurised air and fuel are burned through the combustion chamber to generate electric power in the ideal brayton cycle. The turbine inlet temperature can be defined as the temperature of the air gas mixture at the inlet of the gas turbine and will influence the gas turbine performance. In deriving the turbine work output, T_1 is denoted as turbine inlet temperature. This relates to the changes that T_1 influences the turbine work output and the resulting net work output. Since atomic mass of the water is less than air of nitrogen and oxygen, the thermal efficiency of gas turbine will not be at peak in offshore condition. Thus, humid air has less density than the dry air and the amount of dry air mass entering the gas turbine reduces, which decreases the performance of the gas turbine under offshore con-

ditions [16].

Consider W and Q are the work done and heat transfer per unit mass respectively. For an ideal Brayton cycle, the following equations can be derived, assuming that the specific heat constant for constant pressure C_p is fixed for the process [16]. During the state 1 to 2 in the T-S diagram, the air is drawn into the compressor where it is pressurised and undergoes isentropic compression in the compressor. The work required by compressor is given by:

$$W_{12} = (h_2 - h_1) = C_p(T_2 - T_1), \tag{2.1}$$

where $h_2 - h_1$ is the heat exchange in terms of the enthalpy differences between the states 1 and 2, C_p is the specific heat constant for constant pressure, and $T_2 - T_1$ is the temperature differences between states 1 and 2.

From the state 2 to 3 in the T-S diagram, the compressed air runs through a combustion chamber and the air is heated up in a constant pressure isobaric process as the chamber is open. The heat addition comes from the fuel using in the combustion chamber is calculated as follows:

$$Q_{23} = (h_3 - h_2) = C_p(T_3 - T_2), \tag{2.2}$$

where $h_3 - h_2$ is the heat exchange in terms of the enthalpy differences between the states 3 and 2, C_p is the specific heat constant for constant pressure, and $T_3 - T_2$ is the temperature differences between states 3 and 2.

From the state 3 to 4 in the T-S diagram, the heated and pressurised air gives up its energy by expanding through a turbine and goes through isentropic expansion inside the turbine. The work output is given by:

$$W_{34} = (h_4 - h_3) = C_p(T_4 - T_3), \tag{2.3}$$

where $h_4 - h_3$ is the heat exchange in terms of the enthalpy differences between the states 3 and 4, C_p is the specific heat constant for constant pressure, and $T_4 - T_3$ is the temperature differences between states 3 and 4.

The thermal efficiency of such a simple Brayton cycle is expressed in terms of the temperatures. For the complete cycle, the net-work output is given by:

$$W_{net} = C_p[(T_3 - T_4) - (T_2 - T_1)]. \tag{2.4}$$

The temperature ratio across the compressor, TR and pressure ratio, PR can be defined for the efficiency of the compressor and its cycle as follows.

$$1 - 1/TR = 1 - 1/PR^{(\gamma-1)/\gamma}, \tag{2.5}$$

where $\gamma = C_p/C_v$, C_p is defined as heat capacity at constant pressure and C_v is defined as heat capacity at constant temperature.

The above equations will be used in our MATLAB Simulink model for the SCGTs onboard the O&G platforms in the subsequent chapters of this thesis.

2.3 Wind Turbine Generation (WTG)

In this section, the wind turbine output power generation, the system architecture of a PMSG, the architecture of the back-to-back (B2B) VSC and its connection to the power network is described. This will be used in our MATLAB/Simulink model for the offshore WTG in the subsequent chapters of this thesis.

2.3.1 WTG Output Power Generation

Wind turbines produce electricity by using the power of the wind to drive an electrical generator [17]. As wind passes over the blades generating lift, a rotational force is exerted. The rotating blades turn a shaft which increases the rotational speed of the generator. The generator uses magnetic fields to convert the rotational energy into electrical energy. This power output goes to a transformer, which steps up the generator terminal voltage to the rated voltage level for the power network. A wind turbine extracts kinetic energy from the swept area of the blades where ρ is the air density, A is the swept area of the rotor in m^2, and v is the upwind free wind speed in m/s.

The power transferred to the wind turbine rotor is reduced by the power coefficient, C_{Pw}. The output power P is measured in kW as follows:

$$P = 0.5 \times p \times \pi \times R^2 \times v^3 \times C_{pw} \times CF \times N_g \times N_b, \tag{2.6}$$

where CF is the capacity factor, R is the radius to tip of the rotor, N_g is generator efficiency and N_b is gearbox efficiency.

A maximum value of C_{pw} is defined by the Betz limit, which states that a turbine can never extract more than 59.3% of the energy from the wind. In practice, wind turbine rotors have maximum C_{pw} values in the range of 25–45%.

The blade tip speed can be calculated from the rotational speed of the turbine and the length of the blades as follows.

$$\omega \times R = \frac{\pi \times D \times RPM}{60}, \tag{2.7}$$

where D is the diameter of rotor and RPM is the rotor speed.

Tip-speed ratio is calculated from the ratio of blade tip speed to wind speed as follows:

$$\gamma_{TSR} = \frac{\omega \times R}{v}, \tag{2.8}$$

where ω is the rotational speed of the rotor. The power coefficient, C_p , varies with the blade tip speed ratio and blade pitch angles, as illustrated in Figure 2.4.

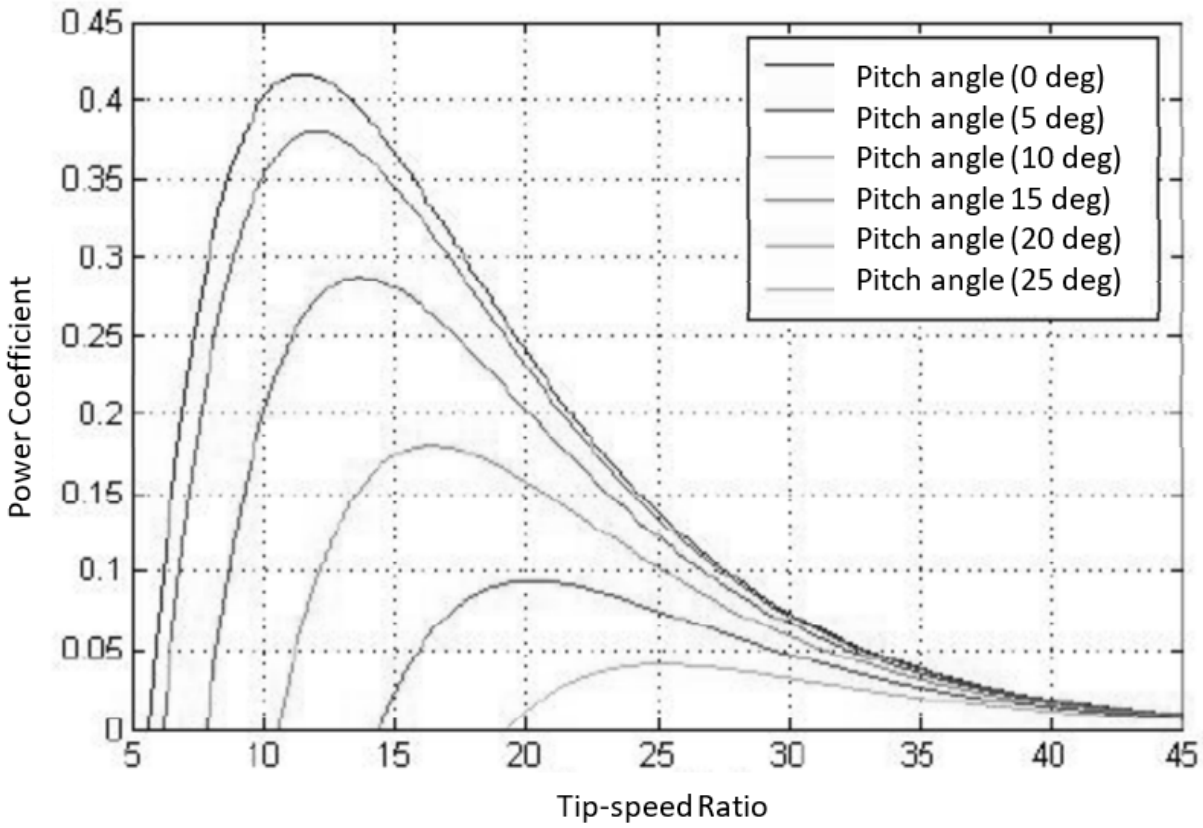

Figure 2.4: Power coefficient versus tip speed ratio for various values of pitch angles [18].

For a variable speed pitch regulated wind turbine, the power production from the wind turbine can be maximized if the system is operated at maximum C_{pw}. As the wind speed changes, the rotor speed should be adjusted to follow the change to maintain the tip speed ratio. This is possible with a variable-speed wind turbine. For varying blade pitch angles, the C_{pw} can maximised at the optimal tip-speed ratio. Simulation results in [18] illustrates that the WTG can be operated for optimum energy capture while limiting the load on the wind turbine for a wide range of wind speeds and operated at high C_{pw} values for most of the time.

For offshore WTG, the rotor size is considerably bigger than onshore turbines. As such, the blades are heavier and rotation must be facilitated by either hydraulic of electric drives. In order to prevent rotor speed from becoming too high, the extracted power from incoming wind must be limited. This can be done by reducing the C_{pw} of the turbine and the C_{pw} value can be adjusted using a change in pitch angle, as shown in Figure 2.4. As the targeted output power can be controlled instantaneously using the angular speed of the WTG , as shown from Equations 2.6 to 2.8, and the realistic limit on output power is the power rating of the converter and generator, only small changes of pitch angles are required to maintain power output at rated power. This enables the WTG to operate at rated power.

In the actual WTG operation, the power curve has to be considered. This is shown by a typical power curve, which details the actual power output of a WTG for wind speeds starting from 0m/s to its cut-in wind speed, followed by the rated wind speed and the cut out wind speed, as shown in Figure 2.5.

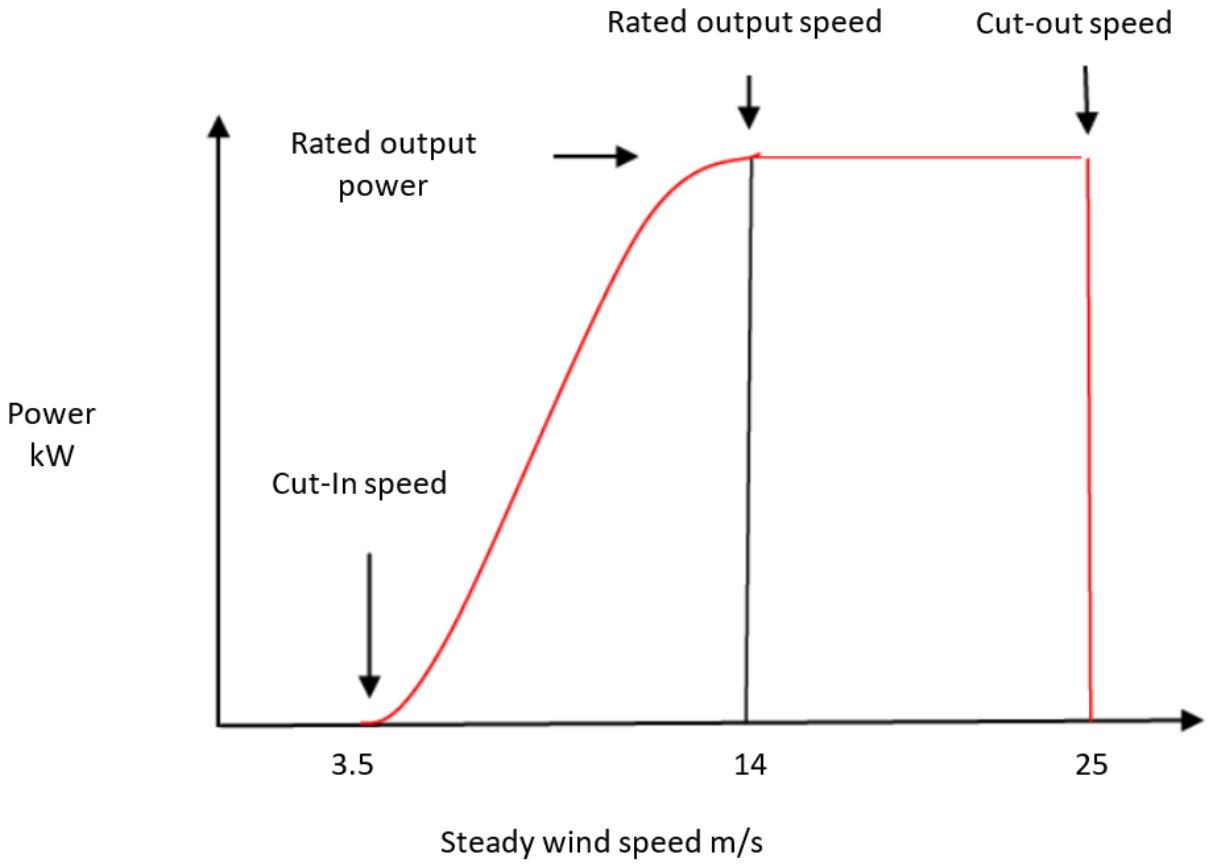

Figure 2.5: Typical power curve of a wind turbine [19].

At low wind speeds below the cut-in speed, the WTG does not output any power. Between the cut-in to rated output speed, output power is below rated. The WTG only operates at rated

power for a range of wind speeds from rated output speed to cut-out speed. When wind speeds exceeds the cut-out speed, the blades can point into the wind to reduce their surface area. Despite this shut off, the yaw drive, located in the wind turbine's nacelle, continuously points the rotor into the wind, even as weather patterns shift as they pass through. In extreme situations, the rotor can be yawed out of the wind and the blades will be locked in a turbine shut down mode. As wind is a natural resource, the stochasticity of wind results in the intermittency of the WTG output power, which will be discussed in Chapter 6.

2.3.2 Permanent Magnet Synchronous Generator (PMSG) System

In this thesis, the PMSG of the WTG is modelled in MATLAB/Simulink, which will be discussed in this section. An overview of the system architecture of PMSG is as shown in Figure 2.6.

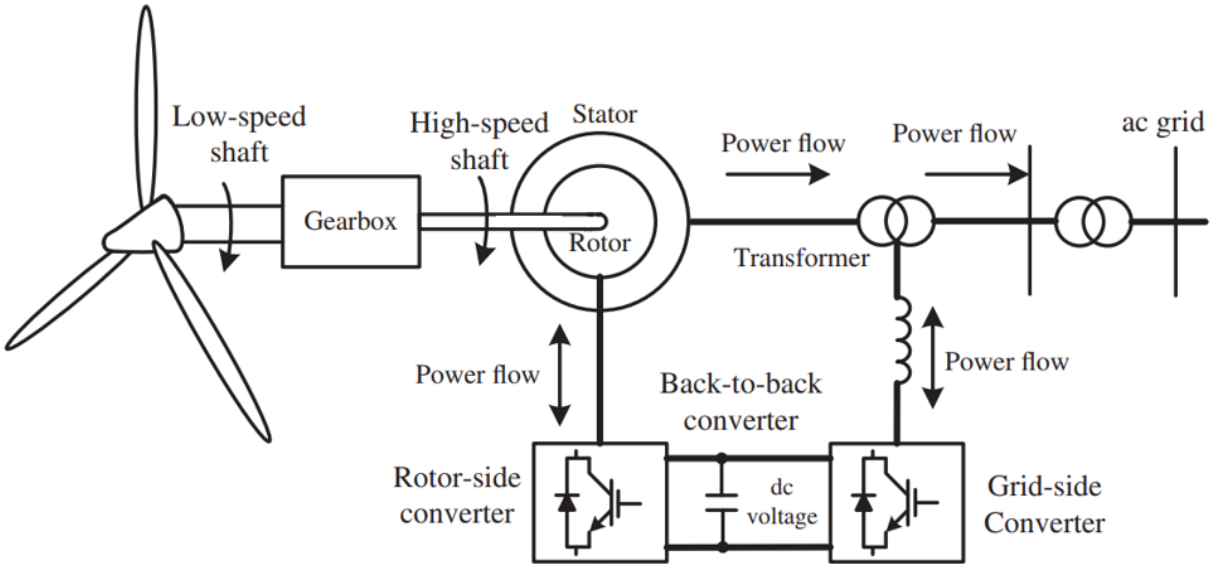

Figure 2.6: System architecture of PMSG [17].

This consists of a synchronous generator, DC-link capacitor and back to back converter interfaces. The PMSG operates with variable wind speed and produces a variable AC voltage with variable frequency. The alternating current (AC) frequency voltage is first rectified by alternating current / direct current (AC/DC) rectifier by the first VSC. Thereafter, the generator output power is converted from direct current (DC) link with AC/DC inverter by the second VSC to supply variable frequency and voltage rated at 690 V.

The power exchange between this converter and the ac grid depends on the operating point of the machine and the desired control over the speed and reactive power of the PMSG. The B2B converter configuration decouples the network electrical frequency from the rotor mechanical

frequency, enabling variable-speed operation of the wind turbine. Finally, a step-up transformer will supply rated voltage of 33 kV to the power transmission in electrical grid. Permanent magnet excitation avoids the field current supply or reactive power compensation facilities needed by wound-rotor synchronous generators and induction generators, and it also removes the need for slip rings [17].

For low power AC-DC converters with no power factor correction (PFC) stage, the minimum capacitance, C is normally set by the allowed mains ripple voltage on the DC-link. This gives a capacitance value of 2 $\mu F/watt$ for a universal main input supply. For higher power AC-DC converters with PFC, the value is set by 'hold-up' or 'ride-through' time on input power loss and a much lower capacitance is possible with energy stored at high voltage. As such, values of less than $1\mu F/watt$ is normal. The hold-up time (t_h) multipled by output power (P_o) and divided by efficiency (η), is calculated as follows [21].

$$C = \frac{t_h \times P_o}{\eta} \tag{2.9}$$

The energy difference in the capacitor between its starting voltage and final voltage at which the converter stops operating to specification is as follows.

$$C = \frac{2P_o \times t_h}{\eta \times (V_{start}^2 - V_{finish}^2)} \tag{2.10}$$

In a transformer, the volt per turn on the secondary winding is the same as in the primary winding. The stepping up or stepping down of the voltage can be determined by the ratio of turns in the primary and secondary windings. In our application, a high-voltage power transformer is used to step up the voltage and which reduces the current, resulting in a lower power loss in the transmission line.

On the secondary winding side, the magnetic flux induces an electromotive force (EMF). Due to induced EMF in the secondary winding, current flows to the external load which is connected to its terminals. The power is effectively transformed from the primary to the secondary winding in this way. Transformers can be connected in configurations such as either wye/wye (Y/Y) delta/delta (Δ/Δ), Y/Δ or Δ/Y. The efficiency of a transformer can be calculated by gaining the ratio of the output power to the input power [20].

It is important to note that no transformer will have an efficiency of 100% which introduces the possibility of a non-ideal transformer, resulting in losses. The unknown parameters of any given transformer may be found by employing a method of using the open and short circuit tests and performing calculations on the results gained. Thereafter, the calculated results can be used to determine the efficiency of the transformer [20]. This can potentially be used to improve our

model, if test results can be made available.

2.3.3 Back-to-back (B2B) Voltage Source Converter (VSC)

In this section, the B2B VSCs and the its properties are discussed. The B2B converters consists of two three-phase Pulse Width Modulated-Voltage Source Converters (PWM-VSCs) that is the rotor-side converter (RSC) and the grid-side converter (GSC), linked via a common dc bus. An advantage of this architecture is the capacitor decoupling between the grid inverter and the generator inverter. Besides affording protection, this also separates control of the two inverters, which allows independent compensation of asymmetry both on the generator side and the grid side.

The RSC is connected to the rotor windings and the GSC is connected to the ac grid via a coupling reactor. The RSC controls the wind turbine speed and reactive power consumption by modifying the rotor currents. The GSC mainly keeps a steady dc voltage level on the B2B dc bus (which is of primary importance for the correct operation of the RSC) and provides, to some extent, reactive power support to the ac grid. The architecture of both converters allows bidirectional power flow making the B2B converter a rotor slip-power recovery device (i.e. recovers the power generated in the rotor windings that otherwise would have been lost as heat in the windings) [21].

In order to use the DC-link, the DC-link voltage must be stepped up to an amplitude greater than that of the grid line-line voltage, to achieve total control of the grid current. The power flow of the grid side converter is controlled in order to maintain a constant DC-link voltage, while the control of the generator side is set to meet the demand on magnetization and the reference speed. A Boost Converter is used to step up the voltage from the input supply to the output of the load. Similarly, boost converter operation is usually used in the application when an output voltage is larger than its input voltage and to stabilise the dc link voltage. This converter is the switch-mode supply and the output voltage is adjusted based on the duty cycle of transistor. It is required to have a transformer, requiring conversion to ac and back for converters with a voltage boost ratio [21]. The ideal boost converter has “infinite” to maximum ratio and the input current is the output current times the boost ratio.

In order to achieve variable speed operation, the wind turbines equipped with a PMSG will require a boost DC-DC converter inserted in the DC-link. This is included in our MATLAB/Simulink model used in the subsequent chapters.

2.4 Battery Energy Storage System (BESS)

The use of batteries as a system to interchange energy with the grid is well known. There are several types of batteries used in renewable energy systems: lead acid, lithium, nickel and etc. Batteries provide rapid response for either charge or discharge, although the discharge rate is limited by chemical reactions and the type of battery. They act as a constant voltage source in power systems. New trends in the use of batteries for renewable energy systems focused on the integration with several energy sources (wind energy, photovoltaic systems, etc.) and also on the integration with other energy storage systems complementing them. Also, there are attempts to optimize battery cells in order to reduce maintenance and to increase its lifetime [22].

2.4.1 Characteristic of Lithium-ion Energy Storage

Lithium-ion energy storage solution has been making remarkable progress to improve environmental sustainability in the offshore and marine industry. Some examples include the electric car ferry, the offshore drilling rig, and etc. In 2015, a fully electric car ferry vessel was operational with an on-board BESS, which reduces the carbon emissions, as compared to vessels on diesel generation. The electric vessel is recharged using hydroelectric power from the existing electric utility grid infrastructure [23]. In 2018, the drilling rigs of West Mira installed 6 MW power of energy storage solution for operation in the Nova field at North Sea. The batteries will be charged from the rig's diesel-electric generators, in the event of peak loads [23].

The minimum battery capacity is sized to accommodate the design load over the specified autonomy time, where C_{min} is the minimum battery capacity calculated in (Ah) as follows [22].

$$C_{min} = \frac{E_d(K_a \times K_t \times K_c)}{(V_{dc} \times K_{dod} \times K_e)}, \tag{2.11}$$

where E_d is design energy over the autonomy time (VAh), V_{dc} is nominal battery voltage, K_a is battery ageing factor (%), K_t is temperature correction factor (%), K_c is capacity rating factor (%), K_e is System efficiency (%), and K_{dod} is maximum depth of discharge (%).

While energy density of energy storage is vital to system integration in offshore O&G platforms due to limited space available onboard, specific energy is worthwhile to be considered due to weight limitation in the building of structures for offshore O&G platforms. Figure 2.7 presents lithium-ion batteries that has the lowest energy density and specific energy in BESS as compare with other mediums such as diesel, liquid hydrogen, methanol and ethanol. These data in term of energy density and specific energy are comparable to articles [24], [25]. The energy density, E_d is calculated as follows.

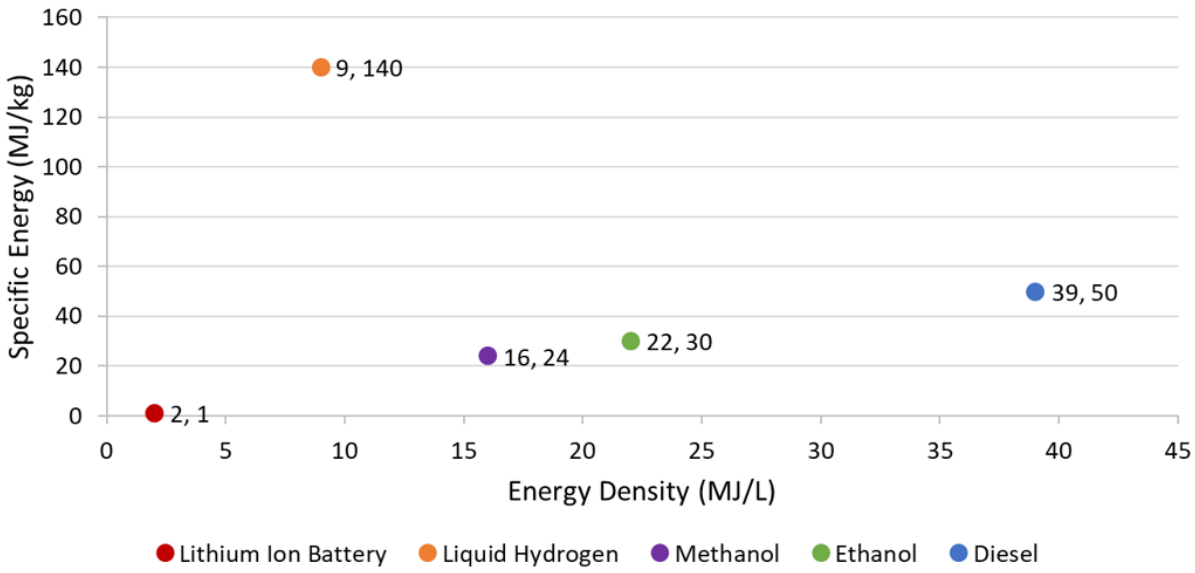

Figure 2.7: Energy density and specific energy for different mediums of energy storage from the references in [24], [25].

$$E_d = \frac{E}{V}, \tag{2.12}$$

where E is the energy that the medium has and V is volume of the medium. The specific energy, E_s is formulated mathematically in the following equation.

$$E_s = \frac{E}{m}, \tag{2.13}$$

where m is mass of the medium.

Considering the different mediums of energy storage, sustainable options with a lower carbon emission include lithium-ion batteries and hydrogen etc. Although hydrogen has a higher energy density, it requires a large H_2 storage capacity, which is not achievable onboard the O&G platform, as discussed in Section 1.1. It is possible to generate hydrogen using electrolysis, which will then have to be fed into a fuel cell to output power. The entire process requires larger footprint area which is not possible to install onboard the O&G platform.

This concept applied similarly to diesel as the energy storage which require additional footprint to place diesel engine with generator that would contribute more in carbon emission that not relevant in this research project's objectives. Moreover, diesel has the lower efficiency than lithium-ion batteries in energy conversion technology. Furthermore, more time requires for energy transfer from diesel engine to generator delays response from diesel to supply output power to power grid.

Other battery options like nickel metal hydride (Ni-MH) are more recyclable but has a 40% lower energy density, as compared to lithium-ion. Newer technologies with a higher energy density include lithium-sulfur batteries, redox flow batteries and etc, which are not mature as yet. It might take a few more years for these technologies to mature, which will propel the viability of our application. Considering the above, lithium-ion is selected as the energy storage device in our application and will be modelled.

2.4.2 BESS in Grid-connected Applications

There has been intensive research on the integration of BESS with WTG for output power enhancement in various applications. This is also fuelled by the fact that BESS has decreased swiftly in cost over the years due to high industry demand stemming from the need to improve power stability with increased penetration of renewables. An example of BESS integrated with WTG is as shown in Figure 2.8. The WTG is interconnected with BESS at the point of common coupling (PCC) to generate output power to the grid. Under this configuration, the control strategy in BESS can be charged and discharged to provide power smoothing to the grid, in the presence of fluctuation in wind power, due to the stochasticity of wind speed. This study has explored a large BESS capacity of approximately 20 % of the total output power to smooth out the intermittency in wind power and improve the output transient stability at the load [26].

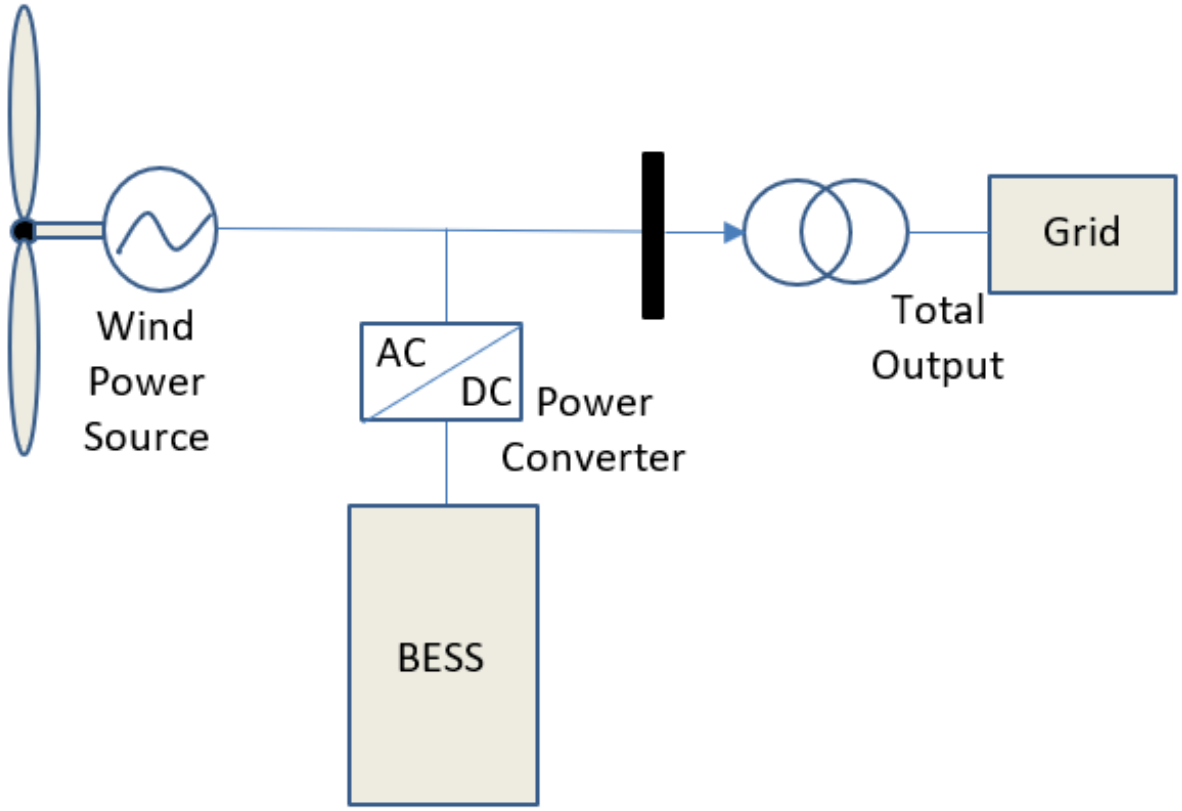

Figure 2.8: BESS integrated with WTG at PCC [26].

As indicated in Figure 2.8, the control strategy in BESS can either discharge by injecting power to PCC when there is low demand from WTG or charge when there is higher penetration from WTG. The net power, P_{net} in the system can be represented by:

$$P_{net} = P_{WTG} + P_{Bess}, \tag{2.14}$$

where P_{WTG} is the power from WTG and P_{Bess} is the power from BESS.

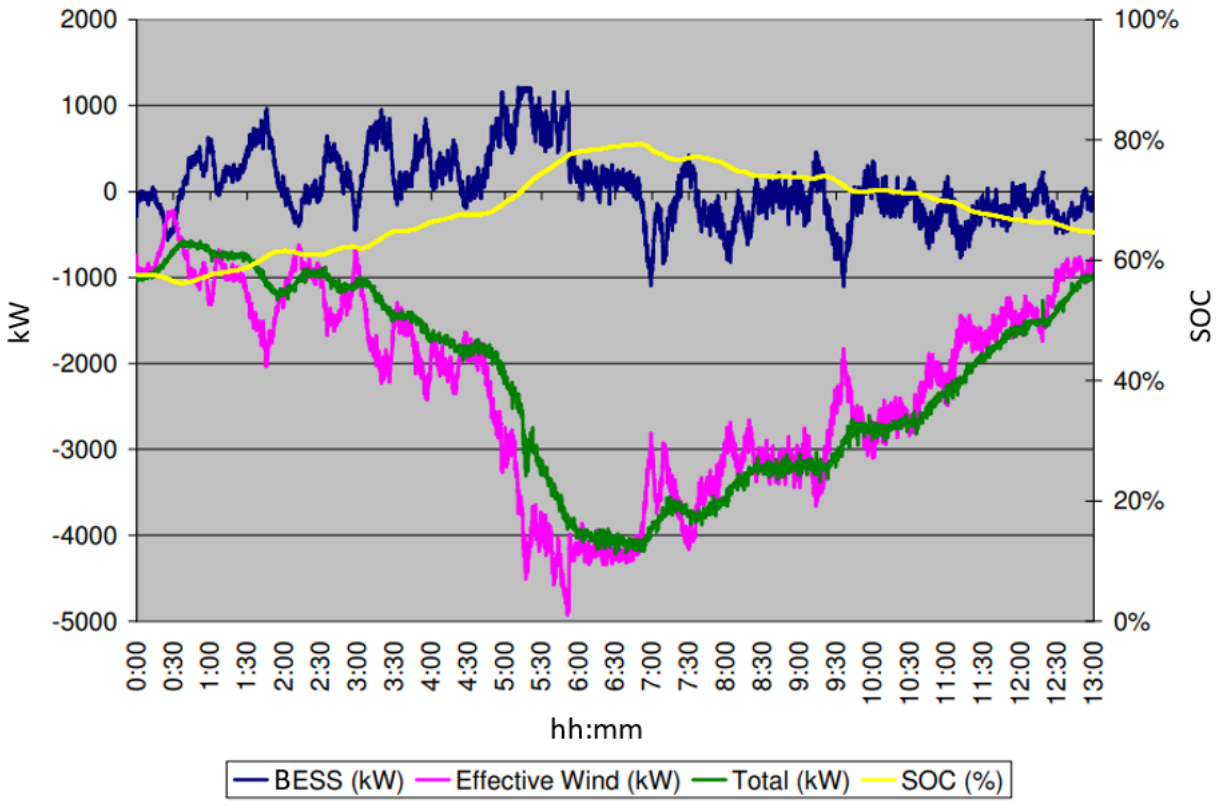

Figure 2.9: Renewable energy output smoothing by the BESS (blue line = output of the BESS; pink line = output of wind energy; green line = combined output of wind energy and BESS measured at the point of interconnection of the grid; and yellow line = SOC of battery) [27].

In another study where the BESS is integrated with an onshore wind farm, the output power smoothing capability of the BESS in the presence of fluctuations in wind energy is illustrated in Figure 2.9. This is enabled by a control scheme that is developed to regulate the output from the BESS, using the feedback at the PCC to enhance the power quality at load, which is vital to provide fast response in balancing transient power fluctuations in generation or the load demand.An EMS control strategy is designed in the BESS for system reliability, power system stability and enhancement in transient stability. These can be achieved by using a power conversion system which is connected to BESS and deployed at the sub-station of the power grid. This control strategy has the ability to regulate grid frequency, maintain the battery state of charge (SOC), smooth output power and provide economic dispatch. An illustration of the

BESS regulating grid voltage and frequency is as shown in Figure 2.10. In this study, the BESS has a control module, which focus on grid frequency regulation and voltage support, in the event of a fault in the 3-phase line to maintain voltage close to nominal. This is compared to the results without BESS where a higher steady state voltage and frequency deviation is observed [28].

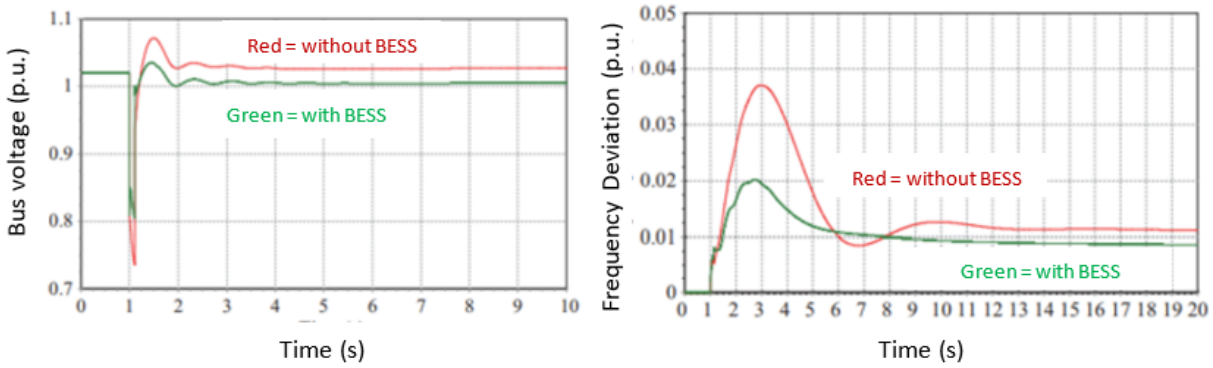

Figure 2.10: BESS regulating voltage and frequency [27].

The above studies investigate the integration of BESS with WTG in grid-connected configuration. Such a configuration will result in a higher CAPEX of O&G platforms as subsea transmission cables are required to connect the system to the onshore power grid. Hence, the focus of this thesis is to study the off-grid configuration, which is more challenging due to limited power capacity from offshore power generation. When applied towards our proposed system on offshore O&G platforms, the feasibility of the design and development has to be considered in two areas, namely the sizing of the BESS considering its footprint and the meeting of the IEC standards 61892-1 on voltage and frequency deviation limits for the O&G platforms [27]. As such, an integrated system consisting of an offshore floating wind farm and O&G production platforms with a BESS is proposed in the scope of our work. The sizing of the BESS and an energy management strategy are proposed to meet IEC standards 61892-1 in the event of stochastic wind speed and dynamic loads.

2.5 IEC Standards for Offshore O&G Platform

The Norwegian power grid is divided in three parts, main transmission grid, regional grid and local grid. Norway is part of Nordel system, ruled by the “Nordel Grid Code”. The Nordel Grid Code corresponds to the minimal requirements that must be fulfilled by the participants. Each Transmission System Operator (TSO) has its own code which completes the Nordel code [[29]. Today, integration of wind farms has an important role on power transmission systems due to their large power generation and requirements of security of power supply. Hence, wind farms are also subjected to specific rules and regulations to transfer and integrate power to the existing power grid. The NORSOK standards [30] control provisions for electrical installations at all voltages to provide safety in the design of electrical systems, selection, and use of electrical

equipment for generation, storage, distribution, integration and utilization of electrical energy for all purposes in offshore units, which are being used for the purpose of exploration or exploitation of petroleum resources.

NORSOK standards does not apply for the electrical installations in rooms used for medical purposes or in tankers but applies to all electrical installations. The installation may be permanent, temporary, transportable or hand-held, to AC installations up to and including 35000 V and DC installations up to and including 1500 V. This ensures that frequency and voltage variations are within permissible limits defined by the NORSOK standards, even in the event of perturbations to the system. The limitations as specified in Table 2.1 are the general requirements according to NORSOK standard E-001 found in [30], which again refers to IEC standards 61892, Edition 1. Please note that the transient frequency deviation limit has changed from 5 % in Edition 1 to 10 % in Edition 2 of the IEC 61892-1 standards [13].

Table 2.1: Voltage and Frequency Deviation

Operation	**Voltage Deviation**	**Frequency Deviation**
Maximum Continuous Deviation	+/-6 / -10%	+/-5%
Maximum Cyclic Deviation	+/-2%	+/-0.5%
Maximum Transient Deviation	+/-20%	+/-10%
Maximum Transient Recovery Time	+/-1.5sec	+/-10sec

In the subsequent chapters of this thesis, the transient and continuous deviations will be checked against the requirements above so as to assess if they meet the IEC 61892-1 standards.

2.6 Configurations for Electrification of Offshore O&G Platforms

In this section, different configurations developed for electrification of offshore O&G platforms are examined and studied in detail. This provides the know-how to generate sufficient power for the load on offshore O&G platforms. These configurations are categorised broadly as follows:

1. Grid-connected offshore O&G platforms with secondary power generation of offshore WTG

2. Micro-grid offshore O&G platforms with secondary power generation of offshore WTG and/or BESS

3. Integration of O&G platforms with offshore WTG based on an economic analysis

Each of the categories above are presented in Sections 2.6.1, 2.6.2 and 2.6.3 respectively.

2.6.1 Grid-connected Offshore O&G Platforms with Secondary Power Generation of Offshore WTG

In the first category, grid-connected offshore O&G platforms provided with secondary power generation of offshore WTG are discussed in [31–34]. These provide the current leading technology of power transmission from onshore power grid to improve in frequency and voltage stability for load consumption in integration of offshore O&G platforms with offshore WTG. However, such power stability results are not possible to achieve in a micro-grid system, which is not connected to the grid. In addition, there is an increased cost of running a HVAC or HVDC line back to the main land for transmission distances less than 100km or more respectively.

In [31], the integration of OWF with onboard GTG to electrify O&G platforms, as shown in Figure 2.11, enables both frequent and voltage transient deviation mitigation when there is excess output power from WTG to inject into power grid. This system configuration is feasible as OWF is situated nearby offshore O&G platforms which requires subsea cabling to connected them together. On top of this, surplus output power from OWF can supply to multiple nearby O&G platforms or inject excess output power to onshore power grid via subsea cabling. The design has been discussed in [31] to optimally reduce carbon footprint across the cluster of O&G platforms. The simulation has been presented in MATLAB/Simulink. With the increased capacity in OWF connected to offshore O&G platforms, this will further reduce transient deviations of both voltage and frequency. However, there is an economic problem that needs to be addressed before this configuration is suitable for development into a business model.

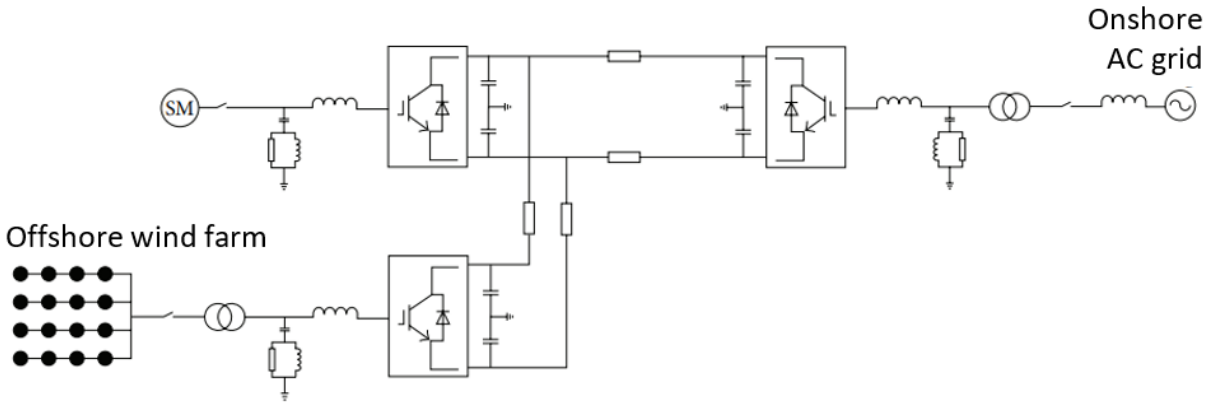

Figure 2.11: One proposal of the 1000*MW* OWF integration [31].

In [32], it is presented that OWF is able to reduce the fluctuation of voltage and frequency

control when the control system provides the required electrical power to O&G platforms in a grid-connected configuration in 2013. The control and stability study has presented the configuration of a wind farm with multiple O&G platforms in an offshore AC grid , and connected via HVDC power transmission to the onshore grid, as shown in Figure 2.12. The simulation test is performed in MATLAB/Simulink with the scenarios of loss of wind power and sudden increase of load by connecting O&G platforms. All of these scenarios are matched with the requirements from IEC6189-1 to keep voltage and frequency within acceptable limits. In the scenario of total loss of wind power in OWF, there is an oscillation seen in the grid-connected HVDC transmission link on the offshore converter side, which is longer than the recovery of wind power to offshore load. In the scenario of sudden connection with an O&G platform, there is 0.1 Hz dip in frequency and existing O&G platforms has a dip in voltage of 0.1 $p.u.$.

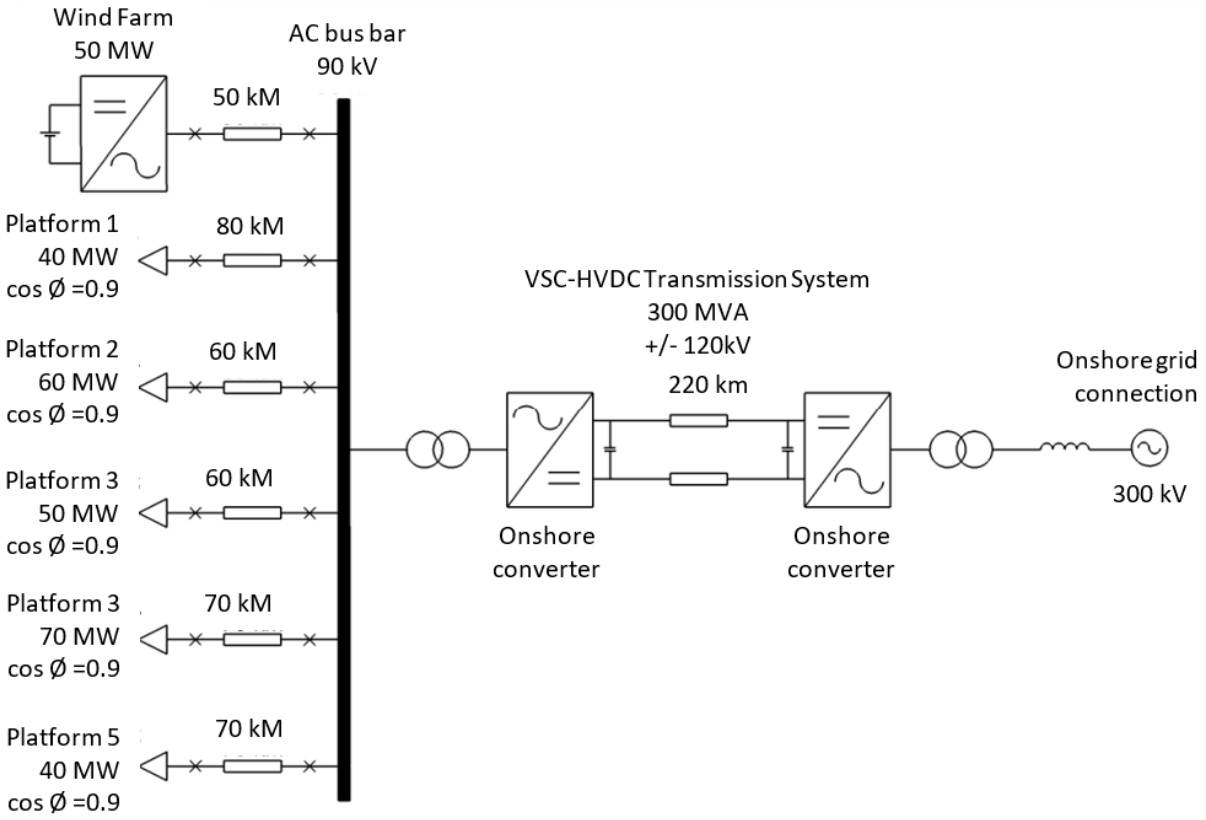

Figure 2.12: Overview of the system consisting of OWF supplying to five O&G platforms [32].

In [33], two wind farms are connected to four O&G platforms and linked to the onshore power system through a HVDC line, as shown in Figure 2.13. It is shown that OWF can improve the frequency and voltage stability during sudden faults in the power supply in 2013. [33] focuses on the fault analysis in electrical power supply of OWF connected to nearby grid-connected O&G platforms without GTG. However, power transmission subsea cables between onshore to O&G platforms will become too expensive as O&G platforms are usually of great distance away from shore. Simulation test has concluded that the topology of OWF with mul-

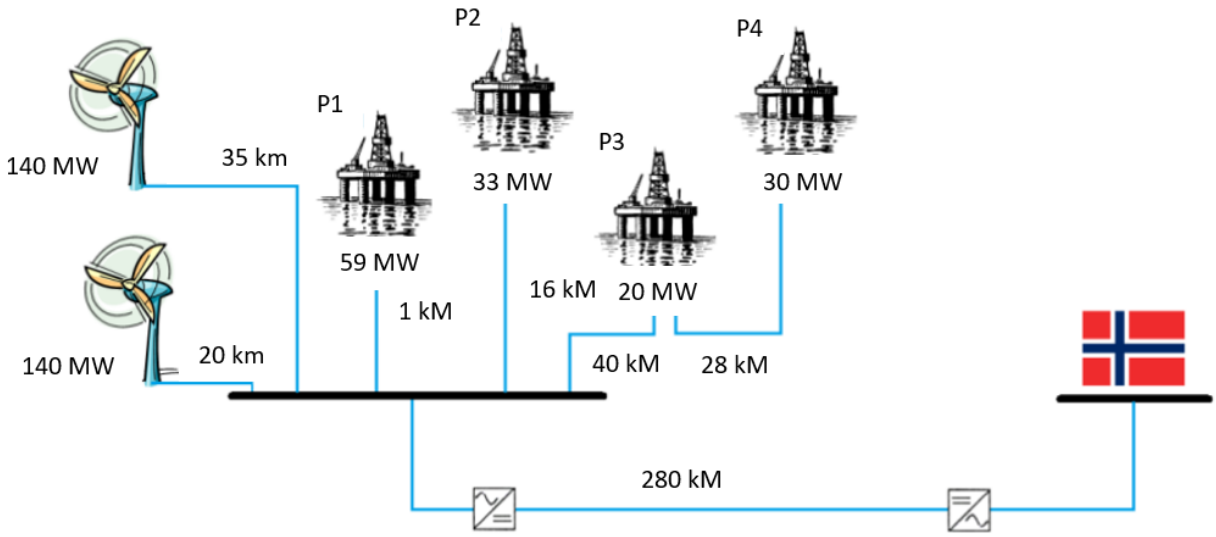

Figure 2.13: Model overview of OWF connected to nearby grid-connected O&G platforms without GTG [33].

tiple grid-connected O&G platforms can provide the greatest reduction in power transmission loss. Moreover, investigation in the simulation has showed that WTG connected to the system is able to recover back faster to normal operation due to short circuit on the main offshore AC bus. Another investigation in this paper has shown reactive power can be reduced in O&G platforms if shunt capacitors are introduced on each platform. In addition, shunt capacities can reduce the size of converter and transformer in offshore systems. Future work has mentioned that the placement of DC-chopper in WT can improve transient stability.

In [34], the integration between OWF and grid connected O&G platforms are shown in a multi-terminal VSC-HVDC configuration. This system configuration as shown in Figure 2.14 is able to secure power back to operation in the event of loss of power supply regulating terminal without the need of communication between terminals. A simulation model is presented and developed in 2008 [34]. Test scenarios have focused on the step changes in power demand, which includes on connected passive load from O&G platforms, onshore grid set to draw 40 *MW* power and sudden loss of all wind power. The result has showed on graph that these scenarios caused minor oscillations on DC voltage and these oscillations are effectively attenuated quickly. The VSC-HVDC system can be used for immediate response automatically to dynamic operation, such as a sudden power loss by no wind profile. This maintains the demand of DC power flow on the grid.

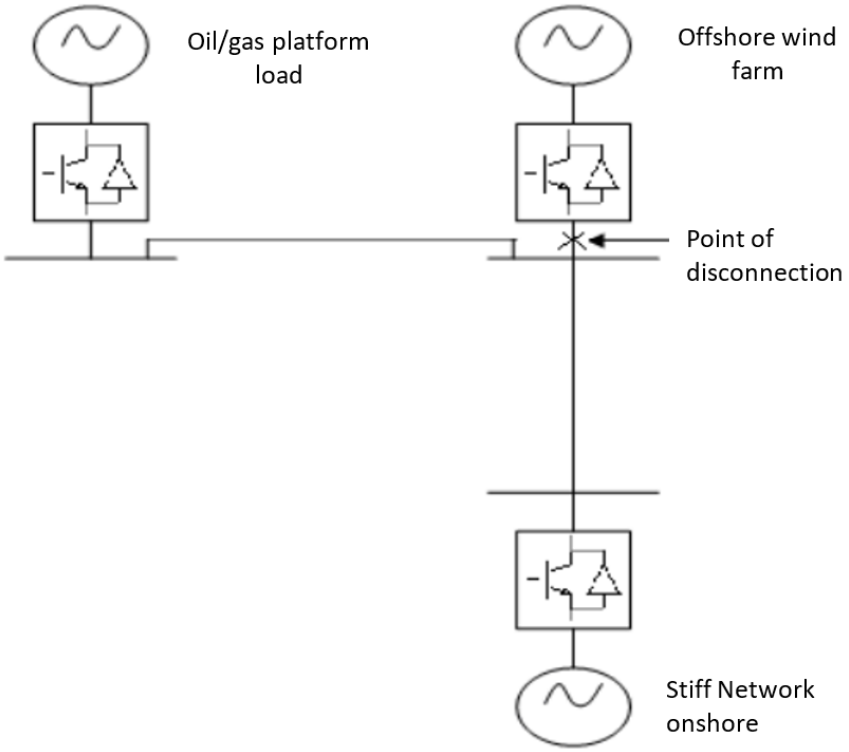

Figure 2.14: Proposed interconnection of O&G platform, OWF and onshore grid [34].

2.6.2 Micro-grid Offshore O&G Platforms with Secondary Power Generation of Offshore WTG and/or BESS

In the second category, the micro-grid configuration for offshore O&G platforms with offshore WTG and/or BESS is covered in [8], [3], [1] and [11]. These works provide different power distribution approaches to supply output power from WTG to non-critical loads, which reduces the power drawn from the GTG. This improves power stability in the system and greater improvement in transient stability can be obtained. In the current state of the art found in [11], an EMS is incorporated with the BESS

As presented in [8], typical O&G platforms are equipped with ULQ platform, a CPF platform and a WHP platform. These platforms are powered by three sets of SCGTs, which are used as EGs and rated to meet the load demand of the platforms. In the typical O&G platforms, two EGs will always be running and one EG is on standby mode, as shown in Figure 2.15. It has been investigated that the integration of OWF with O&G platforms is able to balance the number of start and stops of gas turbine onboard so as to reduce energy losses and increase fuel savings. In this configuration, two GTs will be supplying electrical power to O&G platforms and there will be lower efficiency as each GT provides only half of the load. Thus, the model in the simulation integrated four sets of 5 MW WT with two sets of 23 MW GTs to electrify the load and the second GT will mostly be turned off for fuel saving. With 20 MW of WT installed,

the default operating strategy results in the gas turbines operating at many hours at low loading, resulting in increased mechanical wear and low efficiency. By allowing start/stops of GT, this avoids the low-loading of GT. The operating of such a GT strategy resulted in more than five hundred times of GT start/stops annually.

This is partially due to the intermittency of wind, which requires support from the GTs. The wind profile is simulated based on a one-year wind speed time-series at 20-minute resolution, which was measured from an offshore meteorological measurement station at a North Sea oil platform in 2012. As such, the second GT will have a shortened lifespan due to wear and tear from the start/stops. It is concluded that the future work can focus on the operational strategy to minimise the start and stop time of GTG when integrated with OWF to secure a technically stable and economic operation. This could optimise OPEX savings and reduce mechanical wear and tear.

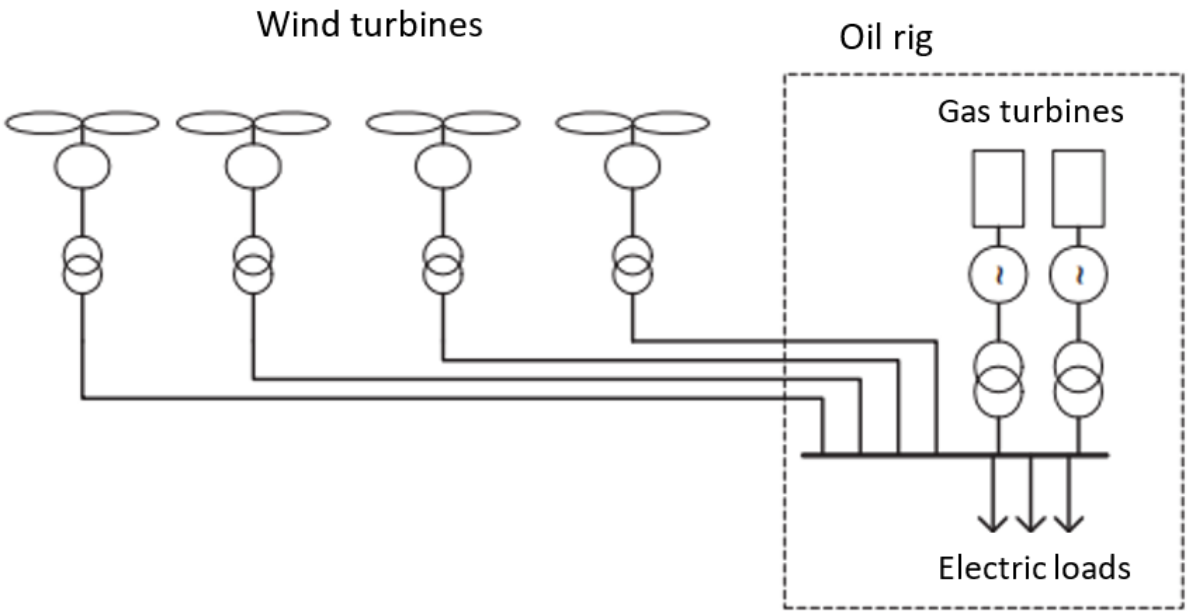

Figure 2.15: Simplified illustration of oil-rig electrical system with connection of offshore wind turbines [8].

In 2014, it was presented in [3] that the WTG control system can provide significantly faster voltage and frequency support than GTG when there is sudden change of power demand from load. The focus of this work was on OWF integrated with O&G platforms to improve the robustness and stability of the system, as shown in Figure 2.16. There are two scenarios that are considered in this work. The first scenario is to electrify O&G platforms with built-in GT in off-grid configuration via HVAC transmission. The second scenario is to supply power to maintain power flow in HVDC transmission to the O&G platforms with built-in gas compressor to drive

synchronise generator and connected to onshore grid for surplus power transmission. These scenarios have been used to study the results during cut out and cut in wind power without tripping the power in the hybrid configuration above. The parameters used in the O&G platforms is of typical rating as the realistic model is classified as confidential.

Based on Fino-project shown in [35], offshore WTG has a higher energy capacity, which increases the electrical power supply to O&G platforms, as compared to onshore power. The simulation program power systems computer aided design (PSCAD) has tested that the WT controllers are able to sense the frequency drop and change the power output significantly faster than gas turbine. The result has revealed that there is cost saving in operation with an approximately 5% reduction in gas turbine efficiency. Moreover, there is higher cost saving, as compared with OWF connected to mainland power grid.

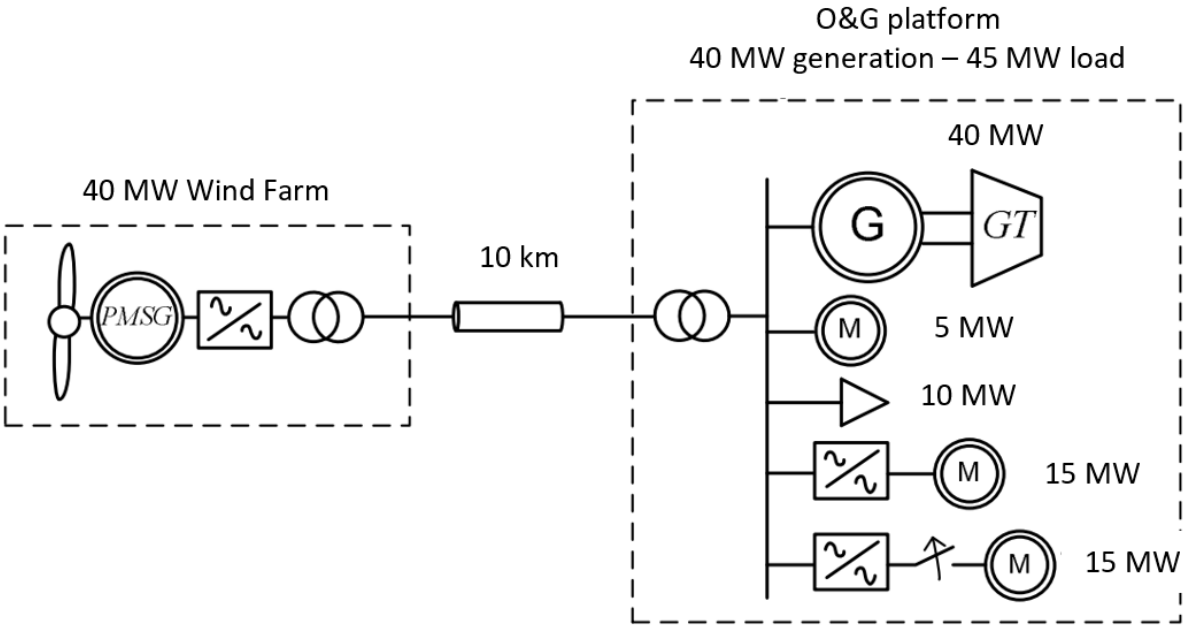

Figure 2.16: Overview of the case study used or frequency stability analysis [3].

In 2017, it was shown that the WTG can supply power to flexible load on O&G platforms to reduce wind power fluctuation and balance power generation and consumption. The flexible load represents a water injection system (WIS) which has a variable speed drive on motor control [1]. A SLM method was proposed to integrate OWF with Offshore O&G platforms by HVAC transmission in hybrid configuration for fixed and flexible load, as shown in 2.17. The integration of WTG will cause oscillations in the rotor of synchronous generator and that of other directly connected AC motors to increase. By applying SLM, there will be a reduction in disturbance to angular speed of the flexible load generator rotor, However, a time delay of 1 second in SLM, will cause a higher perturbation in the rotor angular speed signal. Thus, further research on SLM is required.

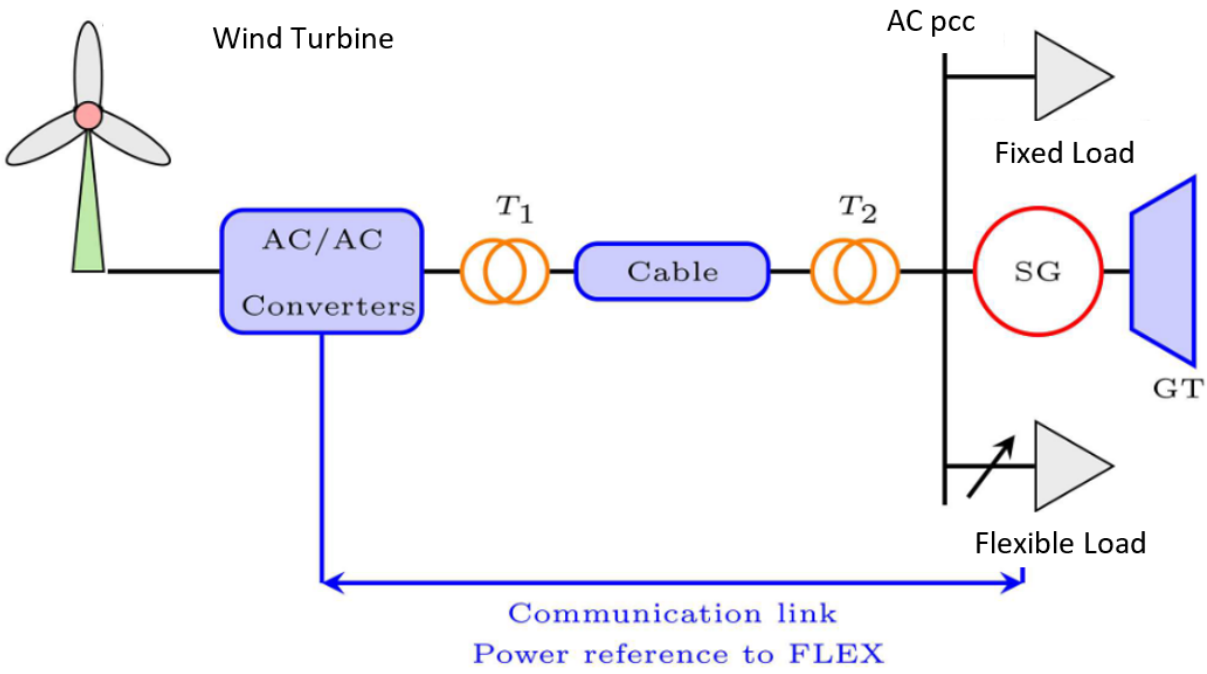

Figure 2.17: O&G platform with WTG and WIS [1].

In 2019, the current state of the art to incorporate EMS into the integration of offshore O&G platforms with combined offshore WTG and BESS was presented in [11]. The system configuration is shown in Figure 2.18. As shown in this figure, a stochastic wind speed was considered and a EMS was used to supply power to flexible loads. In the event of a shortage of power from WTG, the EMS injects power from the BESS to the meet the load requirements. Likewise, a sudden surge in load demand, which is one of the disturbances that the system is facing in a standalone micro grid, will need the EMS to provide regulation through the injection of power from the BESS. This EMS has been tested in simulation in terms of transient stability improvement. However, the reported EMS includes a low-pass filter, which reduces the the rate of response from BESS. This will be addressed in our proposed EMS later in Chapter 6. In addition, it is not known if the excess output power in power grid can be charged into BESS, which will be demonstrated in Chapter 6.

All of the above articles presented in this section aim to reduce carbon emissions from the usage of traditional power generation from open-cycled gas turbines. However, there is inevitable technical challenges in transient stability due to the fluctuation in voltage and frequency deviation from the WTG that was proposed to achieve the goal to reduce carbon emissions. As such, this will be addressed in the subsequent chapters in this thesis.

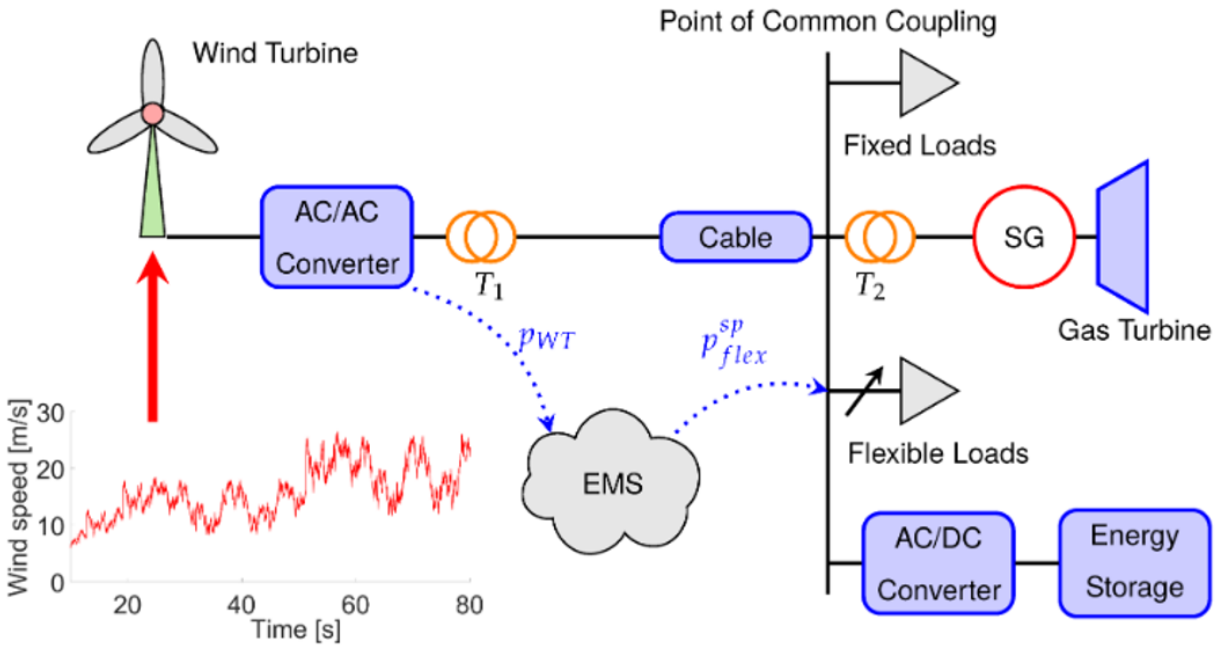

Figure 2.18: Integration of offshore O&G platforms with combined offshore WTG and EMS embedded in BESS [11].

2.6.3 Integration of O&G Platforms with Offshore WTG based on an Economic Analysis

In the third category, a review on the economic analysis of the integration of O&G platforms with offshore WTG is presented. Although all of the studies conducted on the integration of offshore wind with O&G platforms in Sections 2.6.1 and 2.6.2 provide the technological feasibility of such a concept. It is vital to consider the the estimated costing in term of Capex with Opex, to build a successful business model. This has yet to be fully addressed in the current literature.

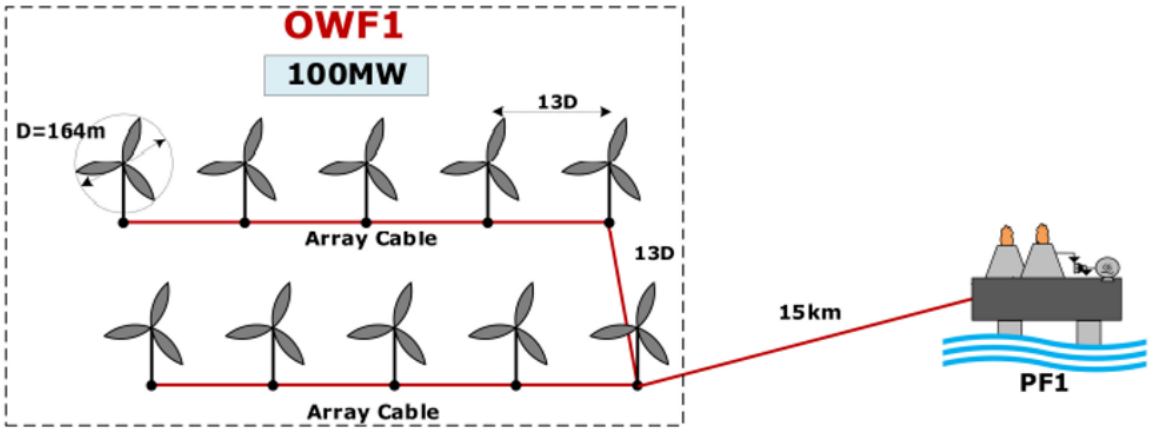

Figure 2.19: OWF integrates with offshore O&G installation [36].

In 2021, a rigorous research study on the technical and economic aspects of transient stability is presented in [36]. The economic aspect is vital in this project to develop a feasible business model The system architecture considered in [36] is shown in Figure 2.19. An overview of cost estimation was provided to predict the capital infrastructure of the system. An offshore wind system architecture which mimicked Hywind Park was used to electrify offshore O&G installations. There is a balance of plant cost, which includes all the components to provide a comparison between the costs of an onshore and OWF. Given the cost of export cabling, the onshore wind farm results in a higher cost than OWF with fixed foundation installation technology. In addition, the wind capacity in OWF is higher than that of the onshore wind farm. Moreover, OWF is a more green and sustainable power source than onshore wind farm to integrate with offshore O&G installation. This provides the motivation to consider the CAPEX and OPEX of our proposed system in this thesis.

2.7 Summary

This chapter reviews the necessary background and the different configurations for the electrification of offshore O&G platforms, which aim to achieve transient stability and carbon emission reduction. Section 2.1 provided an outline of a typical configuration of offshore O&G platform where two sets of GTGs will be in running mode while the third GTG will be in standby mode to meet the different power rating of the equipment in the load. This has provided the necessary background information to develop the research problem. Likewise, the simulation models considered in this thesis are based on the system performance calculations covered in Sections 2.2 and 2.3.1. It is taken into consideration that GTG requires more fuel and air to increase higher temperature for power generation whereas WTG is dependant on the wind profile, which might result in the WTG running below rated power at cut-in or cut-out wind speeds. In addition, for WTG based on the PMSG where the synchronous generator with DC-link is not directly connected to power grid, the WTG will not be able to assist in mitigating transient voltage and frequency deviation. To solve this problem, various energy storage technologies are considered to provide rapid response to support the loads, in the event of dynamic load changes or perturbations from the loss of wind power. This is reviewed in Section 2.4 where the energy density and foot print of the BESS is computed so that the BESS can be installed onboard the O&G platform. This is followed by the BESS characteristics and its application in grid-connected systems. A review of the IEC standards 61892-1 is covered in Section 2.5. Lastly, the development of different configurations for the electrification of offshore O&G platforms are classified into three categories, which highlights the gap in the existing literature and the necessary considerations in this thesis.

Chapter 3

Power System Stability Analysis

3.1 Introduction

Throughout the 20th century and today, the number of renewable energy installations have multiplied due to awareness for the environment, increase in fossil fuels' energy price and growth in energy consumption for industrial, transportation and residential purposes. This has led to a worldwide effort from the International Maritime Organisation (IMO) to reduce annual greenhouse gas (GHG) emissions from the shipping industry by at least 50% by 2050 [37]. In the marine and offshore industry, the Norwegian Ministry of Climate and Environment introduced the Norwegian CO2-tax in 1991, in addition to the European union emissions trading system (EUETS) regulation, resulting in the O&G industry paying both CO2-tax and EUETS pricing for GHG emissions [38]. Norway has also committed to the European union (UN) Framework on Climate Change to reduce GHG emissions by at least 40% by the year 2030 [31]. This contributes to the push for carbon footprint reduction, which is discussed in Section 1.1 in Chapter 1.

In the context of the offshore O&G industry sector, traditional O&G platforms are mainly powered by onboard SCGTs. These SCGTs typically have efficiency levels ranging from 25% to 30% with newer models not exceeding 40% [10], [39]. As such, they are less energy efficient, compared to the onshore combined-cycle gas turbine, which will produce 50% more energy with the same amount of fuel, as discussed in Section 2.2. In addition to producing more than double the amount of GHG emissions, the installation of SCGT also requires a significant amount of space and cost in building the loading-bearing infrastructure on the O&G platforms. Therefore, there has been increasing interest in exploring alternative renewable energy sources (RES) for electrification of O&G platforms [40].

O&G platforms are typically at least 100 to 200 *km* away from the coast [41] For distances above 100 *km*, the high voltage direct current (HVDC) transmission systems are currently most cost-efficient for transmitting energy from the onshore grid to the offshore O&G platforms, as

compared to high voltage alternating current (HVAC) transmission systems. Such examples include Troll [34], Valhall [32] and etc. However, with many O&G fields in shallow waters being depleted, O&G exploration companies are moving to greater depths to access more abundant O&G reservoirs in deeper waters, resulting in higher costs for HVDC power transmission [4]. In addition, other challenges include potential limitations on transmission capacity from onshore power substations, additional infrastructure cost in building an onshore power substation for remote locations, and etc [42].

In recent developments, offshore WTG have been considered as an alternative source of energy for electrification of O&G platforms [1]. Offshore wind installation in deep waters is considerably more expensive largely due to the costly installation of submarine cables to transmit generated energy to the onshore grid. As the cost of WTG power transmission contributes more than half of overall CAPEX cost, there is high cost savings in the power distribution of an integrated WTG to O&G platforms, thereby removing the need for a costly power transmission line to the onshore grid [3]. Based on the latest case studies of integrating offshore wind with O&G platforms, it has been shown to be techno-economical to power O&G platforms using offshore wind energy in deep waters [31]. O&G platforms in Beatrice oil field has been supplied electricity by two 5 MW wind turbine which are installed adjacent in offshore [7]. In order to address the intermittency of wind, on-board SCGTs are required to be on "stand-by" mode, which can be started up almost instantaneously, in the event of a sudden drop in wind speed. The fuel efficiency of SCGTs reduces drastically under low loads and SCGTs in "stand-by" mode consumes at about 20% of the amount of fuel required in "full power" mode, which contributes towards increased GHG emissions [8].

In this chapter, an integrated system consisting of an offshore floating wind farm consisted of two WTG and O&G production platforms with a BESS is proposed. With a BESS, the third SCGT will no longer be required onboard on "standby" mode, resulting in reduced GHG emissions while maintaining the overall output power quality. The main technical challenge is to improve output power quality in the system which is the key focus in this chapter. An important first step is to carry out power stability analysis in a conventional system that will influence transient stability and determine output power inject into load consumption. In order to overcome offshore wind power intermittency, which may result in insufficient output power to load, an energy storage system is introduced to integrate with conventional system for power system stability that will effectively improve transient stability. The integration of offshore wind with O&G platform and an energy storage system is referred as our proposed system in the subsequent chapters. Although there have been a handful of energy storage technologies available for use in the industry, BESS has a fast transient response to smoothing control which is considered in this project and given its comparable size to replace a GTG on board, which is discussed in

Section 2.4 in Chapter 2.

This chapter will present the load flow analysis and power system stability results that will lay the foundation for the transient stability studies on the proposed configuration which will be demonstrated in next Chapter 4. The outline of this chapter is as follows. Section 3.2 presents the detailed configuration for the proposed system. Four different test scenarios are presented in Section 3.3. Simulation results of the conventional system and proposed system for the four test cases, will be shown in Section 3.4. A summary is provided in Section 3.5.

3.2 Proposed System Configuration

As described in this section, the proposed system can be situated near the coast of Scotland with two wind turbines at the location of Hywind park and one conventional three bridge linked O&G platforms in the North Sea. The O&G platforms will be 55 *km* away from the coast of Peterhead and 40 *km* from Hywind Park. The proposed system overview illustrated integration of WTG in Hywind Park and nearby offshore O&G platform in North Sea is as shown in Figure 3.1.

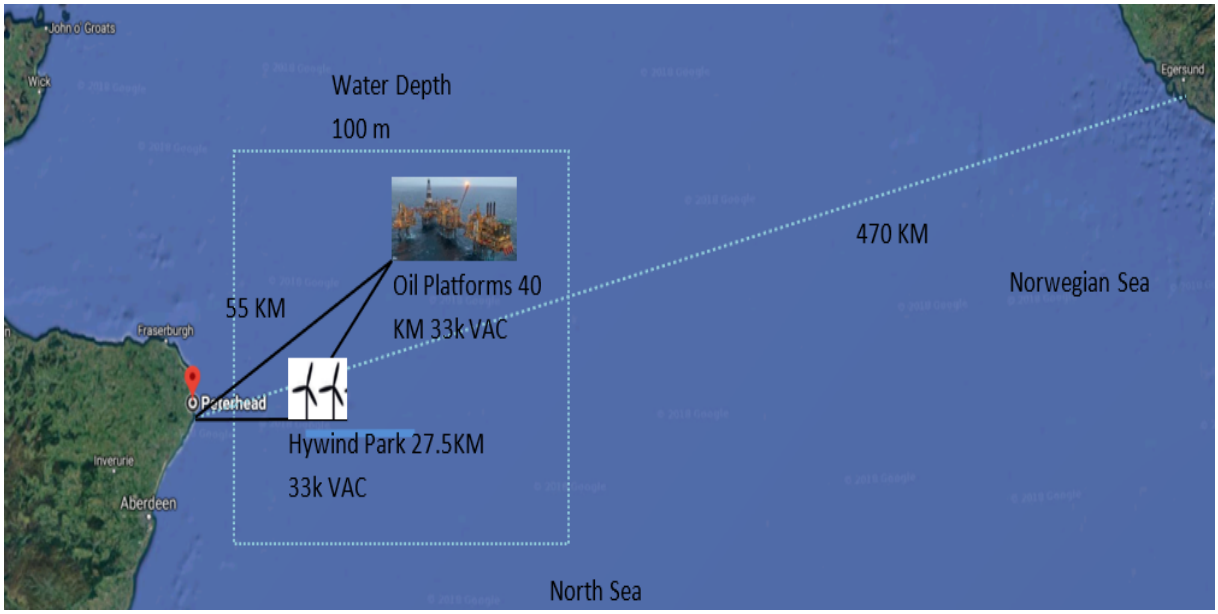

Figure 3.1: System overview of Hywind Park and Buzzard North Sea in North Sea.

The detailed configuration of the proposed system is presented as follows. The offshore O&G platform has the peak load consumption of 11 *MW* that is of realistic sizing in load demand as smallest power consumption of 5.5 *MW* in O&G platform presented in [43]. As discussed in [44], a typical O&G platforms of 10 *MW* power is needed for small fields. The typical system is assumed to have two SCGTs running onboard, which are the EG and emergency essential generator (E.EG), and these are integrated with offshore WTG. In our proposed system, two separate BESS are used in this simulation study, namely BESS 1 (3 *MW*) used in Case 1 and an

additional BESS 2 (1 *MW*) used in Case 2 and 3 in Section 3.4. In the rest of this section, the sizing of the GTG on the O&G platforms, WTG and BESS will be discussed in more detail.

3.2.1 O&G Platforms

Typical O&G platforms are equipped with three platforms consist of a utility and living quarter platform, a processing and heating platform and a wellhead platform. These platforms are powered by three sets of SCGTs, which are used as EGs and rated to meet the load demand of the platforms. In the typical O&G platforms, two EGs will always be running and one EG is on standby mode. The EGs burn extracted natural gas from the field under normal operating conditions, which powers the three platforms via three main switchboards that are rated at 11 *kV*. The output voltage is stepped down via integral transformers in distribution panels to 3,3 *kV* and 400 *V*, to power the water injection pumps, gas compressors, drilling unit, utility loads and etc [45].

In this chapter, the O&G platforms are equipped with 2 x SCGTs (13 *MW*), where one SCGT acts as an EG and the other serves as an E.EG. There is usually a third SCGT and is usually on "standby" mode. This SCGT has been removed, which allows integration of the 4 *MW* BESS onboard O&G platform where 2 *MW* of BESS is stack on top of the other 2 *MW* of BESS, as discussed in Section 2.4.

3.2.2 WTG

Approximately 25 *km* off the coast at Peterhead, north east of Scotland, Statoil Wind Limited (SWL) has been awarded an Exclusivity Agreement by The Crown Estate (TCE) for the deployment of floating WTG Units in an area known as the Buchan Deep which is an area of deep water (95 to 120 *m*), as shown in Figure 3.1. SWL is planning to deploy a small pilot wind farm (Pilot Park) comprising of five Hywind Scotland WTG Units with a total maximum capacity of up to 30 *MW*. The project has a technical design lifetime of 20 years.

The Hywind units are floating structures consisting of standard wind turbine on a spar buoy type substructure. Each WTG Unit have a hub (centre) height of 101 *m* above Mean Sea Level (MSL), with a draft of between 78 *m* and a rotor diameter of 154 *m*. The substructure is made of steel and will be partly filled with ballast water and solid ballast. The WTG Units will be attached to the seabed by a three-point mooring spread. There will be a maximum of five inter-array cables each of which will have a maximum length of 3 *km*. The inter-array cables will have a transfer voltage of 33 *kV*. Electricity will be transmitted as HVAC. The cables, which will be armoured, will be approximately 0.5 *m* in diameter [46].

In this chapter, two floating WTG units with a total power generation capacity of 12 *MW* will be considered in the simulation study. The proposed system consists of two sets of 6 *MW* Siemens (Model: SWT-6.0-154) PMSG floating WTGs connected in parallel, which mirrors the Hywind Park configuration in the North Sea [47]. Each WTG consists of a synchronous generator, DC-link capacitor and B2B converter interfaces. The PMSG operates with variable wind speed and produces a variable AC voltage with variable frequency. The AC frequency voltage is first rectified by AC/DC rectifier. Thereafter, the generator output power is converted from DC link with AC/DC inverter to supply variable frequency and voltage rated at 690 *V*. Finally, a step-up transformer will supply rated voltage of 33 *kV* through a 40 *km* HVAC power transmission cable, which is stepped down to 11 *kV* output on the power bus of the O&G platforms.

3.2.3 BESS

There are several types of batteries commonly used in renewable energy systems, e.g. lead acid, lithium, nickel cadmium and etc. In this system, a BESS utilizing Li-ion batteries is proposed, primarily due to its high energy density and declining cost [48]. Although BESS with a small capacity of 600 *V* offers bidirectional power flow and can be used for power system stability strategy in the event of voltage drop on the grid-connected WTG in [49], the feasibility study on larger capacity with more than 1 *MW* BESS integrates with WTG in standalone microgrid for power stability has yet to be fully investigated. This technical challenge will be demonstrated in this chapter. The 4 *MW* BESS is installed onboard the platforms and connected to the 11 *kV* main switchboard on offshore O&G platforms.

Considering the sizing of the GTG, WTG and BESS in Sections 3.2.1, 3.2.2 and 3.2.3, the test model in a microgrid configuration is developed in MATLAB/Simulink, as shown in Figure 3.3. This model is simulated for four different test scenarios, corresponding to faults in the primary power generation from the EG and secondary power generation from the WTG.

3.2.4 BESS Model in Simulation

In our MATLAB Simulink model for the BESS, there are electrical equipment that comprise of 2 *MW* of Lithium-ion batteries pack with 2 *MW* of bi-directional converter which is connected to 2 *kVA* transformer for discharging/charging electrical power in the micro grid as shown in Figure 3.2. BESS is designed in 40-foot container with built in heating, ventilation, and air Conditioning (HVAC) similarly to industrial manufacturer [50]. While this figure depicted the schematic diagram which represents electrical equipment in the simulation model, the electronic devices of BESS's controllers that control the depth of discharge/charge to keep batteries pack in healthy state and improve its lifespan is being modeled for simulation. The detail equivalent

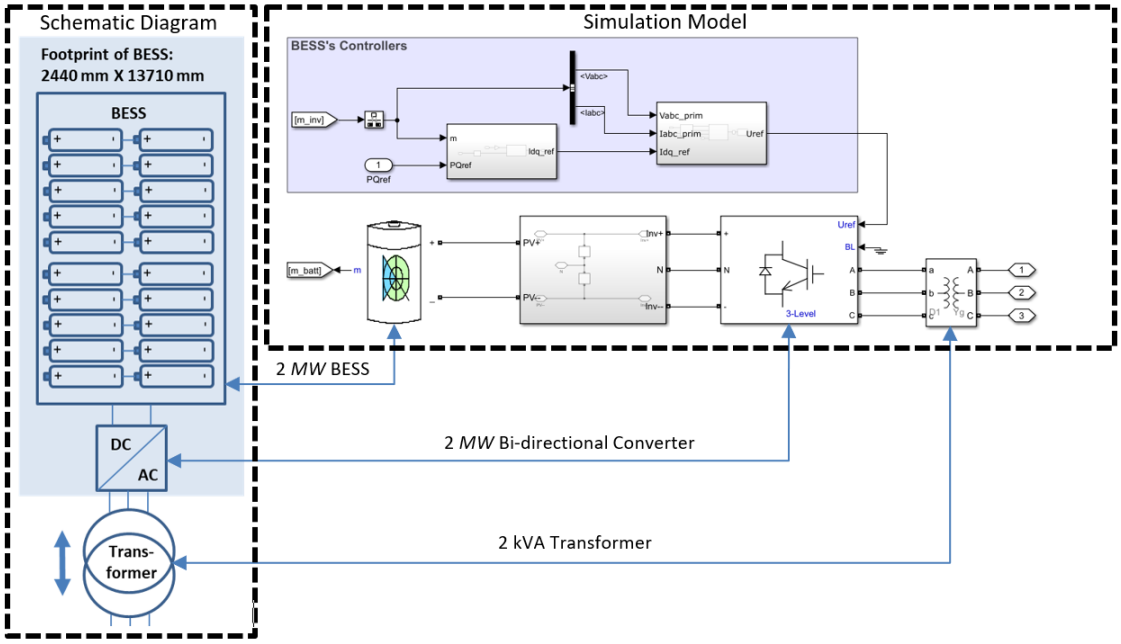

Figure 3.2: Schematic diagram of BESS modeled in simulation.

model of controllers' components are describe in detail on Chapter 6.

3.3 Test Scenarios

In this section, four test scenarios are simulated in the MATLAB/ Simulink with SimScape/ SimPowerElectronics and results are presented in Section 3.4. The four test scenarios corresponding to faults in the primary power generation from the EG and secondary power generation from the WTG. are described in Table 3.1. Throughout the four test scenarios, a constant rated wind speed of 12 m/s is assumed. The simulation study is based on the ability of the power system, to maintain electrical power to load when subjected to transient fault such as the loss of a large energy generation source.

Table 3.1: Four scenarios test for conventional and proposed system

Scenario	Event
1	No wind
2	EG and E.EG are tripped and WTG is turned on
3	E.EG and WTG are tripped and EG is turned on
4	EG and WTG are tripped and E.EG is turned on

For these four test scenarios, the simulation results for the both conventional and proposed systems are presented in Section 3.4. For a fair comparison, the conventional system is assumed to have two SCGTs running onboard, which are the EG and E.EG.

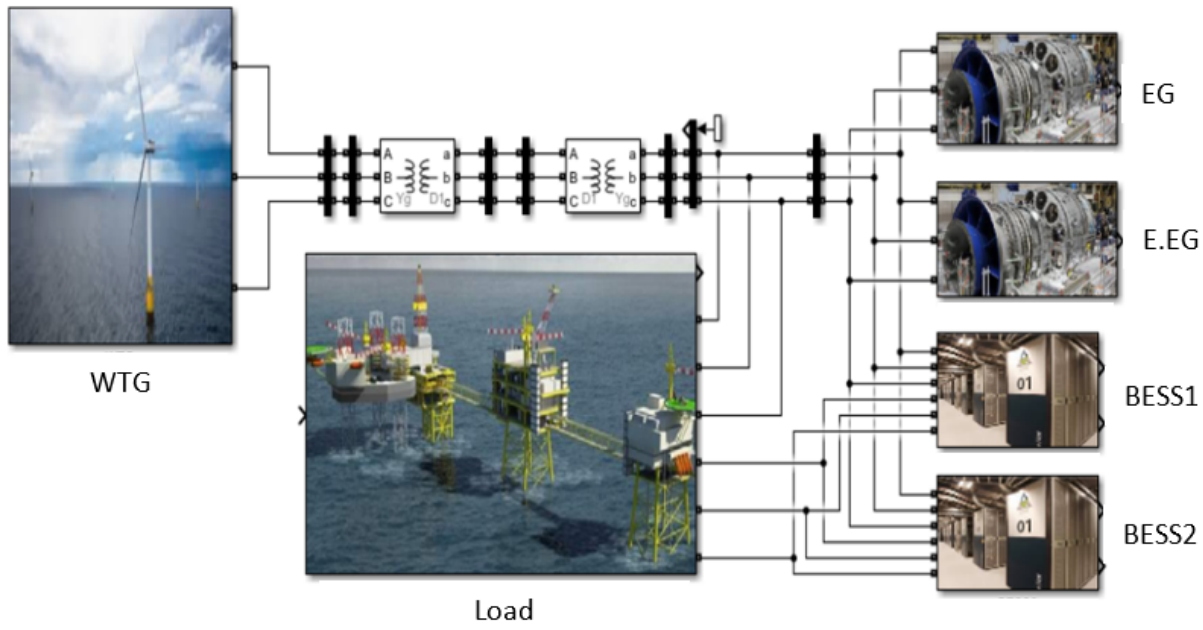

Figure 3.3: Test model in MATLAB/Simulink

3.4 System Simulation Results

3.4.1 Case 1: Essential Generator (EG) is tripped and WTG is turned on

In this case study, the conventional system is started in Scenario 1 where there is no wind and switched to Scenario 2 where the EG is tripped and E.EG is not in standby mode. It can be seen from Figure 3.4 that the EG is supplying electrical power to O&G platforms consistently at about 1 $p.u.$ in Scenario 1.At time, $t = 10.8s$, the EG is suddenly disconnected and tripped at 10.8 s, which corresponds to Scenario 2. At the same time, the WTG is turned on to supply electrical power to O&G platforms from 10.8 s onwards. It can be seen from Figure 3.4 that there is a high surge of output power to the load of 1.3 $p.u.$ between 10.8 s and 11.3 s, which settled down to 1.08 $p.u.$ after 0.5 s. In this case, it is shown that the output load power profile has a maximum transient deviation of 30 % and the maximum continuous deviation is +8 %.

Similarly, the proposed system is started in Scenario 1 and switched to Scenario 2, where the EG is suddenly disconnected and WTG is turned on. BESS 1 is also switched on between Scenario 1 and Scenario 2. In Scenario 1, the EG is supplying power to electrified O&G platform, as shown in Figure 3.5. It is observed that when the EG is tripped and WTG is turned on, the maximum transient deviation in load power is 14 %. This is a reduction of 16 %, as compared to the conventional system in Figure 3.4. In addition, the load power is maintained around 1.08 $p.u.$ after the transient period. It can be seen that the BESS has discharged between 10.8 s and 11.6 s to supply power to load. At time, $t = 11.6s$, the WTG supplies power to load.

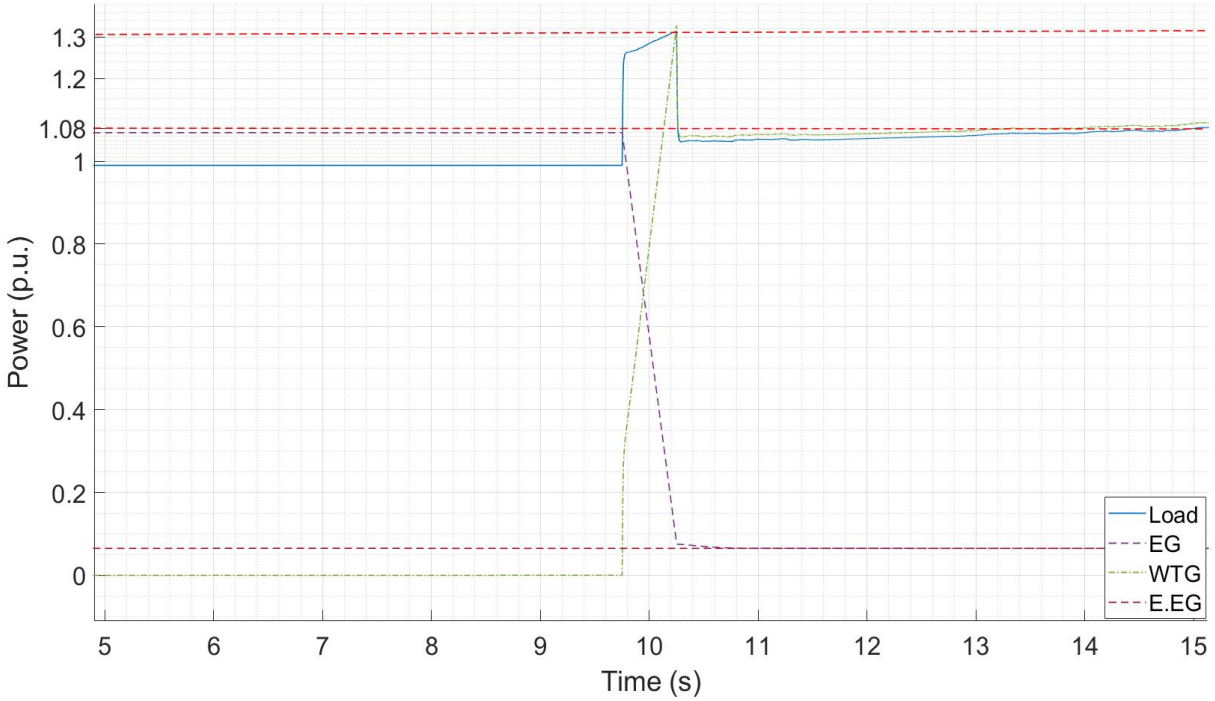

Figure 3.4: Conventional system of power flow in $p.u.$ when EG is disconnected and WTG is turned on (Pbase =11 MW).

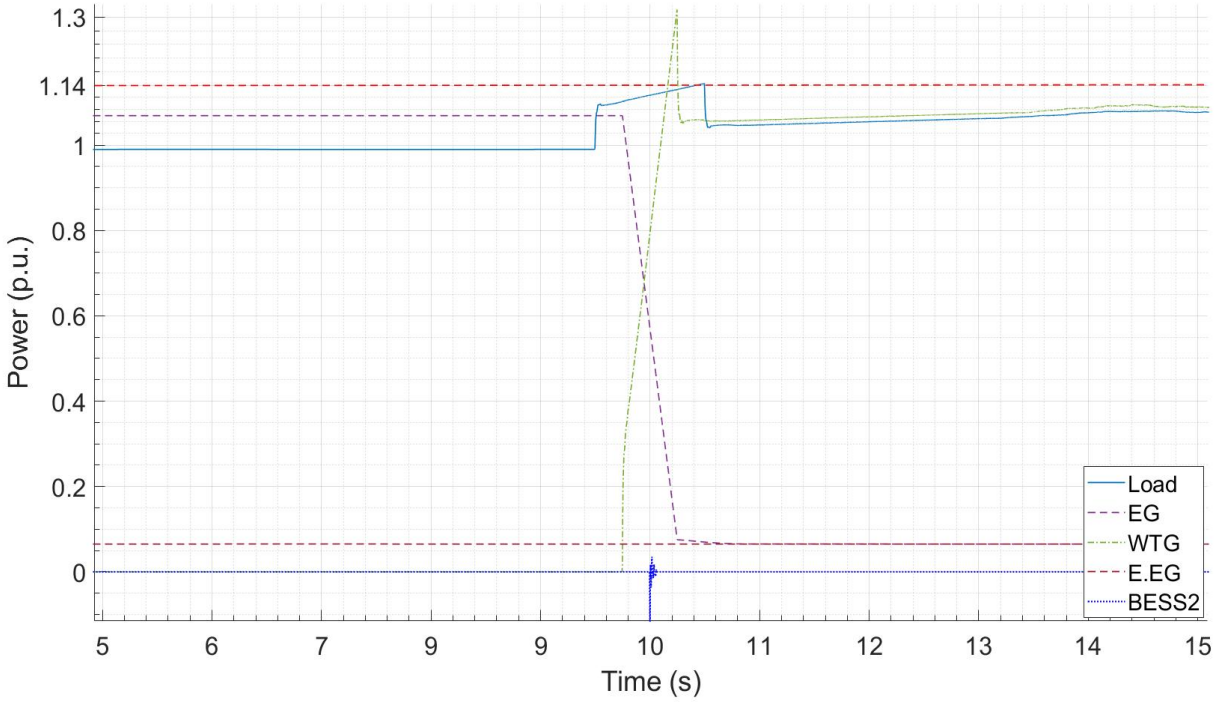

Figure 3.5: Proposed system of power flow in $p.u.$ when EG is disconnected and WTG is turned on (Pbase =11 MW.

3.4.2 Case 2: WTG is disconnected and EG is turned on

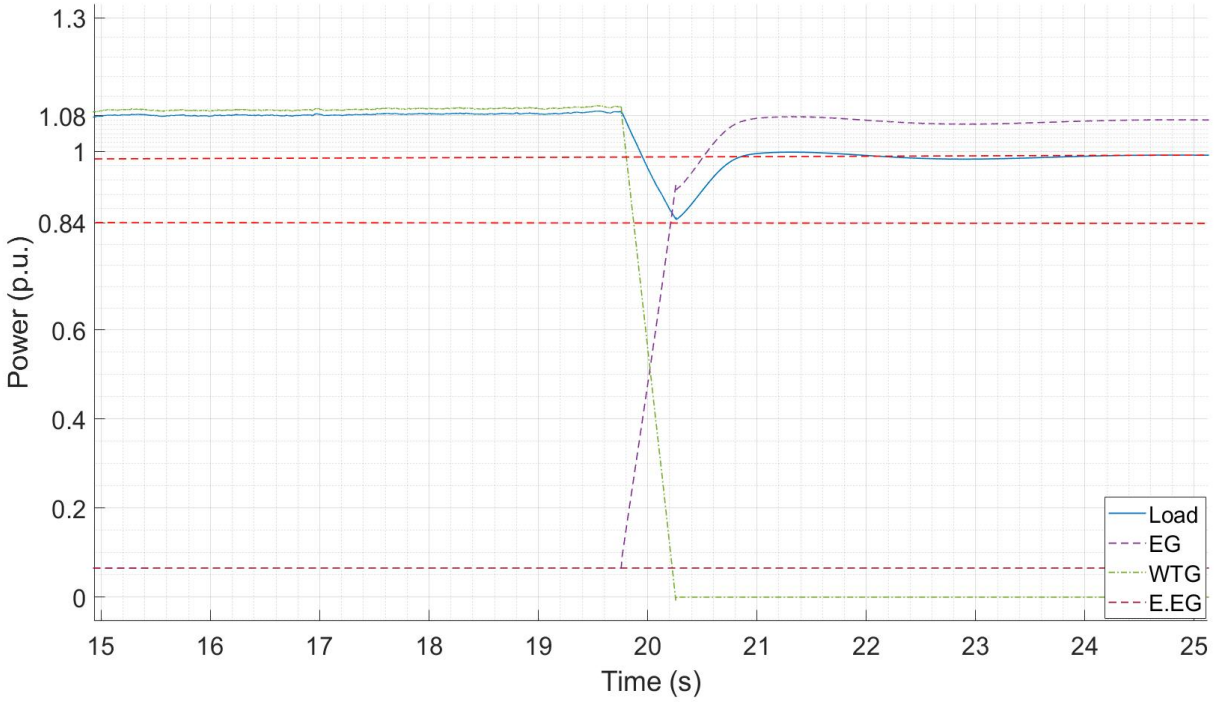

Figure 3.6: Conventional system ofpower flow in $p.u.$ when WTG is disconnected and EG is turned on (Pbase =11 MW).

In this case study, the conventional system is started in Scenario 2 and switched to Scenario 3, where the WTG is disconnected and the EG is turned on. In Scenario 2, the WTG has been supplying power to the electrified O&G platform consistently around 1 $p.u.$. There is a trip to WTG at 20.9 s and the EG is turned on at this point of time. As shown in Figure 3.6, there is a significant drop to 0.84 $p.u.$ to the load. Moreover, the transient recovery time is up to 1 s. In this case, it is shown that the output load power profile has a maximum continuous deviation of approximately -2 %. However, the maximum transient deviation of 16 % and a maximum transient recovery time of 1 s.

Likewise in the proposed system, Scenario 2 is switched to Scenario 3, where the WTG is disconnected and EG is turned on. BESS 2 is switched on between Scenarios 2 and 3. In Scenario 2, the WTG has been supplying power to the electrified O&G platform, which is around 1 $p.u.$. At 20.9 s, the WTG is tripped and EG is turned on, as shown in Figure 3.7. It is observed that the transient deviation in load power is approximately -10 %. This is significantly lower as compared to the conventional system, as shown in 3.6, where the transient deviation is -16 %.

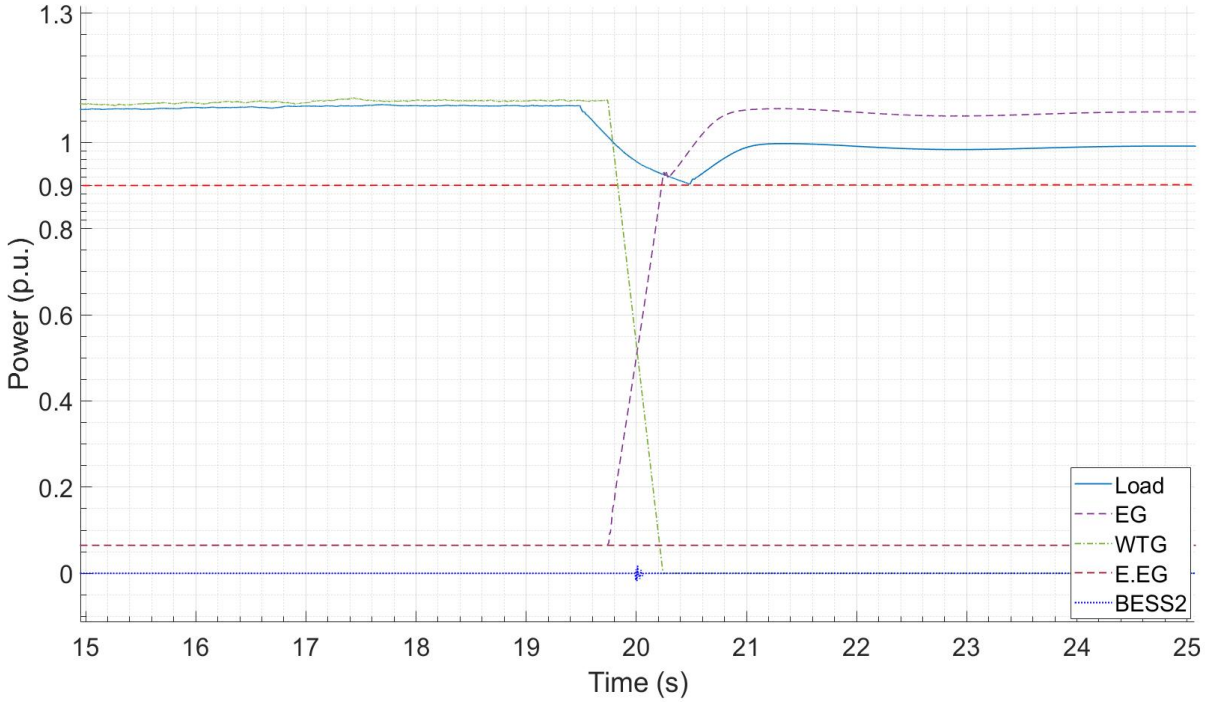

Figure 3.7: Proposed system of power flow in $p.u.$ when WTG is disconnected and EG is turned on (Pbase =11 MW).

3.4.3 Case 3: EG is disconnected and Emergency Essential Generator (E.EG) is turned on

In this case, the power system stability of the load power is studied when the EG fails and the E.EG is turned on. In Scenario 3, the EG has been supplying electrical power to load on O&G platforms continuously. In this simulation case, the EG is disconnected at 30.8 s. The E.EG is then turned on to supply electrical power at rated level. It can be seen for the conventional system in Figure 3.8 that there is similarly a significant drop to 0.81 $p.u.$ to the load. Similar to Case 2, it is shown that the maximum transient deviation of 16 % and a maximum transient recovery time of 1 s are observed in Figure 3.9. This is expected as the EG and E.EG are modelled with the same specification. In both Scenarios 3 and 4, the EG and E.EG are supplying power to the same load, which explains the same transient response observed in Cases 2 and 3.

In proposed system, Scenario 3 is switched to Scenario 4, where the EG is disconnected and E.EG is turned on. BESS 2 is switched on between Scenarios 3 and 4. At 30.8 s, the EG is tripped and E.EG is turned on, as shown in Figure3.9. It is observed that the transient deviation in load power is approximately -10 %, similar to Case 2. This is significantly lower compared to the conventional system where the transient deviation is -16 %.

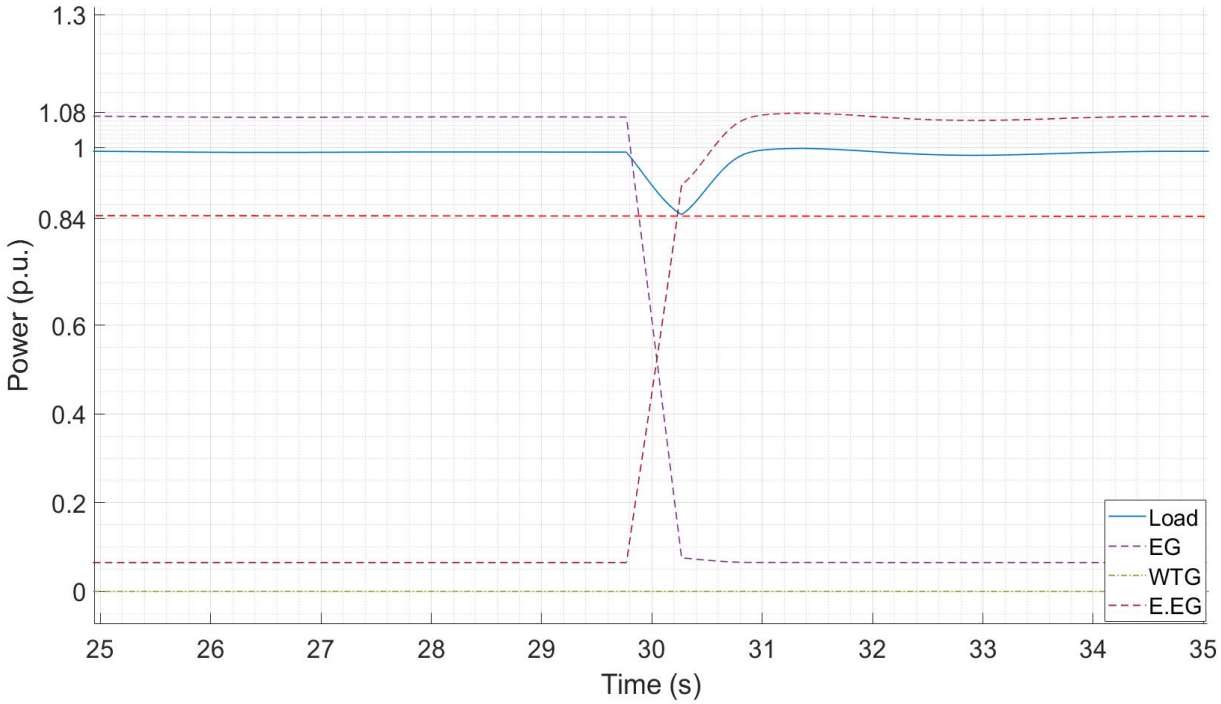

Figure 3.8: Conventional system of power flow in $p.u.$ when EG is disconnected and E.EG is turned on (Pbase =11 MW).

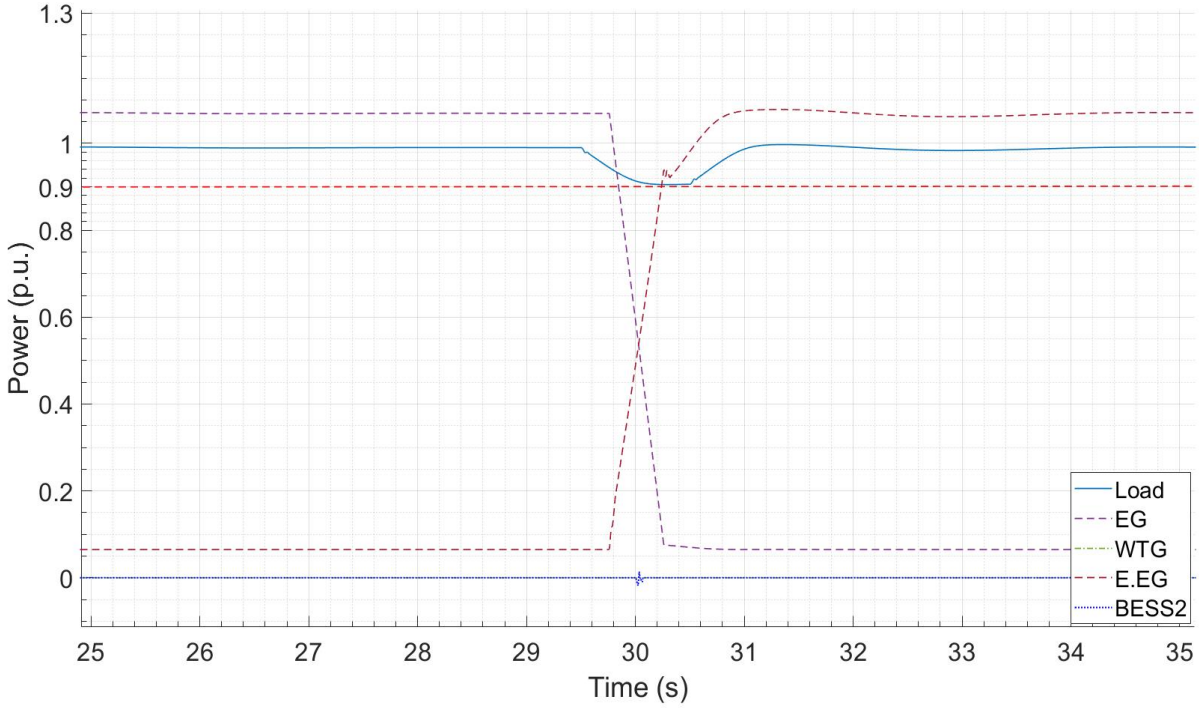

Figure 3.9: Proposed system of power flow in $p.u.$ when EG is disconnected and E.EG is turned on (Pbase =11 MW).

3.5 Summary

Offshore O&G exploration companies are moving to greater depths to access more abundant O&G reservoirs in deeper waters, resulting in higher costs for HVDC power transmission. As such, an integrated system is proposed and sized, which comprises of two offshore WTG and O&G production platforms with a BESS in this chapter.

The proposed system is modelled in MATLAB/Simulink and simulated with SimScape and SimPowerElectronics for four test scenarios, corresponding to faults in the primary power generation from the EG and the secondary power generation from the WTG. The simulation results have shown that the proposed system configuration provides improved results, as compared to the conventional system. It is also shown that the output power to load is maintained and the proposed system is feasible for the integration of offshore WTG with nearby offshore O&G platforms and on-board BESS.

As compared to the conventional system, the proposed system reduces the transient deviation in load power from -16 % to -10 % during a switch from the EG to the E.EG. When the energy generation is switched from the EG back to the WTG, the transient deviation in load power is reduced by 16 %. In the load flow analysis, both the conventional and proposed system has shown to be capable of maintaining output power to load close to 1 $p.u.$ after the transient period.

Our simulation results have proven that the proposed system with 4 MW of BESS capacity has significantly improved the transient stability of the output power, in the presence of faults in the WTG. However, it is not feasible to increase the BESS capacity on-board the offshore O&G platform, due to the space constraint and weight limitation. To the best of our understanding, no research has been carried out to size on-board BESS for transient stability enhancement, which will be addressed in the subsequent chapters.

Chapter 4

Transient Stability for Variations in BESS Sizing

4.1 Introduction

In Chapter 2, integration of offshore wind with O&G platforms is discussed for decarbonisation in offshore industry. Till today, this concept is still being researched on to establish a feasible business model. To the best of our knowledge, the integration of offshore floating WTG with offshore O&G platforms in the standalone microgrid configuration is a business model, currently in development in the North Sea. Since typical O&G platforms have limited space onboard, which is mainly taken up by the SCGT, necessary consideration has to be made to ensure that proposed technology can be installed, while reducing carbon emission and meeting IEC standards. Existing literature has shown that the carbon footprint can be reduced on offshore O&G platforms by integrating with offshore WTG in Section 2.6. The feasibility of combined offshore wind with O&G platforms and BESS in a microgrid configuration has been studied in Chapter 3.4, which is demonstrated through load flow analysis and its power system stability. With a BESS, the third SCGT will no longer be required onboard on "standby" mode, resulting in reduced GHG emissions while maintaining the overall output power quality. It has also been demonstrated that transient stability issues in the conventional system without BESS can be potentially be mitigated by the proposed system with 4 MW BESS, as shown in Chapter 3.

In this chapter, an investigation on transient voltage and frequency deviation on both conventional and proposed system will be carried out to compare with the IEC standards, which are discussed in Chapter 2.5. A commercial software application, ETAP, will be used to generate transient stability results that will be compared with the IEC standards for both conventional and proposed systems. The simulation will consist of a lower capacity of BESS and WTG, in order to understand if transient stability requirements in the IEC standards can be met with a lower WTG capacity and variations in BESS sizing. Two systems are proposed: System 1 will

consist of a 1 *MW* BESS and System 2 will consist of 2 *MW* BESS. It has also been reviewed in Section 2.6 that cost analysis is vital for the development of the business case for the proposed system. It is expected that there will be an increase in CAPEX and OPEX, which will rise due to additional secondary power generation from WTG and support from BESS. However, there will also be an offset in costs from the removal of the third SCGT. As such, the CAPEX and OPEX comparison among BESS, GTG and WTG will be carried out to lay the necessary foundation for techno-economic analysis in this chapter.

The outline of this chapter is as follows. Section 4.2 presents the detailed configuration for the proposed systems. Four different test scenarios are described in Section 4.3 to study the ability of the power system to maintain electrical power to loas when subjected to transient faults in the energy generation sources. The simulation results are presented in Section 4.4 with a summary of results in Section 4.5. Section 4.6 analyses the economic analysis. This chapter is summarised in Section 4.7.

4.2 Proposed System Configuration

The proposed system configuration is as shown in Figure 4.1. In this section, detailed system configuration for the proposed system is presented as follows.

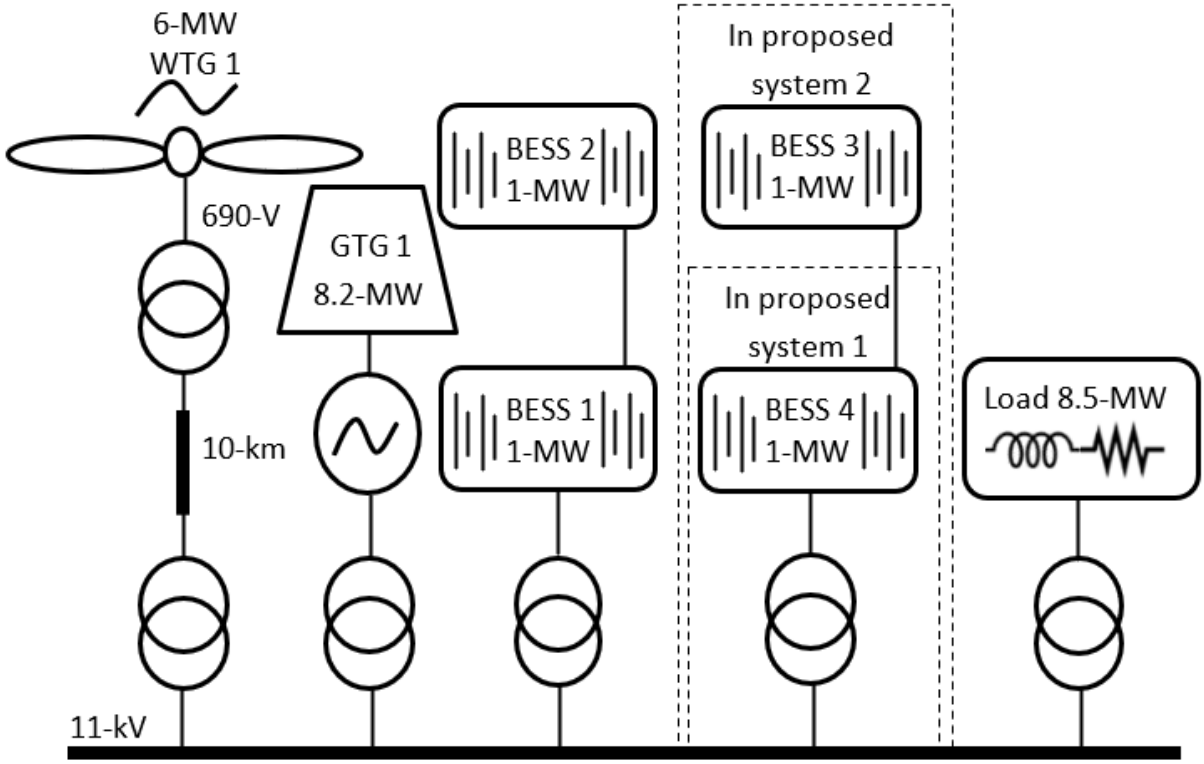

Figure 4.1: Proposed offshore integrated system.

4.2.1 O&G platforms

It has been reviewed in Section 2.6 that the actual load consumption on the O&G platforms varies between fixed and flexible loads [1]. For fixed load demand, the power rating is the minimum required to operate air compressors, motors with pumps to extract O&G out from the reservoir. On the other hand, flexible load demand requires additional water pumps to operate and inject into the reservoir to increase higher amount of extraction in O&G out. Likewise, the actual load demand in offshore O&G platform consists of fixed load and flexible load.

In the conventional system, the O&G platforms are equipped with 2 x SCGTs (13 MW), where one SCGT acts as primary energy generation while the other serves as redundant energy generation to share the load equally. There is usually a third SCGT and is usually on "standby" mode. In the proposed system, the third SCGT is removed, which allows integration of the 2 MW BESS onboard the O&G platform. The conventional O&G platform will be based on a fixed load demand of 8.5 MW as referenced from [44].

4.2.2 WTG

Both the conventional and proposed system consists of one 6 MW Siemens (SWT-6.0-154) PMSG floating WTG which mirrors the Hywind Park configuration in the North Sea [47] as discussed in Chapter 3. The WTG is of type 4 which comprise of synchronous generator, a bi-directional AC-DC converter. The type 4 generator is decoupled from the grid by the bi-directional AC-DC converter through the DC-link. Finally, a step-up transformer will supply rated voltage of 11 kV through a 30 km HVAC power transmission cable to the power bus of the O&G platform. The power loss in transmission cable is not taken into the consideration in this project and it is assumed that the WTG will project a required power rating of 6 MW when it is turned on.

4.2.3 BESS

The development of BESS is in fast pace which attract the attention to prefer this technology as an energy storage system. As mentioned in Chapter 2 due to space constraint on O&G platform, BESS utilizing Li-ion batteries is proposed. Considerations on its energy density, footprint and declining cost [48] is described in Section 3.2.3. The BESS offers bidirectional power flow and can be used in the control strategy to provide smoothing control and dispatch for the O&G platforms installed with renewable systems [49]. The 2 MW BESS is installed onboard the platforms and connected to the 11 kV main switchboard on O&G platforms.

4.3 Test Scenarios

In this section, four test scenarios are simulated in ETAP and results are presented in Section 4.4. The four test scenarios corresponding to faults in the primary power generation from the GTG and secondary power generation from the WTG. are described in Table 4.1. Through the four test scenarios, a constant rated wind speed of 12 m/s is assumed. The simulation study is based on the ability of the power system, to maintain electrical power to load when subjected to transient fault such as the loss of a large energy generation source. Usually, the duration of the trip event to study transient stability is around 3 to 5 seconds [33].

Table 4.1: Four test scenarios

Scenario	Event
1	Continuous wind
2	WTG 1 is tripped and GTG 2 is turned on
3	No wind
4	GTG 2 is tripped and WTG 1 is turned on

For these four test scenarios, the simulation results for the conventional and proposed system 1 and 2 are presented in Section 4.4. The simulation results are compared against the IEC standards 61892-1 for maximum continuous deviation and maximum transient recovery time, as shown in Table 2.1 in Section 2.5. For a fair comparison, the conventional system is assumed to have two SCGTs running on board, which are the GTG 1 and GTG 2.

4.4 Simulation Results

In this section, the load flow analysis from the generation sources and loads, voltage deviations and frequency deviations in the four test scenarios from Section 4.3 will be presented. Numerical values on the criteria according to the IEC 61892-1 standards will be highlighted. The necessary checks if the IEC standards have been met will be performed in Section 4.8.

4.4.1 Case 1: Load Flow Analysis from Scenario 1 to 2

In this case study where WTG is tripped and GTG 2 is turned on, it can be seen from Figure 4.2 that Load in the conventional system has a significant surge of 1.28 $p.u.$, followed by drop of output power to the load of 1.12 $p.u.$ and the recovery time takes up to about 6 s. This is due to the ramp up from GTG 2 which is started up to share the load with GTG 1. In this case, a transient deviation of 28 % in the conventional system is observed from its initial load of 1.02 $p.u.$. Meanwhile, it is shown that Load with BESS 1 in proposed system 1 and Load with BESS

2 in proposed system 2 have shown a significantly lower surge in transient period at 20 % and 14 % respectively.

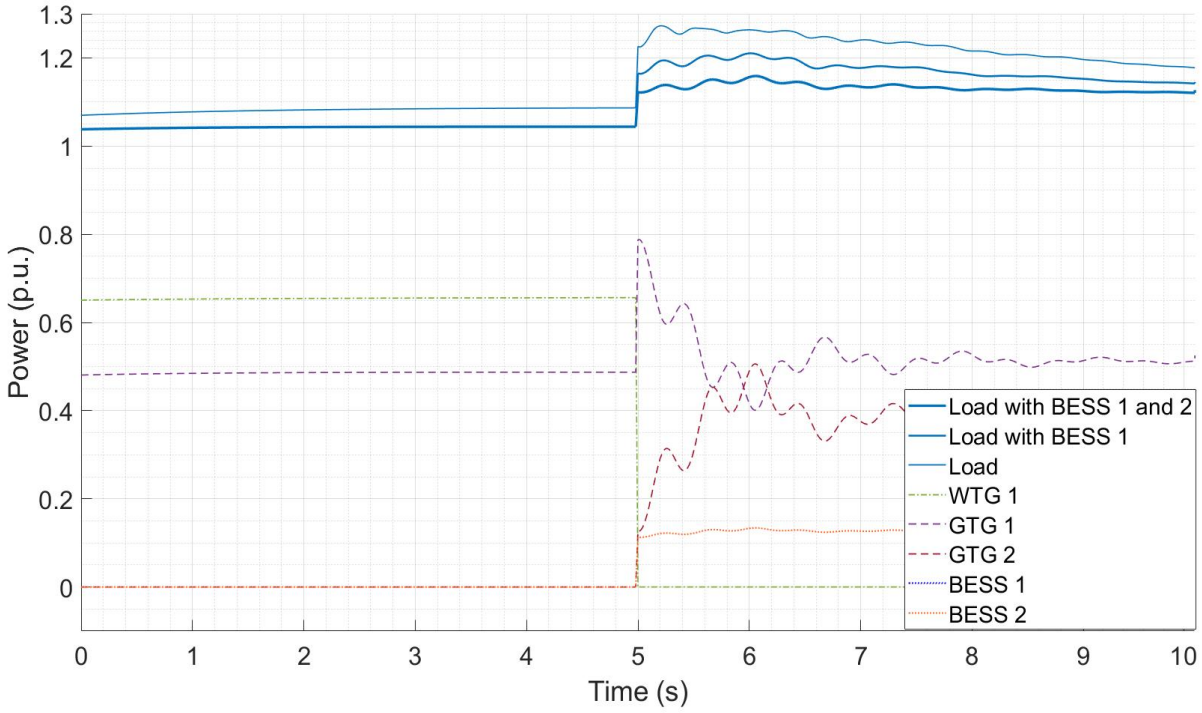

Figure 4.2: Power flow in $p.u.$ when WTG 1 is disconnected and GTG 2 is turned on (Pbase =8.5 MW).

4.4.2 Case 2: Voltage Analysis from Scenario 1 to 2

In voltage deviation, it can be seen from Figure 4.3 when the WTG is tripped and GTG 2 is turned on, there is a significant surge of output voltage of Load in the conventional system which has a maximum transient deviation of 13 % from its initial voltage of 1.03 $p.u.$ and the maximum continuous deviation is 9.4 %. The Load with BESS 1 in proposed system 1 has showed a significantly lower surge in transient deviation of 10 % with continuous deviation of 8.1 %. The Load with BESS 1 and 2 in proposed system 2 has shown the lowest surge in transient deviation of 8 % with continuous deviation of 5.7 %.

4.4.3 Case 3: Frequency Deviation from Scenario 1 to 2

In Figure 4.4, it can be seen that Load in the conventional system has a surge of output frequency which has a maximum transient deviation of 2/-3 % from its initial frequency of 1 $p.u.$ and a maximum continuous deviation is 0.1 %. Load with BESS 1 in the proposed system 1 has showed lower surge in transient period of 1/-2.5 % with continuous deviation of 0.1 %. In addition, Load with BESS 1 and 2 in the proposed system 2 has the lowest surge in transient period

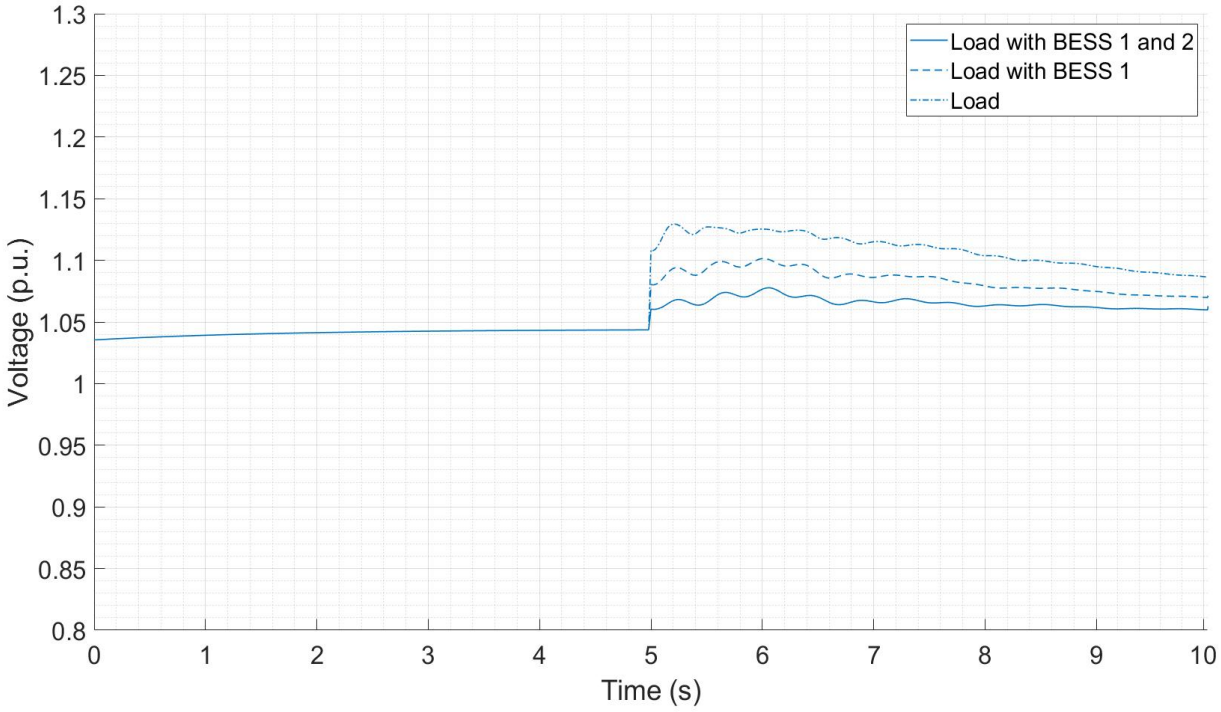

Figure 4.3: Voltage in $p.u.$ when WTG 1 is disconnected and GTG 2 is turned on (Vbase =11 kW).

of 1/-1.5 % with continuous deviation of 0.05 %. All three systems meet the requirements on maximum continuous frequency deviation of $\pm$5 % and maximum transient frequency deviation of $\pm$10 % in IEC 61892-1 in Table 2.1.

4.4.4 Case 4: Load Flow Analysis from Scenario 3 to 4

In this case study when GTG 2 is tripped and WTG is turned on, as shown in Figure 4.5, it is observed that maximum transient deviation of Load in the conventional system in load power is 21 % as the initial load is 1.23 $p.u.$. The load power is maintained around 1 $p.u.$ after the transient period with a maximum continuous deviation is 1 %. There is a similar significant surge in Load from BESS 1 in the proposed system 1 with 22 % in maximum transient deviation. The Load from BESS 1 and 2 in proposed system 2 has a further reduction of only 1 % in maximum transient deviation as BESS 1 and 2 are switched on throughout the scenario 3 and 4.

4.4.5 Case 5: Voltage Analysis from Scenario 3 to 4

In voltage deviation, it can be seen from Figure 4.6 that there is a significant dip of output voltage to 0.94 $p.u.$ and surge back of 1.04 $p.u.$ to the load in the conventional system when GTG 2 is tripped and WTG is turned on. In this case, it is shown that the output load power profile has a maximum transient deviation of -20 % from its initial voltage of 1.14 $p.u.$ and there is maximum

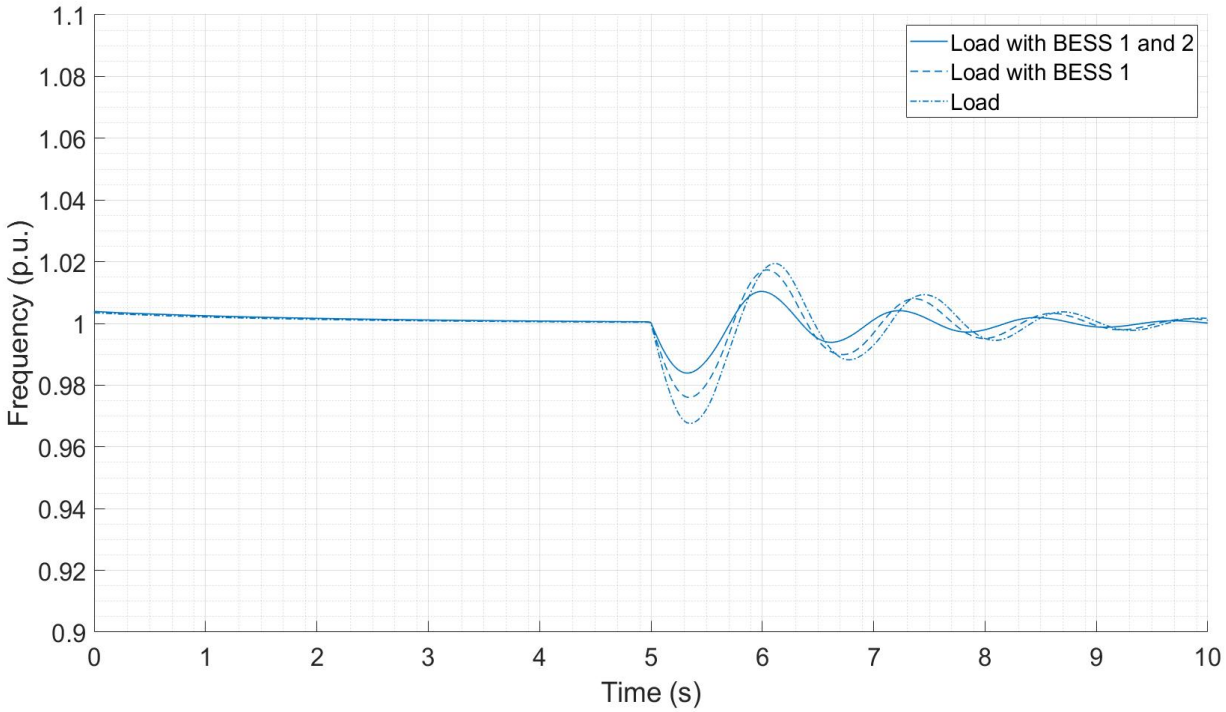

Figure 4.4: Frequency in $p.u.$ when WTG 1 is disconnected and GTG 2 is turned on (Fbase =50 Hz).

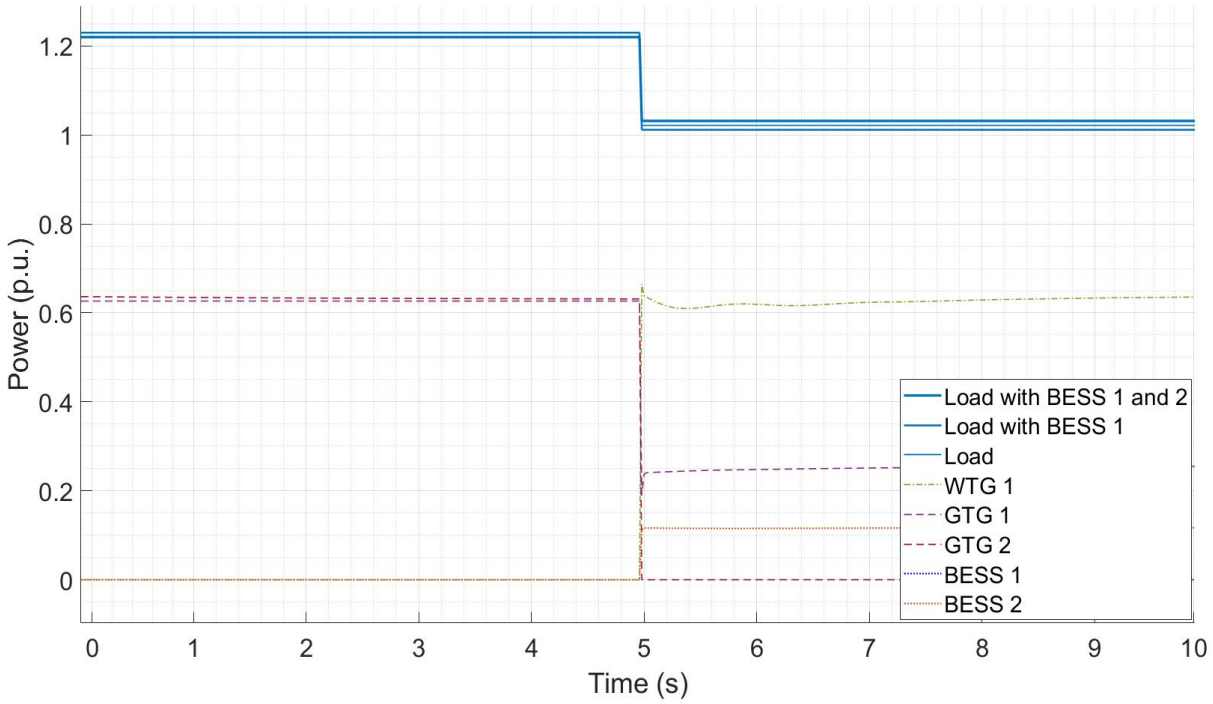

Figure 4.5: Power flow in $p.u.$ when GTG 2 is disconnected and WTG 1 is turned on (Pbase =8.5 MW).

continuous deviation in -10 % . Load with BESS 1 in the proposed system 1 has showed a lower surge in transient deviation of 19 % with continuous deviation of -11 %. Moreover, Load with BESS 1 and 2 in proposed system 2 has showed the lowest surge in transient deviation of -18 % with continuous deviation of -9.5 %.

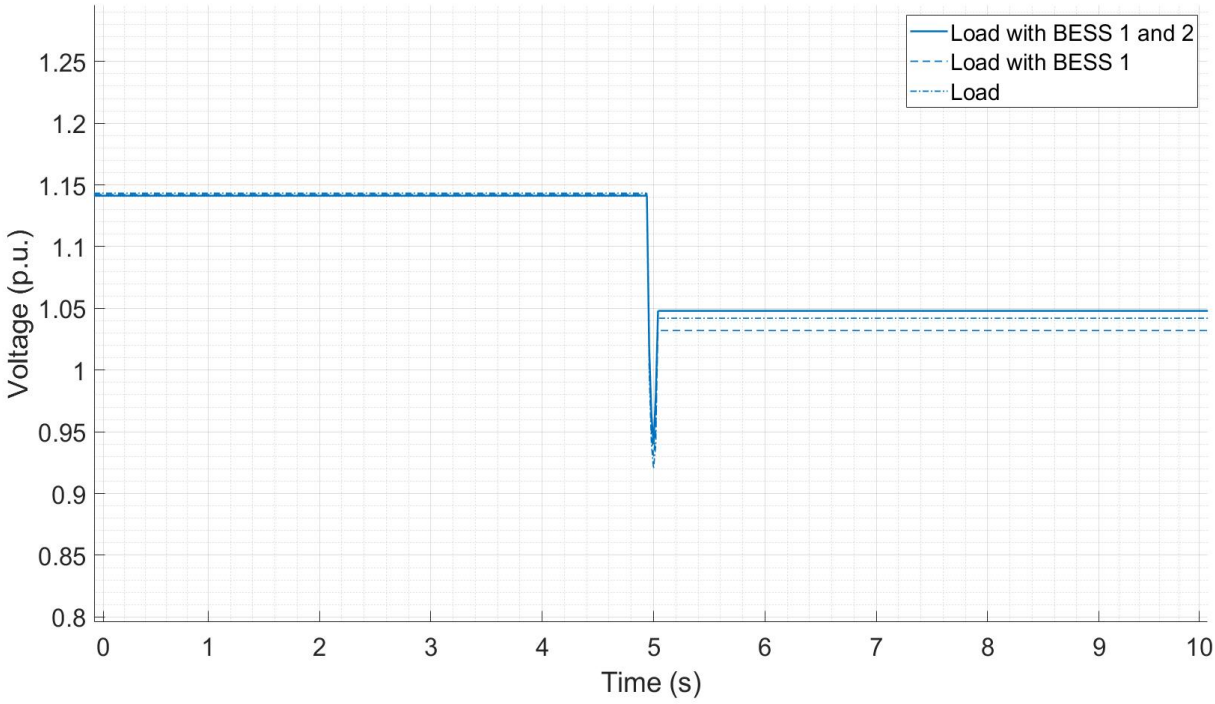

Figure 4.6: Voltage in $p.u.$ when GTG 2 is disconnected and WTG 1 is turned on (Vbase =11 kW).

4.4.6 Case 6: Frequency Deviation from Scenario 3 to 4

In frequency deviation of conventional system when GTG 2 is tripped and WTG is turned on, it can be seen from Figure 4.7 that there is a surge in maximum output frequency of 1.01 $p.u.$ with dip in maximum output frequency of 0.99 $p.u.$ to the load and the recovery time takes up to about $3s$. In this case, it is shown that the output load power profile in the conventional system has a maximum transient deviation of -1 % from its initial frequency of 1 $p.u.$ and the maximum continuous deviation is 0.01 %. The Load with BESS 1 in proposed system 1 showed significant surge in transient period of 0.5 % with continuous deviation of 0.01 %. Although the Load with BESS 1 and 2 in proposed system 2 showed the highest surge in transient period of 1.5 % with continuous deviation of 0.01 %, all three systems meet the requirements on maximum continuous frequency deviation of ± 5 % and maximum transient frequency deviation of ± 10 % in IEC 61892-1 in Table 2.1.

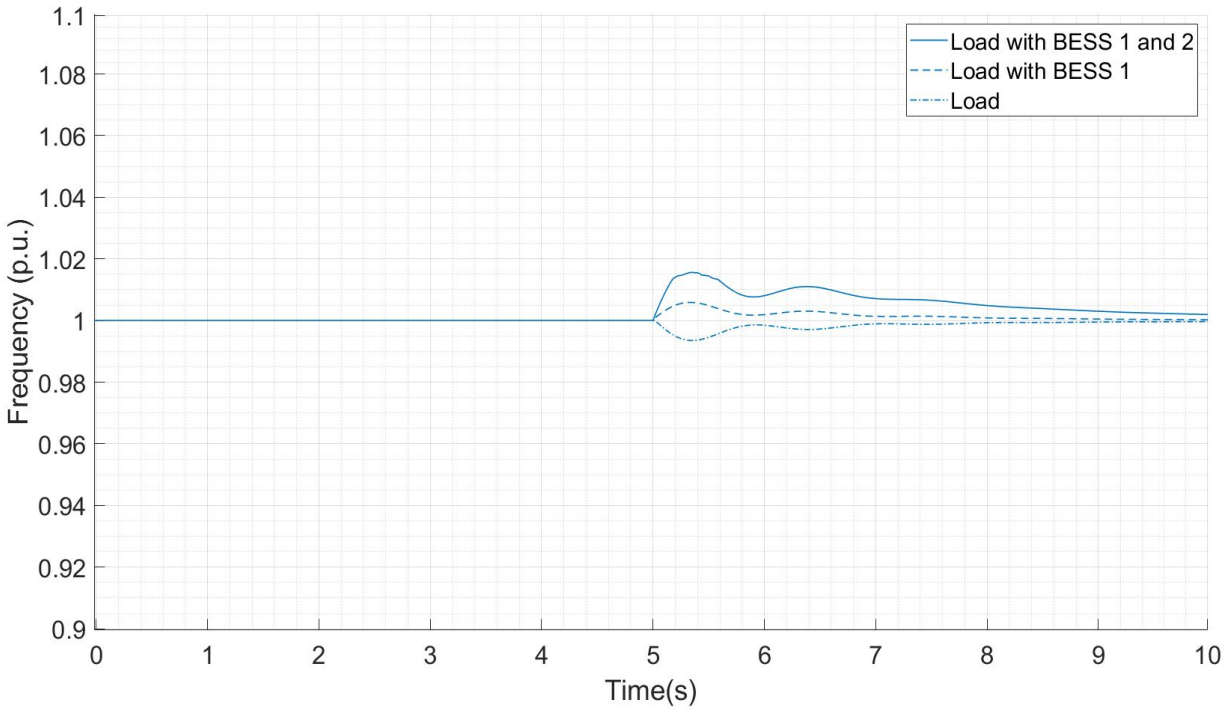

Figure 4.7: Frequency in $p.u.$ when GTG 2 is disconnected and WTG 1 is turned on (Fbase =50 Hz).

4.5 Summary of Simulation Results

In this section, a summary of simulation results will be presented and the necessary comparison against the IEC 61892-1 standards in Table 2.1 will be conducted. The criteria to be checked include the maximum transient voltage deviation, maximum transient frequency deviation and maximum continuous voltage deviation.

It has been discussed in Sections 4.4.3 and 4.4.6 that the requirements on maximum continuous frequency deviation of ± 5 % has been met in all three systems. The simulation results of all cases of voltage deviation and frequency deviation from Case 1 to 6 are presented in Figure 4.8. For the observed frequency response in Case 3, proposed system 1 has the lowest frequency deviation of 1.9 % while conventional system has highest frequency deviation of 3.3 %. For the observed frequency response in Case 6, the conventional system has the lowest frequency deviation of -0.5 % while proposed system 2 has the highest frequency deviation of 1 %. The requirement on maximum transient frequency deviation of ± 10 % in IEC 61892-1 is met in all three systems.

For the observed voltage response in Case 2, the proposed system 2 has the lowest voltage deviation of 8 % while the conventional system has the highest voltage deviation of 11 %. Sim-

ulation results show that all systems are within the maximum transient voltage deviation of ± 20 % but the conventional system and proposed system 1 did not meet the maximum continuous voltage deviation of 6 % after 1.5 *s*. Simulation results show that the conventional system has a maximum voltage deviation of -20 %, which is barely adequate to meet maximum voltage deviation, as compared to proposed system 2 which can be lowered to -18 %. In view of the results on the maximum continuous voltage deviation, the proposed system 2 is preferred.

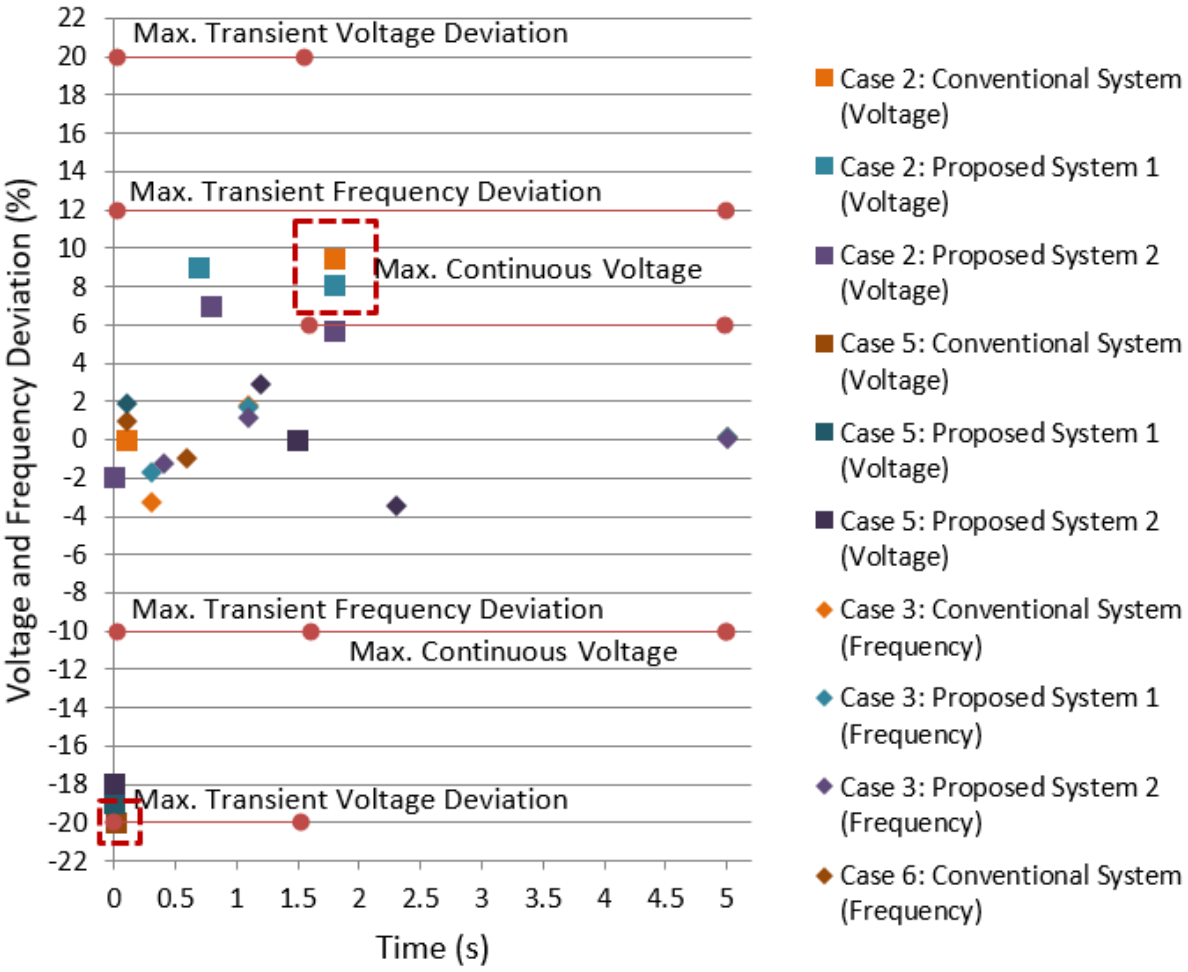

Figure 4.8: Results of voltage and frequency deviation in simulation to compare against the IEC standards 61892-1.

4.6 Cost Analysis for Proposed System 2

In this section, the cost of the preferred proposed system 2 from Section 4.5 is computed. Based on the CAPEX and OPEX from the cost analysis in United States (US) [57], [58], [59], [60], the mathematical functions of CAPEX and OPEX cost of 2 GTG, 1 WTG and 2 MW $BESS$ onboard the O&G platform are written as follows:

The capital cost of GTG, GTG_C onboard the platform can be calculated by:

$$GTG_C = GT_{10MW} \times 2 \times 1415, \tag{4.1}$$

where represents 10,000 kW and GT is approximately $ 1415 per kW.

The capital cost of WTG, WTG_C onboard the platform can be calculated by:

$$WTG_C = WTG_{6MW} \times 2870, \tag{4.2}$$

where offshore WTG_{6MW} represents 6000kW and GT is approximately $ 2870 per kW.

BESS has the lifespan of ten years and would require double times of the capital cost for lifespan of twenty years. Thus, the capital cost of BESS, $BESS_C$ onboard the platform can be calculated by:

$$BESS_C = BESS_{1MW} \times 1930 \times 2 \times 2, \tag{4.3}$$

where $BESS_{1MW}$ represents 1000kW and GT is approximately $ 1937 per kW.

The opex cost of GTG, $GTG_{O\&M}$ onboard the platform can be calculated by:

$$GTG_{O\&M} = GT_{10MW} \times 2 \times 89.4, \tag{4.4}$$

where GT_{10MW} represents 10 000 kW and OPEX of GT is approximately $ 89.4 per kW.

The OPEX cost of WTG, $WTG_{O\&M}$ onboard the platform can be calculated by:

$$WTG_{O\&M} = WTG_{6MW} \times 80, \tag{4.5}$$

where WTG_{6MW} represents 6000kW and O&M cost of WTG is approximately $ 137 per kW.

BESS has the lifespan of ten years and would require double the opex cost for lifespan of twenty years. Thus, the operational and maintenance (O&M) cost of BESS on board the platform can be calculated by:

$$BESS_{O\&M} = BESS_{1MW} \times 10 \times 2 \times 2, \tag{4.6}$$

where $BESS_{O\&M}$ represents 6000 kW and O&M cost of WTG is approximately $ 10 per kW.

A cost analysis of CAPEX and OPEX for proposed system 2 is shown in Figure 4.9, which

comprises of 2 GTG, 1 WTG and 2*MW* BESS for proposed system 2. Both pie charts corresponding to CAPEX and OPEX have revealed that GTG has the highest cost of 53% in CAPEX and 78% in OPEX. The BESS has the lowest cost 15% in CAPEX and 1% in Opex.

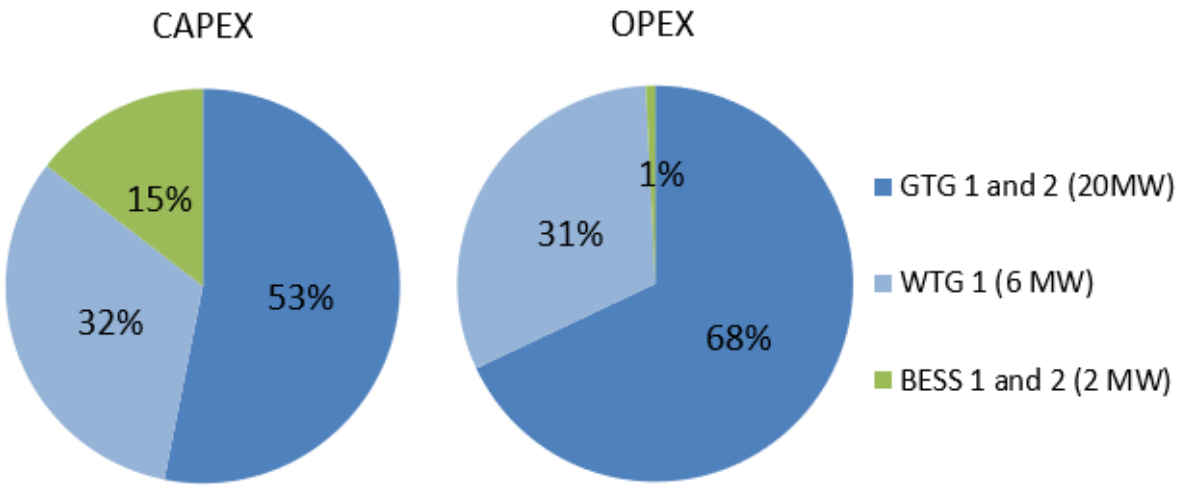

Figure 4.9: Cost analysis of CAPEX and OPEX of proposed system 2.

4.7 Summary

In this chapter, an investigation on transient voltage and frequency deviation for both conventional, proposed system 1 and proposed system 2 has been carried out. A commercial software application, ETAP, is used to generate transient stability results that will be compared with the IEC standards for both conventional and proposed systems, which are discussed in Chapter 2.5. In order to understand if transient stability requirements in the IEC standards can be met with a lower WTG capacity and variations in BESS sizing, the simulation will consist of a lower capacity of BESS and WTG. There is a proposed system 1 with 1*MW* of BESS and proposed system 2 with 2*MW* of BESS to integrate with 2 GTG and 1 WTG. Four test scenarios corresponding to faults in the primary power generation from the GTG and secondary power generation from the WTG are described. Simulation results have shown that proposed system 2 meets all the IEC standards 61892-1 in O&G industry for transient deviation in both voltage and frequency deviation and is the preferred system. It is also shown that proposed system 2 is able to enhance the output power quality by lowering the maximum voltage transient from 11 % to 5.7 % in Section 4.4.3 and maximum transient frequency deviation of 1.8/-3.3 % in Section 4.4.2, in the event of a sudden trip in WTG due to inadequate wind speed. In addition, it is also shown that the conventional system barely meet the IEC standards with a maximum voltage deviation of -20 %, which can be lowered by proposed system 2 to -18 % in Section 4.4.5, in the event of a trip in GTG. As such a cost analysis has been performed for the configuration of proposed sys-

tem 2 to lay the foundation for economic analysis. It has been shown that BESS has the lowest CAPEX and OPEX, as compared to GTG and WTG. The sizing of 2 MW BESS is adequate to meet both transient voltage and frequency deviation in IEC standards 61892-1. It is worhtwhile investigating if the output power can be further enhanced with an increase in BESS capacity due to its low CAPEX and OPEX, which will be conducted in the next chapter.

Chapter 5

Transient Stability with Costs Enhancement

5.1 Introduction

As discussed previously in Chapter 3, BESS has also been proposed to integrate with an offshore floating wind farm and offshore O&G production platforms for load flow analysis without considering voltage and frequency deviation [51]. A subsequent study conducted in Chapter 4 on transient stability analysis with ETAP on offshore O&G platforms with WTG and 2 MW of BESS has shown that the voltage and frequency deviations meet the IEC standards 61892-1 for O&G industry [61]. It has also been demonstrated in Chapter 4 that the BESS is capable of improving the transient stability of the system and the CAPEX and OPEX of BESS is lower, as compared to the GTG and WTG. As such, it is possible to replace GTG 2 with 2MW of BESS [62]. The dimensions of the GTG and BESS are comparable as described in Section 2.4. This is likely to improve the transient stability further in terms of the maximum continuous voltage deviation, which is the closest to the limits in the IEC standards 61892-1, as discussed in Section 4.5.

In this chapter, the transient stability with an increased capacity of 4MW BESS will be studied. As discussed, this requires the removal of 2 GTGs to install 4 MW BESS onboard the O&G platforms. The system architecture will be discussed in Section 5.2. As Chapter 3 and 4 have studied faults in the primary power generation by tripping the GTG and studying the transient response, this will not be simulated again. Instead, faults in the secondary power generation of the WTG will be studied to investigate if the BESS is able to provide the secondary response to the system in Section 5.3. The primary response from GTG will be limited and slower, as compared to that of the BESS. Similar to Chapter 4, variations in the BESS sizing will be considered, along with the associated cost of increasing the BESS capacity. Based on the cost analysis data given in Chapter 4.6, a detailed techno-economic analysis with increased capacity of BESS will

be studied in Section 5.5.

The outline of this chapter is as follows. Section 5.2 presents the detailed configuration of two proposed systems with varying BESS. Four different test scenarios are presented in Section 5.3. Section 5.4 presents the simulation results of conventional system, proposed system 1 and proposed system 2. The techno-economic analysis with discussion of simulation results will be described in Section 5.5. Lastly, conclusions are presented in Section 5.6.

5.2 System Overview

In this section, the proposed system architecture consisting of 1 GTG, 1 WTG and four modular of 1 *MW* BESS is shown in Figure 5.1.

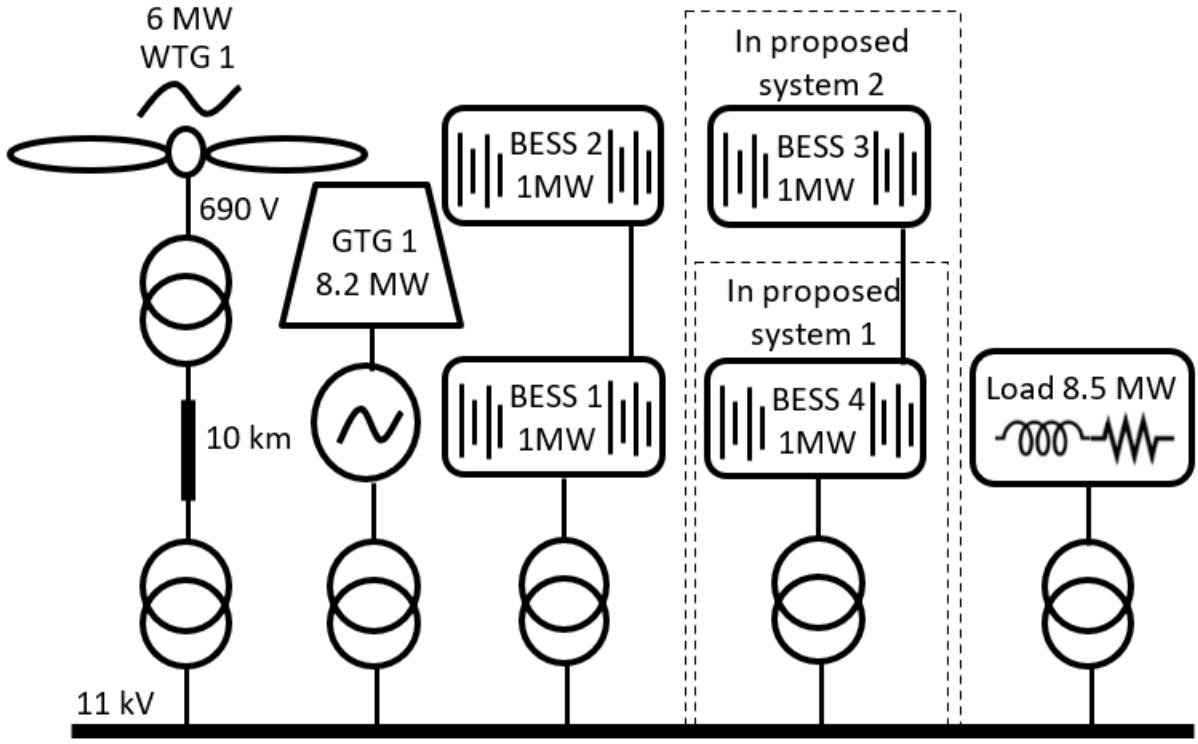

Figure 5.1: Proposed offshore integrated system.

In the typical system, the offshore O&G platforms are equipped with two sets of SCGTs (16.4 *MW*) and standby one set of SCGTs (8.2 *MW*), where two SCGT acts as an EG and the other serves as an E.EG. In our proposed systems 1 and 2 in Chapter 4, one of the EG has been removed, which allows the necessary physical space for the integration of an additional 1 *MW* or 2 *MW* BESS onboard the offshore O&G platform, which is otherwise known as the conventional system. In this chapter, the proposed system 1 consists of 3*MW* of BESS while the proposed system 2 consists of 4*MW* of BESS.

The conventional O&G platform has a fixed load of around 8.5 *MW*, as discussed in [51]. Similarly, the system architecture in the conventional system consists of one set of 6 *MW* Siemens (SWT-6.0-154) PMSG floating WTGs connected in parallel, which mirrors the Hywind Park configuration in the North Sea [47]. The WTGs are situated 10 *km* away with joint HVAC power transmission cable to the output on the power bus of the offshore O&G platform.

5.3 Test Scenarios

In this section, four test scenarios are simulated in the ETAP 19.0 and plotted in MATLAB/Simulink. Throughout the four test scenarios, a constant rated wind speed is assumed. The simulation study is based on the ability of the power system to maintain electrical power to load when subjected to transient fault of WTG. This is conducted for varying sizes in the BESS, as shown in Table 5.1. Usually, the duration of the trip event to study transient stability is at least 3 *s* and beyond for RES connected to BESS that has been demonstrated in [52].

Table 5.1: Conventional System in four scenarios

Scenario	Event
1	Continuous wind
2	Conventional system: WTG 1 is tripped and BESS 1 and 2 are turned on
3	Proposed system 1: WTG 1 is tripped and BESS 1, 2 and 3 are turned on
4	Proposed system 2: WTG 1 is tripped and BESS 1,2,3 and 4 are turned on

The simulation results will be compared against the IEC standards 61892-1 for the maximum transient voltage and frequency deviations found in Table 2.1 on Chapter 2.5. For a fair comparison, both conventional and proposed system are assumed to have a GTG together with a WTG running onboard, which are GTG 1 and WTG 1 respectively.

5.4 Simulation Results

In this section, the transient stability results for voltage and frequency deviations in the conventional system, proposed system 1 and proposed system 2 are presented. These will be based on the scenarios in Table 5.1, which evaluates the ability of each of the systems to maintain electrical power to load when subjected to transient fault of WTG. The conventional system, proposed system 1 and proposed system 2 will be started in Scenario 1 and subjected to Scenario 2, 3 and 4 respectively.

5.4.1 Voltage and Frequency Deviation on Conventional System

In this section, the baseline reference will be established from the conventional system, which is started in Scenario 1 with continuous wind. A fault in the WTG is simulated in Scenario 2 and 2 *MW* of BESS is turned on in the conventional system, in addition to the primary power generation from GTG 1.

As shown in Figure 5.2, there is a significant surge in output voltage to the load, with peak value of 1.11 *p.u.* This is followed by a drop in output voltage to the load with values below 1 *p.u.*. In this case, it is shown that the output load power profile has a maximum transient deviation of 11 % from its initial voltage of 1.02 *p.u.*. This result affirms that the conventional system barely meets IEC standards 61892-1 for maximum transient for voltage deviation, which is 20 %.

In frequency deviation, it can be seen from Figure 5.3 that there is a dip in output frequency at the load to 0.78 *p.u.* immediately after the transient period. In this case, it is shown that the output frequency has a maximum transient deviation of -22% from its initial frequency of 1 *p.u.* This result shows that the conventional system does not meet IEC standards 61892-1 for maximum transient frequency deviation of 10%.

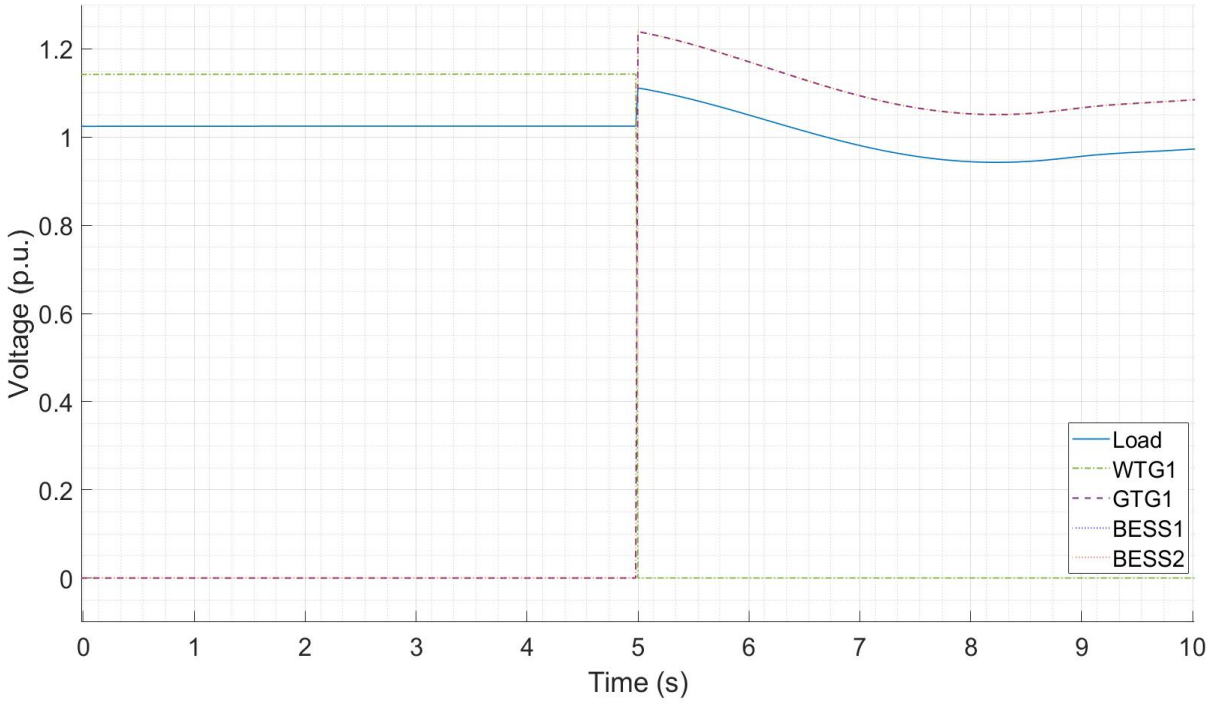

Figure 5.2: Voltage in *p.u.* when WTG 1 is disconnected and BESS 1and 2 are turned on (Vbase =11 *kV*).

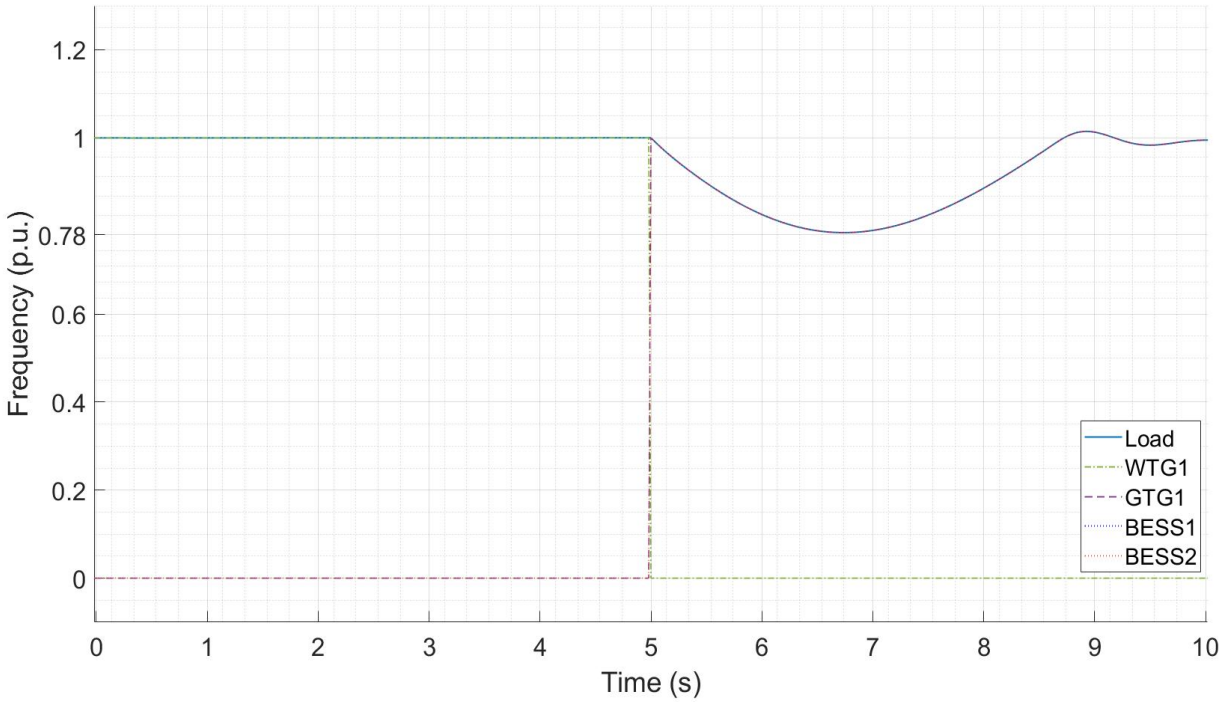

Figure 5.3: Frequency in $p.u.$ when WTG 1 is disconnected and BESS 1and 2 are turned on (fbase =50 Hz).

5.4.2 Voltage and Frequency Deviation on Proposed System 1

In this section, a similar study is conducted on the proposed system 1 with 3MW of BESS. The proposed system 1 is started in Scenario 1 and switched to Scenario 3, where the WTG 1 is suddenly disconnected and BESS 1,2 and 3 are turned on with GTG 1 in operation mode.

It is observed that the maximum transient deviation in voltage is approximately 8 %, as shown in Figure 5.4. This is significantly 3 % lesser as compared to the conventional system. It is also observed that, the output voltage dips below 1 $p.u.$ after the transient period.

It is also shown in Figure 5.5 that the transient deviation in frequency is approximately 11 % which is 11 % lesser as compared to the conventional system. Similarly, this result shows that the proposed system 1 does not meet IEC standards 61892-1 for maximum transient frequency deviation of 10 %.

5.4.3 Voltage and Frequency Deviation on Proposed System 2

In this section, a similar study is conducted on the proposed system 2 with 4 MW of BESS. The proposed system 2 is started in Scenario 1 and switched to Scenario 4, where the WTG 1 is suddenly disconnected and BESS 1,2,3 and 4 are turned on with GTG 1 in operation mode.

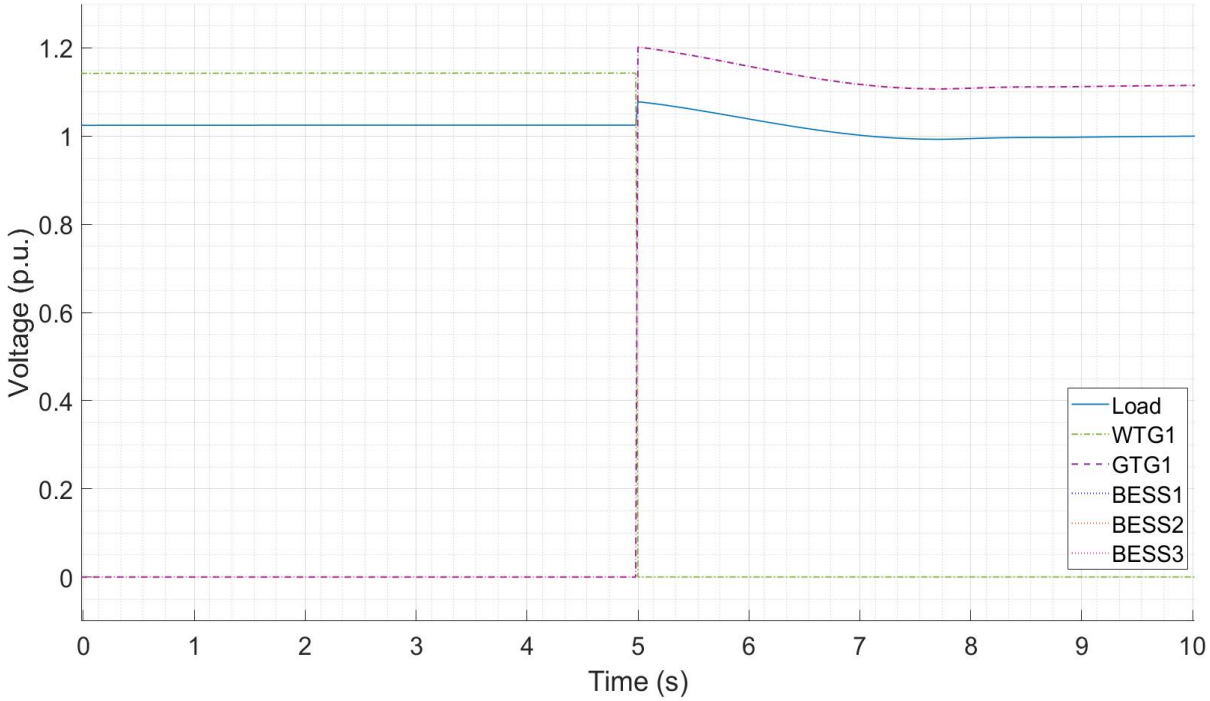

Figure 5.4: Voltage in $p.u.$ when WTG 1 is disconnected and BESS 1, 2 and 3 are turned on (Vbase =11 kV).

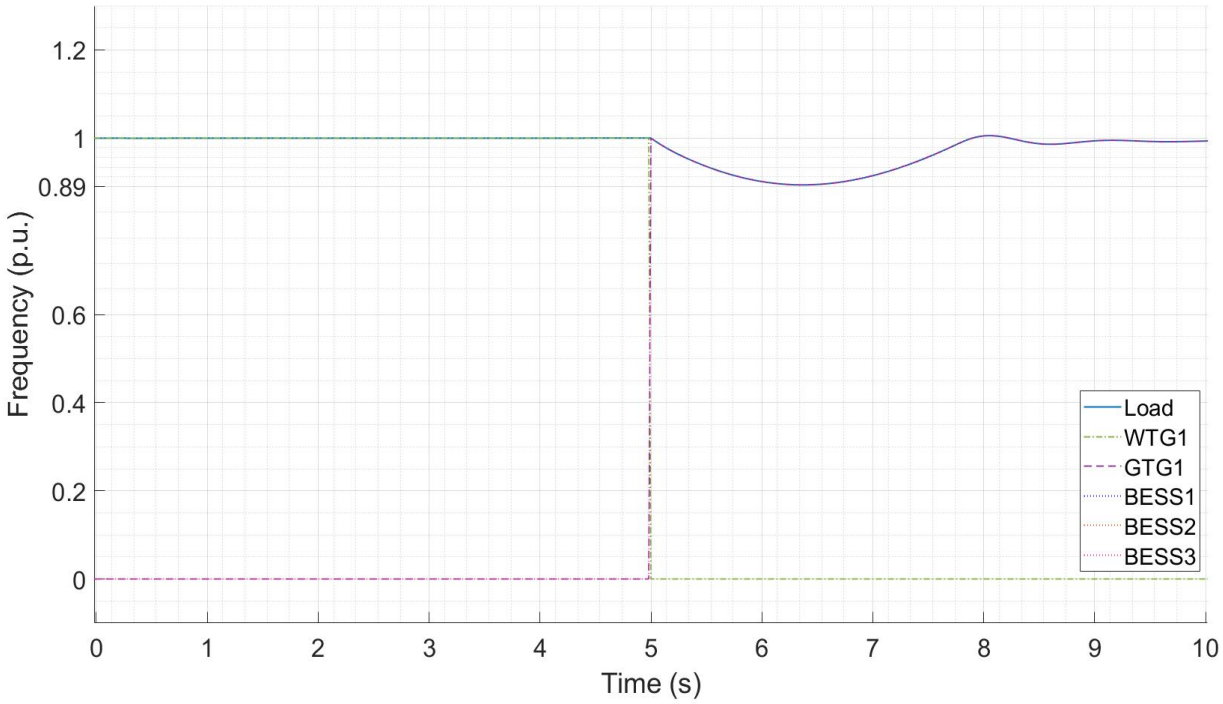

Figure 5.5: Frequency in $p.u.$ when WTG 1 is disconnected and BESS 1, 2 and 3 are turned on (fbase =50 Hz).

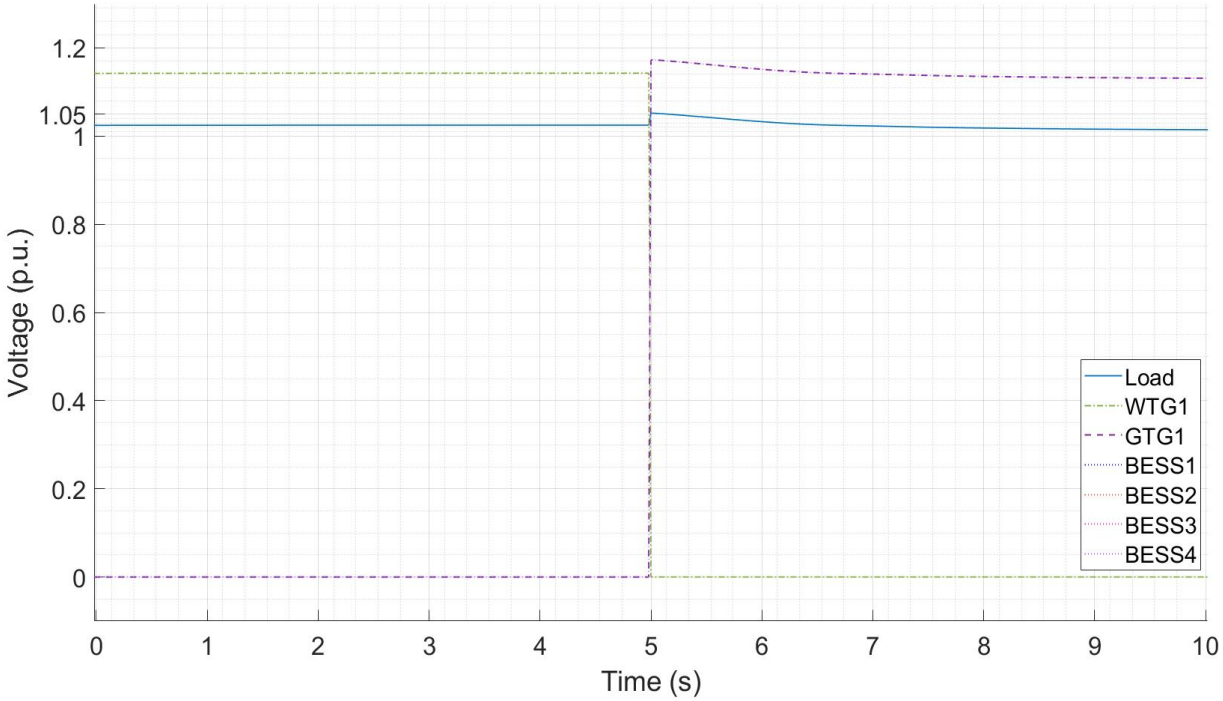

Figure 5.6: Voltage in $p.u.$ when WTG 1 is disconnected and BESS 1, 2, 3 and 4 are turned on (Pbase =8.5 MW).

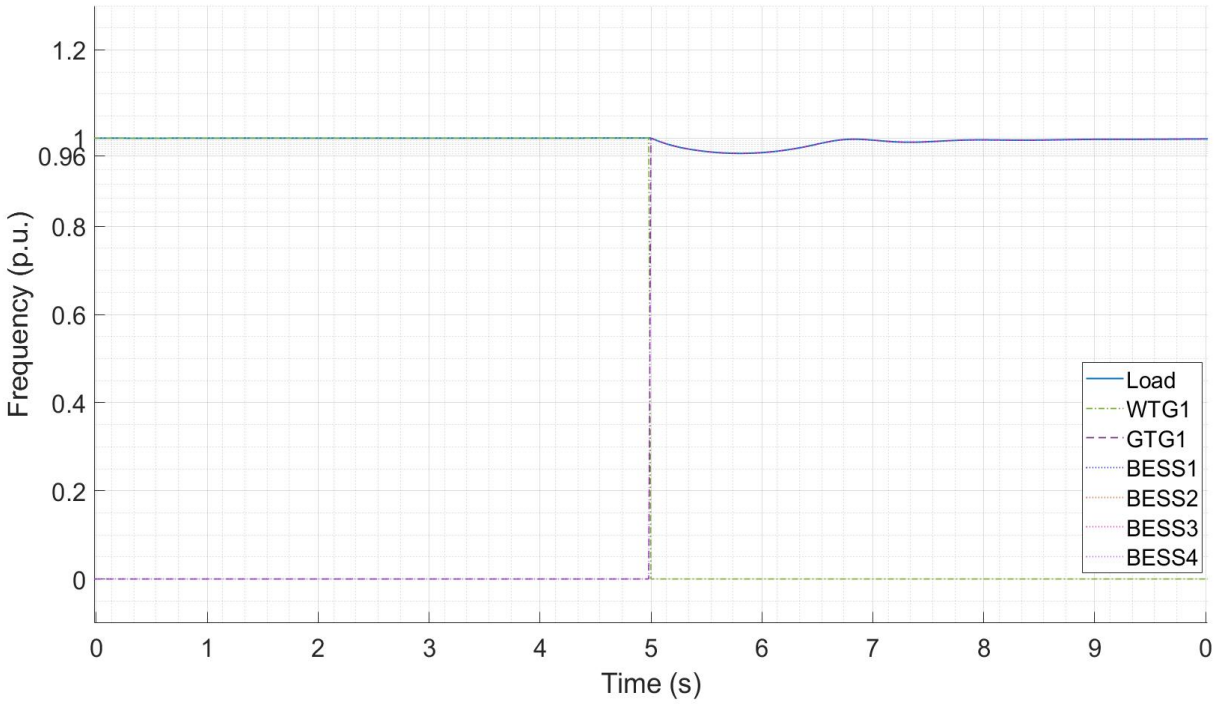

Figure 5.7: Frequency in $p.u.$ when WTG 1 is disconnected and BESS 1, 2, 3 and 4 are turned on (fbase =50 Hz).

In voltage deviation, the output voltage has a surge of 1.05 $p.u.$ as shown in Figure 5.6, which is 5 % in maximum transient deviation. This is significantly lower by 3 % compared to the proposed system 1. In addition, there is a further reduction reduction of 6 % in maximum transient voltage deviation as compared to conventional system.

In frequency deviation, the output frequency has a surge of 0.96 $p.u.$ as shown in Figure 5.7, which is 4 % in maximum transient deviation. This is significantly lower by 7 % lesser as compared to the proposed system 1, as shown in Figure 5.3 (b) where the transient deviation is 11 %. In addition, there is a further reduction of 18 % lesser in maximum transient frequency deviation as compared to conventional system. Overall, proposed system 2 can meet IEC standards 61892-1 for maximum transient voltage and frequency deviation.

5.5 Techno-Economic Analysis of Proposed System 1 and 2

With ongoing R&D in battery technology, the BESS has declined in total costs which makes it more attractive for integration with RES in a standalone micro grid configuration [53]. As such, the E.EG of the conventional system, which is usually in stand-by mode has been replaced with another 2 MW of BESS onboard the platform. In our proposed system 2, another EG is also removed and replaced with, BESS 3 and 4, each with an energy capacity of 1 MW, and connected to the 11 kV main switchboard on offshore O&G platforms. It has been shown in Section 5.4.3 that proposed system 2 meets the IEC standards 61892-1. In order to evaluate the techno-economic feasibility, the costs of the typical system, conventional system, proposed system 1 and proposed system 2 will be computed and analysed in this section.

Based on the CAPEX and OPEX cost analysis in [54], [55], [56], the cost is calculated as follows. Since GTG has a power factor of 0.8, the CAPEX of GTG (GTG_C) onboard the offshore O&G platform is written as follows:

$$GTG_C = 10000 \times 2 \times 1415, \tag{5.1}$$

where the cost of GTG is approximately \$1415/kW for two 10 MW of GTG.

The CAPEX of WTG (WTG_C) on board the platform can be calculated by:

$$WTG_C = 6000 \times 2870, \tag{5.2}$$

where the cost of WTG is approximately \$2870/kW for a 6 MW WTG.

Initial BESS has the lifespan of 10 years and would require double times of the CAPEX for lifespan of 20 years. Thus, the CAPEX of BESS ($BESS_C$) on board the platform can be

calculated by:

$$BESS_C = 1000 \times 1930 \times 2 \times 2, \tag{5.3}$$

where BESS is approximately \$1937/*kW* for four unit of 1 *MW* BESS.

Based on Equations 5.1 to 5.3, the overall cost in term of CAPEX and OPEX in the lifespan of twenty years for a typical system, conventional system, and the proposed systems 1 and 2 is presented in Figure 5.8. It is shown that the typical system has the highest cost, as compared to the other systems. For ease of comparison, all costs have been normalised to the base cost of the typical system. As the typical system comprises of two set of GTGs, it has the highest cost, as compared to the other systems. In this chapter, the conventional system, proposed system 1 and proposed system 2 have only one set of GTG and 1 set of WTG. However, the conventional system, proposed system 1 and proposed system 2 have onboard the O&G platforms, 2 *MW*, 3 *MW* and 4 *MW* BESS respectively. As such, the conventional system has the lowest cost at 84.87 %, which is 15.13 % lower than the base cost. As proposed system 1 requires an additional of 1 *MW* of BESS, it has a higher cost, which is approximately 14.8 % lower than the base cost. Last but not the least, proposed system 2 requires an additional of 2 *MW* of BESS and has a higher cost, which is approximately 14.46 % lower than the base cost.

As shown in Figure 5.6 and Figure 5.7 in Section 5.4, proposed system 2 is able to meet the IEC standards 61892-1 for O&G industry. Although proposed system 2 has a 0.67 % higher cost than the conventional system, it presents a cost reduction of 85.54 % compared to the typical system, while meeting the requirements on the quality of the output power that is specified by the IEC standards.

In order to enhance output power quality and to meet IEC standards 61892-1 for frequency deviation, there is an increase in CAPEX and OPEX from \$0.475 *M* in conventional system to \$0.95 *M* in proposed system 2 throughout the twenty years, as shown in Figure 5.9. However, the overall cost has yet to include the fuel cost and the amount of carbon reduction, which will be further presented in Chapter 6.

5.6 Summary

In this chapter, transient stability with an increased capacity of 4*MW* BESS has been studied. As discussed, this requires the removal of 2 GTGs to install 4*MW* BESS onboard the O&G platforms. Three system configurations with 1 set of GTG and 1 set of WTG are considered. The conventional system, proposed system 1 and proposed system 2 have onboard the O&G platforms, 2 *MW*, 3 *MW* and 4 *MW* BESS respectively. The simulation results of all cases of voltage deviation and frequency deviation are presented in Figure 5.9 for the event of a trip

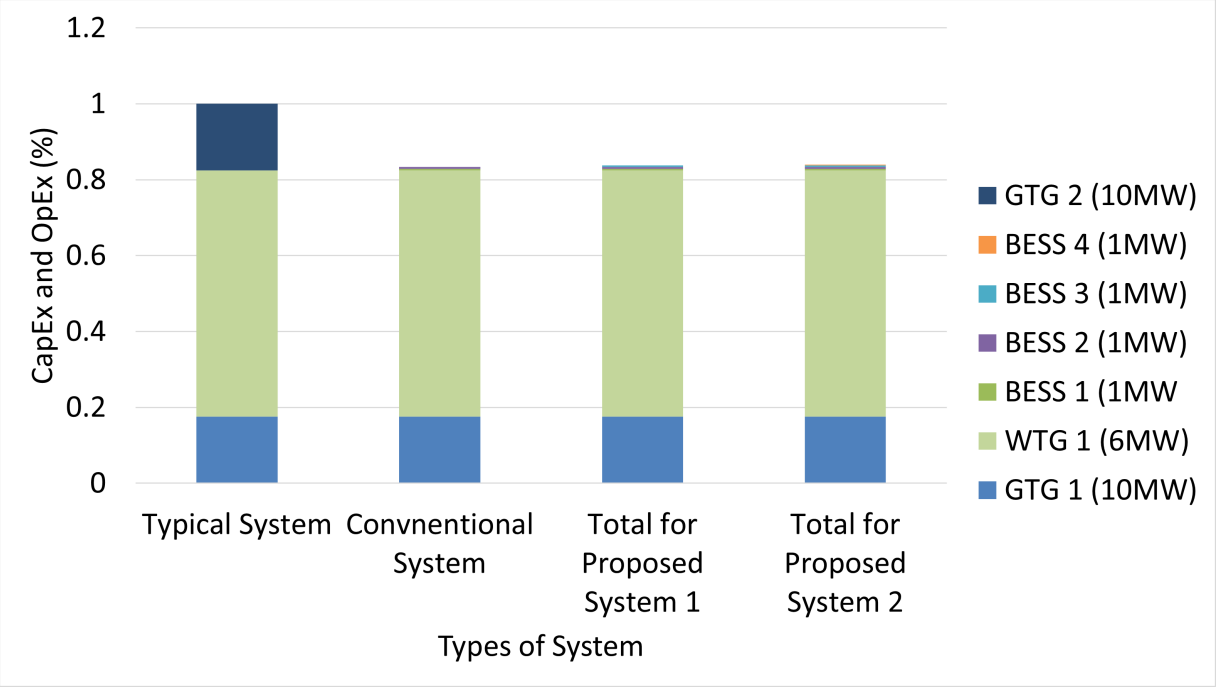

Figure 5.8: Total cost for lifespan of 20 years of CAPEX and OPEX (normalised to the base cost of the typical system).

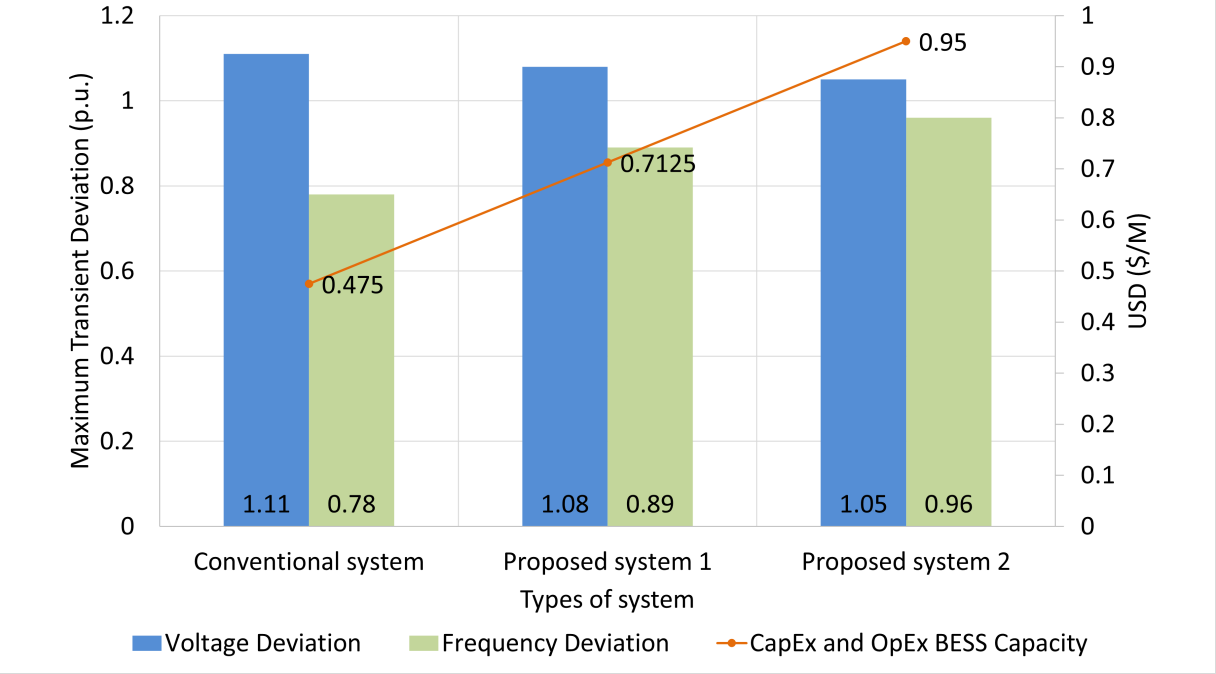

Figure 5.9: Simulation results of voltage and frequency deviation with CAPEX and OPEX for conventional system, proposed system 1 and 2.

due to a fault in the WTG. The simulation results have shown that proposed system 2 has an improved power quality improvement, as compared to the conventional system and proposed system 2.

In the simulation on voltage deviation, an increase in BESS from 2 MW to 4 MW led to a reduction of transient deviation from 11 % to 5 %. For maximum transient frequency deviation, both conventional system and proposed system 1 do not meet the requirements on maximum frequency deviation according to IEC standards 61892-1. This is unlike proposed system 2 which has BESS of 4 MW, which is able to meet the IEC standards. Although proposed system 2 has a 0.67 % higher cost than the conventional system, it presents a cost reduction of 85.54 % compared to the typical system, while meeting the requirements on the quality of the output power that is specified by the IEC standards. In addition, the overall cost has yet to include the fuel cost and the amount of carbon reduction, which will be further presented in Chapter 6.

Chapter 6

Development of an Energy Management System (EMS)

6.1 Introduction

In the developments of offshore O&G platforms, the adoption of IEC standards 61892-1 is used to ensure that voltage and frequency deviation are within ranges for power stability during O&G production [13]. Dynamic load demand and stochastic wind affect output power to load and the transient stability of the system. These conditions commonly lead to large deviations in voltage and frequency, which fail to meet IEC standards 61892-1. The integration of WTG with O&G platform and BESS has shown an improvement in transient stability with increased BESS capacity, as demonstrated in Chapter 5. This methodology is only achieved when there is constant wind speed. Stochastic wind speed will cause a fluctuations in output power. Hence, the models in the earlier chapters may not meet the IEC standards 61892-1, in the event of wind intermittency. Therefore, there is a need to consider a realistic wind profile and dynamic loads from the offshore O&G platforms.

In this chapter, a remaining gap to improve transient stability of the proposed system, in the event of stochastic wind speed and actual load variation will be addressed. In recent publications, there has been a lot of interest in this research area. A control strategy was developed to provide short-term voltage stability control by rapid control of batteries on extra high voltage networks to match supply and demand of the grid with a large penetration of renewable generation. [63]. Subsequently, a lead-lag controller is developed in the BESS to provide improved stabilisation for the transient voltage and frequency of the system [64]. An online EMS in [65] has been proposed to enhance output power quality to meet the load demand. However, the transmission of the signal online may not provide a sufficiently rapid response to address any transient surge in load demand. A summary of recent studies of EMS and control architectures for hybrid RES has been provided in [66]. It has been discussed that the adoption of a certain

energy management strategy is vital to control the flow of energy among the various components (energy sources, storage devices, and loads) in the hybrid energy system. This further affirms that an EMS should be developed when there is a high penetration of wind power, whose intermittency can pose challenges for power stability and reliability of the system.

More recently, the sizing of BESS for offshore O&G platforms has been assessed in capacity allocation for a multi functional energy storage system for O&G applications [12]. For a wind-powered O&G platform, SLM is developed using EMS inbuilt with controllers and control algorithms to control the BESS, so as to provide voltage and frequency support at PCC to the load [11]. This is the latest state of the art in this area, which will be further reviewed in this chapter. The authors have also proposed to size the BESS for both inertia support in the system and frequency control which is demonstrated in [67] so as to achieve optimum transient stability of the system. This is similar to our work in Chapter 5 of this thesis, which sizes the BESS to meet the frequency deviation requirements in the IEC standards.

Our proposed EMS is motivated by [1], which designed water injection load to utilise the surplus energy generated from WTG with realistic wind speed at any point of time. This reduced the disturbance on the power grid when there is stochastic wind that will affect transient period in voltage and frequency control. Likewise, we have considered to supply the water injection load with the BESS for transient stability, in the event of loss in wind speed and dynamic loads. In addition, BESS will also be used to store surplus energy from the WTG. Therefore, our motivation to design and develop an EMS into our proposed system that consist of BESS is as follows.

- Rapid response to enhance transient stability in our proposed system.
- Secondary frequency support for the power grid, in the event of dynamic loads with intermittency in wind speed.
- Improvement of output power quality to load without increasing the size of BESS.

This chapter provides an overview of the development of our energy management in our proposed system to improve output power quality to dynamic load, in the event of power intermittency from the WTG. The detailed modelling and sizing of our proposed system with EMS is presented in Section 6.2. Section 6.3 will discuss the main control components of our EMS to regulate the voltage and frequency at the PCC. Section 6.3.3 presents the test scenarios and the optimal controller parameters in the EMS. Simulation results with analysis for all test scenarios are analysed in Section 6.5. Section 6.6 provides a cost evaluation with the savings in carbon emission reduction with our proposed system. Lastly, a summary of this chapter is presented in Section 6.7.

6.2 Sizing of Proposed System with Energy Management System (PSEMS)

In this section, the detailed modelling and sizing of our proposed system with EMS is presented. The overview and sizing of our proposed system with EMS is as shown in Figure 6.1. The system components, which are of similar configuration, used in the previous chapters are presented as follows.

Typical offshore O&G platform are powered primarily by SCGTs onboard the platforms. These GTG are carbon intensive with an efficiency of approximately 35 % [3]. In our proposed system, the GTG is of 10 MVA which delivers 8 MW active power to the 3-phase power grid of 11 kV. Circuit breaker (CB) 3 is placed between the PCC and GTG. The model of WTG is based on a floating 6 MW Siemens (Model: SWT-6.0-154) PMSG connected to a step-up transformer with its detailed model found in [68]. CB 1 is placed in between the PCC and WTG. A variable load is assumed to be between 6MW to 10MW. The base load of 6MW will be referred to as fixed loads and the sum of the fixed and flexible loas will sum up to 10MW. CB 4 is placed between the PCC and Load. The BESS consists of a lithium-ion battery bank which allows bi-directional power flow through the power inverter and is connected via the step-up transformers to the system. CB 2 is placed in between the PCC and BESS.

The sizing of 2 MW BESS is used as its footprint is comparable to one unit of GTG, as shown in Figure 6.2. The footprint dimension of BESS is of 1370 mm in length by 244 mm in width, which is slightly less than GTG of 1400 mm in length by 300 mm in width. If it is possible to achieve good output power quality and meet the IEC standards with 2 MW of BESS, this provides better structural stability to the system as the BESS will not have to be stacked vertically upwards. In addition, the choice of a sizing of 2 MW BESS is also for better comparison with the present state of the art, which uses a 2 MW BESS. At the beginning of this thesis in Section 2.6, the motivation of implementing EMS to use BESS integrated with offshore WTG, to provide voltage and frequency support at the PCC to the load has been discussed. The BESS has also been constantly used in EMS to support the power grid ranging from Kilowatts to Megawatts, demonstrating the effectiveness in terms of its efficiency, reliability, availability and economic operation [69], [70].

In summary, the individual power rating of BESS, GTG and WTG is 2 MW, 8 MW and 6 MW respectively. In order to optimally reducing carbon emission in the system, WTG will be injecting output power to power grid. The GTG, which is of primary power generation initially will take the role of secondary power generation when WTG is turned on. Since the other GTG is replaced by BESS which will be installed onboard O&G platform, WTG and GTG shares

the load equally at rated wind speeds. In the Hywind Park configuration in the North Sea [47], the WTGs are situated 10 *km* away with joint HVAC power transmission cable to the output on the power bus of the offshore O&G platform. As such, losses of output power from the AC transmission line will be assumed to be insignificant in the simulation study.

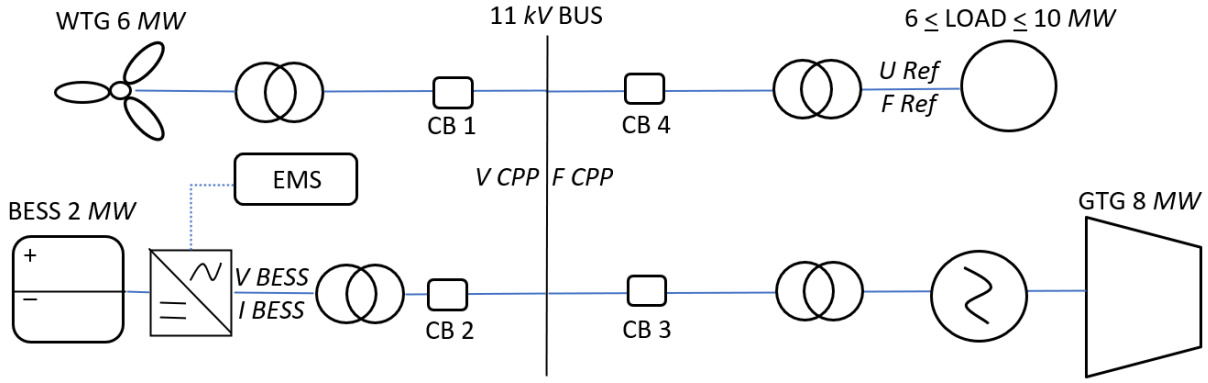

Figure 6.1: The proposed system with allocated EMS overview.

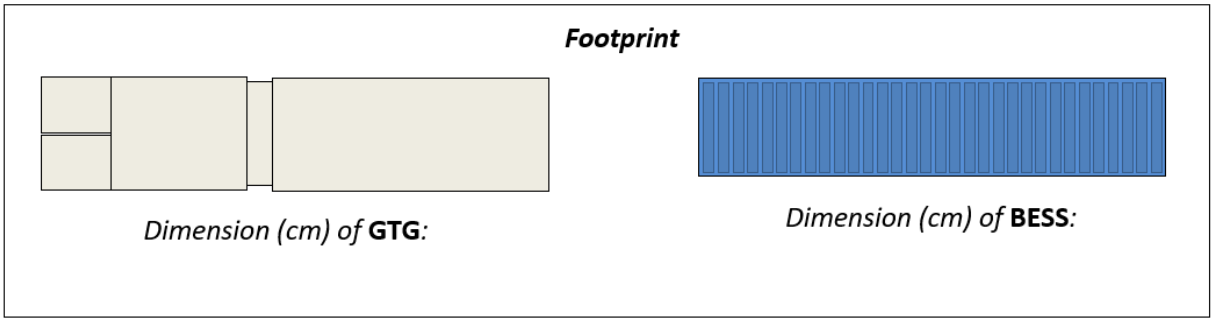

Figure 6.2: Footprint of GTG and BESS comparison.

6.3 Development of the EMS

As discussed in Section 6.2, the footprint of 1*MW* of BESS is comparable to one unit of GTG. If 4*MW* of BESS is used, as demonstrated in Chapter 5, the BESS has to be stacked vertically, which affects structural stability. Hence, it is proposed to study if the EMS is capable of maintaining the output power quality with 2*MW* of BESS, in the presence of wind intermittency and varying load demands. In this section, the components and controllers used in the EMS will be described based on the proposed system in Section 6.2.

A schematic on the overview of the EMS is shown in Figure 6.3. As discussed in Section 2.6.2, the fluctuations due to the intermittency of wind can be supported by the BESS, which has a faster response, as compared to the primary power generation. Hence, the EMS will not be

developed for the GTG as the GTG has a slower rate of dispatch and is primarily supplying fixed loads. The focus of this chapter will be on developing the EMS with the BESS, which is designed to charge and discharge energy from battery bank power to balance the load at PCC as shown in Figure 6.3. Existing technologies are built in the lithium-ion battery bank which potentially improve cycle lifetime, performance and reduces the overall cost with examples found in [71] and [72]. Moreover, BESS is suitable for use during transient period to provide short and fast response time [73].

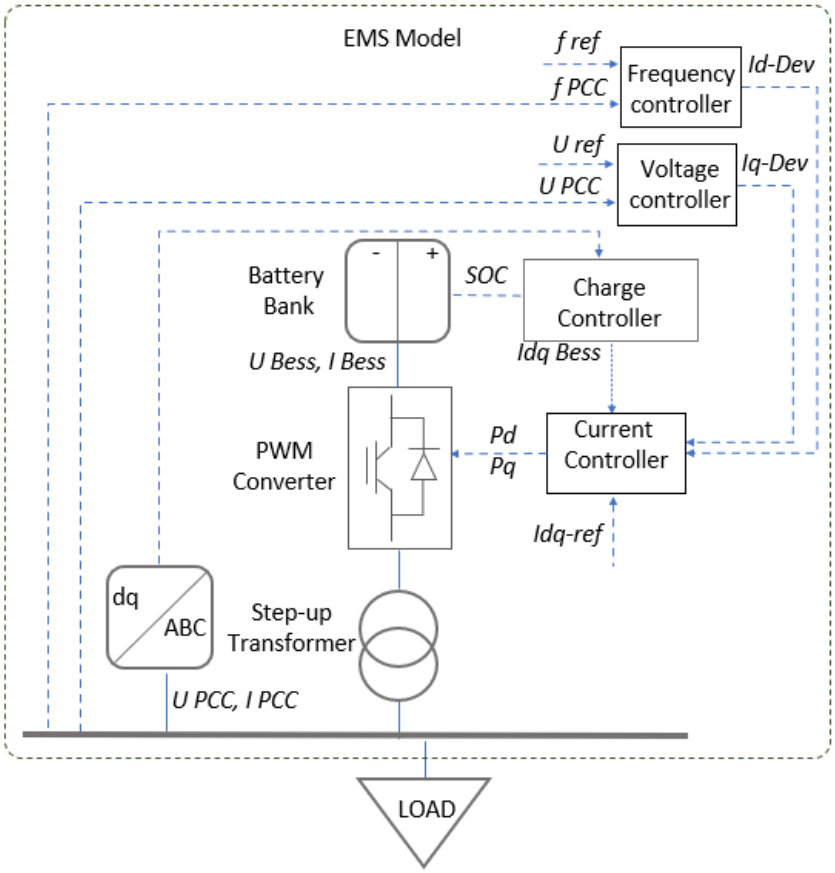

Figure 6.3: Schematic of EMS overview.

In the inverter of the BESS, AC/DC Converter is of a similar type in [74], which is bi-directional and acts either as an inverter to regulate output power to PCC or as a rectifier to regulate excess output power to BESS. On the other hand, the charge controller inject or draw electric current into or from battery bank to maintain a safe level of SOC. There is no doubt that the BESS will be depleted due to constant discharging output power to balance up the total power to meet load demand as there is insufficient output power generated from GTG and WTG during transient period. Hence, BESS will be constantly charged up from the excess power in PCC to maintain its SOC. In addition, the WTG may have inputs on the hourly wind speed forecast, as discussed in [75]. This could be used to provide more output to load and charge the BESS. The demonstration of this scenario will be carried out in Section 6.5.3.

It is expected that the response from BESS to improve transient stability will be rapid as the controllers outputs directly to the VSC known as PWM converter, as shown in Figure 6.3. Despite the fact that the approach in using BESS to balance the load at PCC is comparable to [11], there is a difference in the controller design and implementation. In [11], the scheduling of the flexible loads corresponds to the WTG's instantaneous output, in the event of excess wind, which could be affected by the following:

1. The use of a low pass filter to remove measurement noise on the WTG active power.
2. The communication time constant (delay required for the effective communication between the WT and flexible load with the EMS).

Our EMS has two main components which will be described in detail as follows:

1. Voltage / Frequency controller
2. Current controller

6.3.1 Voltage / Frequency Controller

The design of independent frequency and voltage controllers to generate active and reactive power control signals is shown in Figure 6.4 and 6.5 respectively. The voltage and frequency controllers generate the active current reference signals, I_{d-Dev} and I_{q-Dev} respectively, based on the error, f_{error} and U_{error} between the frequency and voltage from PCC and their references. There is an anti-wind-up limiter in each of the frequency and voltage controllers to prevent a wind-up condition. I_{d-Dev} and I_{q-Dev} show the current offset values require to maintain the set point of active current reference signals while these offset values are sending to the charge controller to control the battery bank for discharging or charging from the PCC. Likewise, power is supplied to or consumed by the PCC depending on the sign of the voltage or frequency errors in the controller.

In the frequency/voltage controller, the functionality of proportional and integral (PI) controller has an identical model described in [64] with anti-windup to prevent undesirable oscillation given a nonlinear system with BESS contributes under the droop setting in GTG. Hence, the equation of the control signals I_{d-Dev} and I_{q-Dev} in frequency/voltage controller is calculated as follows:

$$I_{d-Dev} = K_p(f_{ref} - f_{PCC}) + K_i/T_i \int_0^t [(f_{ref} - f_{PCC})\, dx]_{Y_{min}}^{Y_{max}}, \tag{6.1}$$

$$I_{q-Dev} = K_p(U_{ref} - U_{PCC}) + K_i/T_i \int_0^t [(U_{ref} - U_{PCC})\, dx]_{Y_{min}}^{Y_{max}}, \tag{6.2}$$

where K_p is proportional gain in voltage/frequency controller, f_{ref} is the reference frequency value $[p.u.]$ at PCC, f_{PCC} is the measured frequency deviation value $[p.u.]$ at PCC, U_{ref} is the reference voltage value $[p.u.]$ at PCC, U_{PCC} is the measured voltage deviation value $[p.u.]$ at PCC, K_i/T_i is integral gain in voltage/frequency controller and Y_{max} and Y_{min} is the maximum and minimum values in the anti-windup limiter.

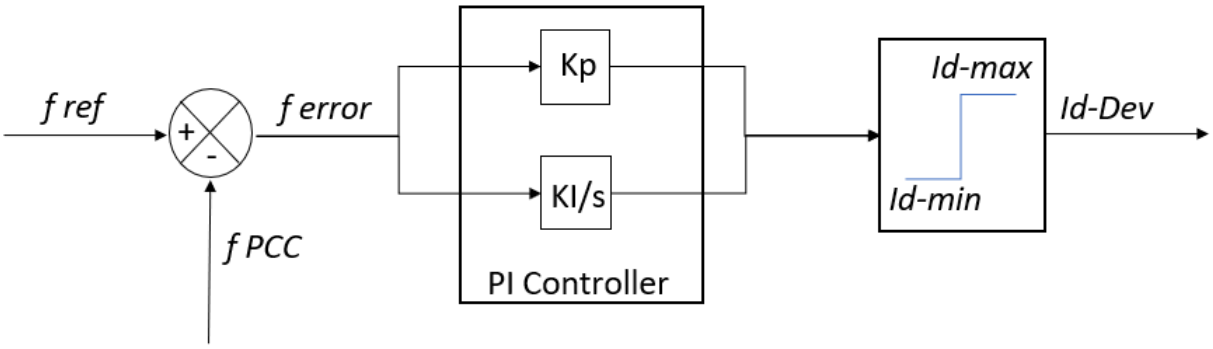

Figure 6.4: Frequency controller model.

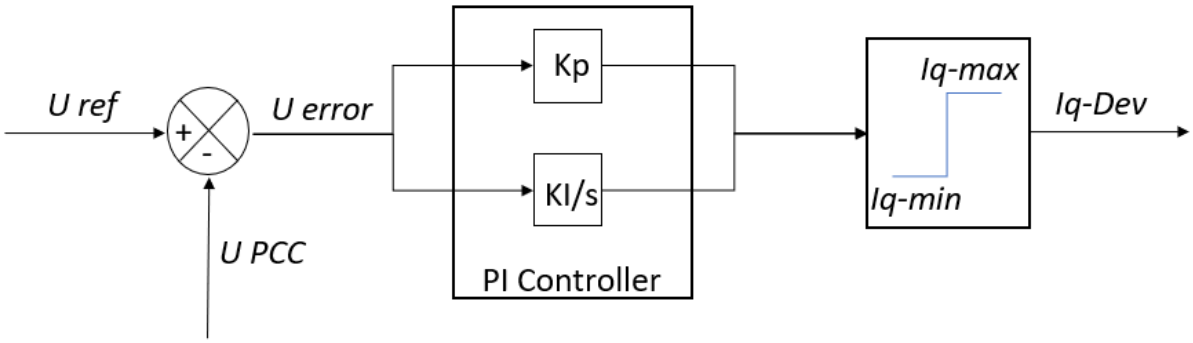

Figure 6.5: Voltage controller model.

6.3.2 Current Controller

The detailed block diagram of the current controller is shown in Figure 6.6 where I_{d-Dev} and I_{q-Dev} are generated from the frequency and voltage controllers in Section 6.3.1. There is similarity in term of the design concept to integrate BESS to the droop control in microgrid which can be found in [11]. The other I_{d-ref} and I_{q-ref} are the signals of nominal power from PCC which are added into current controller assist in regulating optimal output power quality control to meet load demand. The current controller is comparing all of the signals to offset the feedback of the measured current I_{d-BESS} and I_{q-BESS} from the 3 phase distribution lines that is closest to

the BESS. Next, the output signals from current controller has an anti-wind-up limiter to prevent a wind-up condition. This sequence generate P_d and P_q as the optimal output power required on PCC. As such, the resulting controller output is used to regulate the BESS active and reactive current and power, which supports the frequency and voltage at PCC.

The detailed model can be found based on a simple microgrid in the MATLAB/Simulink library.

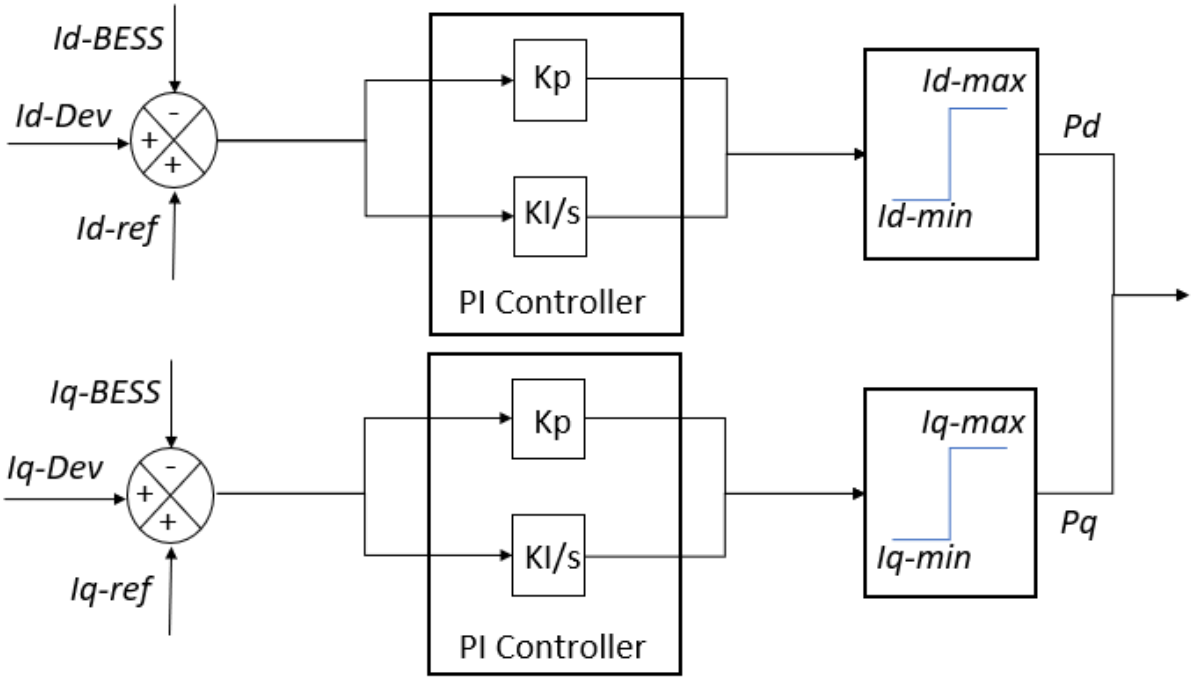

Figure 6.6: Current controller model.

Given that I_{d-Dev} and I_{q-Dev} are described in equation 6.1 and 6.2, the equations of feed forward control in term of frequency, f_{ff} and voltage, U_{ff} in current controller can be defined as:

$$f_{ff} = K_p(I_{d-ref} + I_{d-Dev}) + K_i/T_i \int_0^t [(I_{d-ref} + I_{d-Dev})\, dx]_{Y_{min}}^{Y_{max}}, \tag{6.3}$$

$$U_{ff} = K_p(I_{q-ref} + I_{q-Dev}) + K_i/T_i \int_0^t [(I_{q-ref} + I_{q-Dev})\, dx]_{Y_{min}}^{Y_{max}}, \tag{6.4}$$

where I_{d-ref} and I_{q-ref} are the reference current control signals from PCC.

Since EMS models of viable controllers have been depicted in Figure 6.4, Figure 6.5 and Figure 6.6, the transfer function of the designed EMS embedded in BESS is presented as follows:

$$I_d(s) = \Delta F_{PCC}(s)[K_P(s) + K_i/s], \tag{6.5}$$

$$I_q(s) = \Delta U_{PCC}(s)[K_P(s) + K_i/s], \tag{6.6}$$

where $I_{dq}(s)$ is the output current of d-axis ($p.u$) and q-axis ($p.u$) within inner loop of VSC, $\Delta F_{PCC}(s)$ is the output transient frequency deviation ($p.u$), $\Delta U_{PCC}(s)$ is the transient voltage deviation, $K_p(s)$ is the proportional gain ($p.u.$) in EMS and K_i/s is the integral gain ($p.u.$) in EMS.

6.3.3 Optimal Proportional and Integral (PI) Parameters

In this section, the optimal PI gain parameters in the PI controller for the best transient response results, in terms of the output voltage and frequency, will be determined and discussed.

The transient response results will be presented in terms of the voltage and frequency deviations, so as to evaluate power stability [10]. Figure 6.7 shows the system's voltage transient response when the GTG and BESS are turned on to meet an increase in load demand. It is shown that there is a surge in the output power when there is a step up in load. For such a step response, the desired response characteristics should have minimal overshoot, short rise time and fast settling time to reach a steady state output. For a range of proportional gain.K_p from 1 to 5 with a constant integral gain of $K_i = 1$, it is observed that the overshoot, settling time and steady state error vary across the range of controller parameters. The output response with $K_p = 3$ and $K_i = 1$ provides a smaller overshoot at 12.5% and settles down to reach a steady state at 1.036 $p.u.$ in the shortest time.

The other parameters $k_P = 1$ and $k_P = 2$ are not chosen to be optimal parameters due to a slower stabilisation and oscillation at steady state. On the other hand, $k_P = 5$ has a lower surge of 1.123 $p.u.$ than $K_p = 3$, which stabilises the fastest at 1.036 $p.u.$ after 12 s.

Figure 6.8 shows the system's frequency transient response when the GTG and BESS are turned on the meet an increase in load demand. It is observed that a range of parameters demonstrate similar frequency deviation. During the simulation in frequency deviation at 10 s, there is a dip of 0.991 $p.u.$ followed by a surge of 1.003 $p.u.$ before reaching the steady state of 1 $p.u.$. This is due a spike of voltage deviation at 10 s, causing a transient frequency deviation, which ends after about 13 s.

The results on voltage and frequency deviations for a varying range of proportional, K_p and integral, K_i values are summarised in Table 6.1.

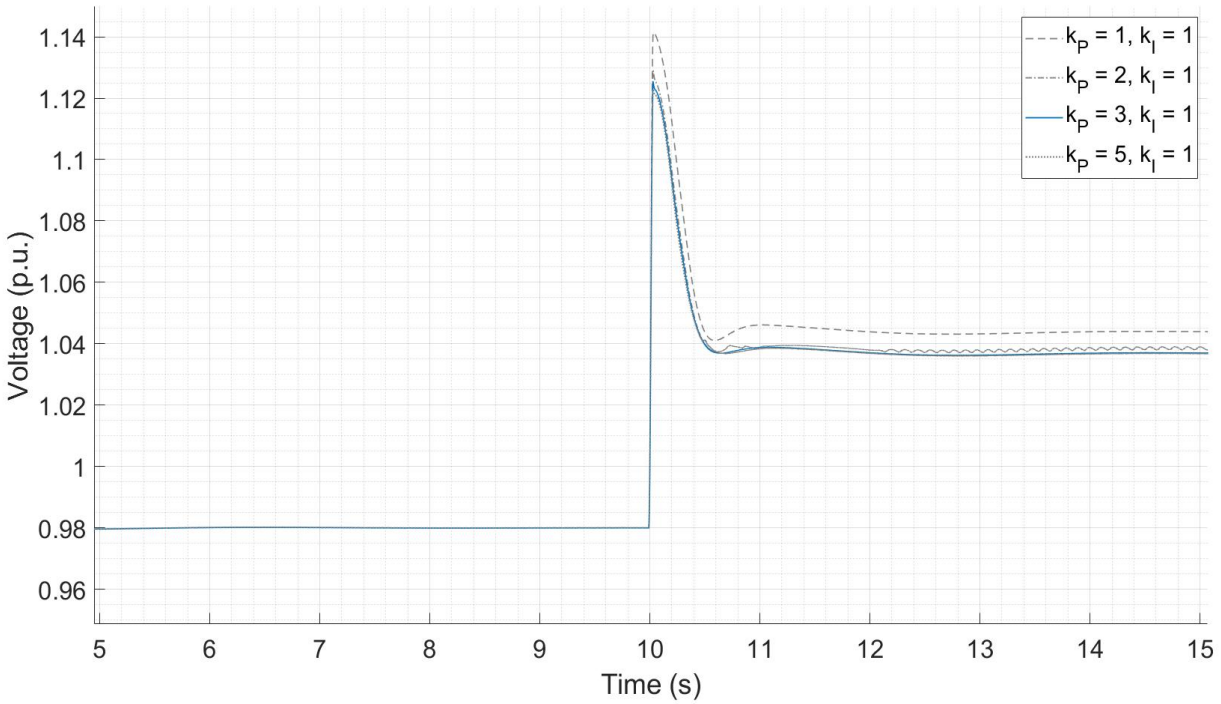

Figure 6.7: Analysis of PI controller's parameters during transient period in voltage (p.u.) when GTG and BESS are turned on. (Base load = 10 *MW*).

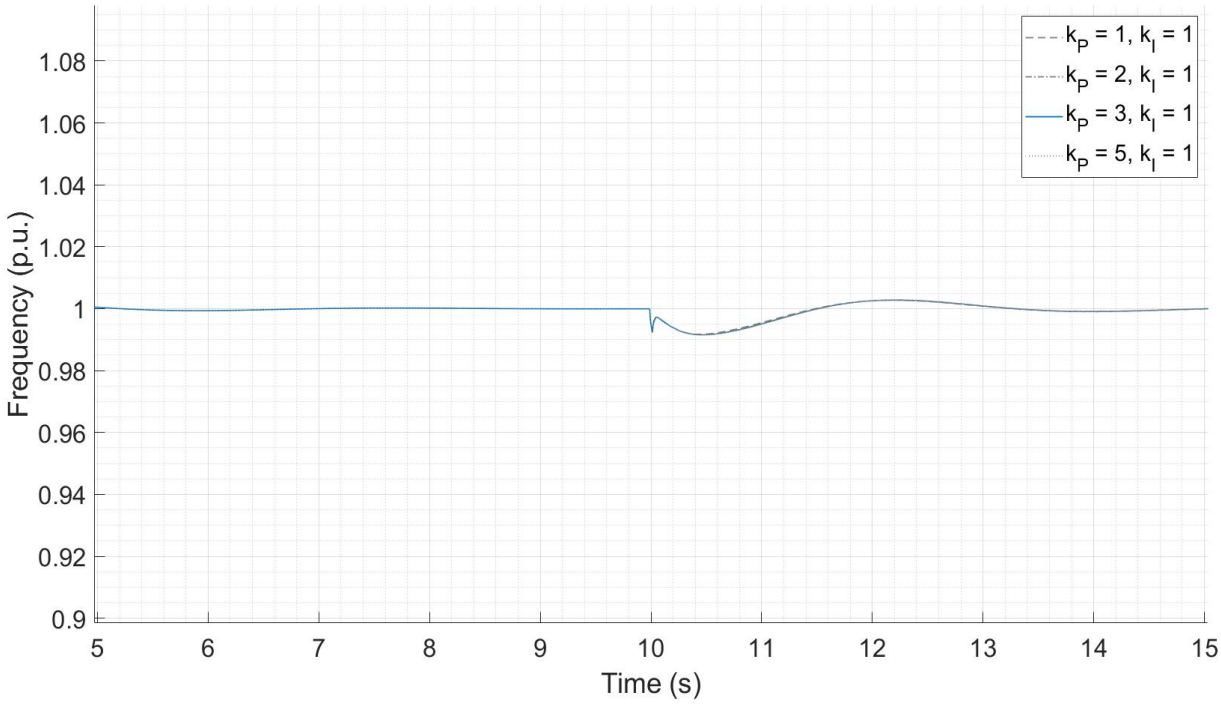

Figure 6.8: Analysis of PI controller's parameters during transient period in frequency (p.u.) when GTG and BESS are turned on. (Base load = 10 *MW*).

Table 6.1: Results of voltage and frequency deviation in optimal PI parameters

Parameters	Voltage Deviation (%)	Frequency Deviation (%)
K_P=1, K_I=1	14	0.3/-0.9
K_P=2, K_I=1	13	0.3/-0.9
K_P=3, K_I=1	12.5	0.3/-0.9
K_P=5, K_I=1	12	0.3/-0.9

6.4 Results and Analysis

In this section, our designed EMS in proposed system will be analysed using the optimal parameters for a PI controller in Section 6.3.3, which will be compared with the state of the art for better power quality in the scenarios due to disturbances of dynamic load and stochastic wind speed. The generated results will be evaluated for maximum/ continuous voltage and frequency deviation in PCC, which affects output power quality to load demand.

6.4.1 Test scenarios

Test scenarios were developed in Chapters 3, 4 and 5 to provide a comparison of transient stability between the conventional and proposed systems. In this section, test events are created to evaluate the transient stability, in the presence of step changes in load and stochasticity in wind. The transient stability results are compared to the IEC standards 61892-1 for the O&G industry, as discussed in the Section 2.5.

The four test scenarios are shown in Table 6.2. The test loads comprise of the fixed and flexible loads, which are discussed in Section 6.2, while primary power generation comprise of the GTG and WTG. The primary power generation will supply output power to load through all four test scenarios. Event 1 simulates the case where the GTG and WTG meet the fixed load demand. Event 2 simulates a step up to power both fixed and flexible loads. The BESS is turned on to study the transient stability results where the BESS rapidly discharges to PCC. In Events 1 and 2, it is assumed that the wind speed stays constant. In Event 3, stochasticity in wind speed is simulated to investigate if the output voltage and frequency at PCC meet the IEC standards. In the last event where the BESS require charging, only the fixed loads will be supplied. This event will also be compared to the IEC standards. Event 4 is worthwhile to be carried out in simulation as it has been aforesaid for an unaccomplished task in the state of the art [67], [11].

As the test scenarios are proposed to demonstrate the superiority of our designed EMS in improving the output power quality, in the event of wind intermittency and load variation, it is important to note that the power generation profiles and the load demand are of actual sizing that corresponds to those in the current state of art for a fair comparison.

Table 6.2: Test Scenarios

Event No	Description	Load Test
1	Disconnected BESS	Fixed
2	BESS is turned on	Fixed, Flexible
3	BESS is turned on with stochastic wind speed	Fixed, Flexible
4	BESS is charging from excess output power in PCC	Fixed

6.5 Simulation Test Results

Given the four test scenarios as shown in Table 6.2, the simulation results are compared against the IEC standards 61892-1 for maximum transient and continuous voltage and frequency deviation in this section. These four scenarios are simulated and plotted in MATLAB/Simulink. With our design in EMS, GTG and WTG will supply output power in PCC simultaneously to balance the load consumption. Meanwhile, the BESS will operate either to discharge output power or charge by consuming excess power from PCC, which provides transient stability improvement. Conventionally, BESS without EMS is proven in the previous Chapters 3, 4 and 5, which has been shown to improve the output power quality [51], [61], [62]. The results are shown in Sections 6.5.1 to 6.5.3.

6.5.1 Case 1: Event 1 is switched to Event 2

At the start of Event 1 extracted from Table 6.2 in Section 6.4.1, GTG and WTG are turned on at $t = 0\ s$ to provide output power for fixed load consumption at 0.6 $p.u.$. A power analysis of individual power generation profiles is provided for our proposed system with energy management system (PSEMS), as shown in Figure 6.9. It can be observed that the start-up in power generation led to a high surge in the primary power generation, The steady state condition is reached at 2 s, where constant output power is provided to the fixed load. At constant wind speed in Event 1, the WTG provides an output power of 0.33 $p.u.$ to fixed load as the primary power generation source with a 9.6 m/s wind speed. GTG provides for the remaining fixed load consumption at 0.28 $p.u.$.

At $t = 10\ s$, Event 1 is switched to Event 2 where the flexible load is turned on together with the fixed loads, totalling to 1 $p.u.$ of load. At the same time, the BESS with a capacity of 0.2 $p.u.$ is turned on to supply output power to improve the transient stability due to load variation

at this time. It can be seen that the GTG responds to the step up in load with a surge of approximately 0.62 $p.u.$, followed by a dip of 0.3 $p.u.$ and stabilised at 11 s. Likewise, the WTG has also responded with a surge of 0.43 $p.u.$, followed by a gradual decline to an output of 0.38 $p.u.$ at 15 s. The BESS embedded with EMS is observed to reach 0.2 $p.u.$ at 10.3 s. It can be seen that both the GTG and WTG has increased their output to meet the increase in load demand as the input from the BESS saturates close to 0.2 $p.u.$. At $t = 15$ s, a lower wind speed of 8 m/s is simulated. As such, the flexible load is disconnected, leaving the fixed load with the primary power generation and BESS. It can be seen that the GTG reacted immediately with a dip of 0.1 $p.u.$ at 16 s, followed by a surge of 0.4 $p.u.$ before stabilising at 0.28 $p.u.$ at 18 s. On the other hand, WTG reacted with a dip of approximately 0.8 $p.u.$ near to 16 s before stabilising at 0.23 $p.u$ at 18.5 s. Likewise, BESS reacted with a dip of 0.16 $p.u.$ before stabilising at 0.16 $p.u$ at 18 s. This meets the fixed load consumption of 0.6 $p.u.$. Throughout the entire simulation test, BESS is close to full charge.

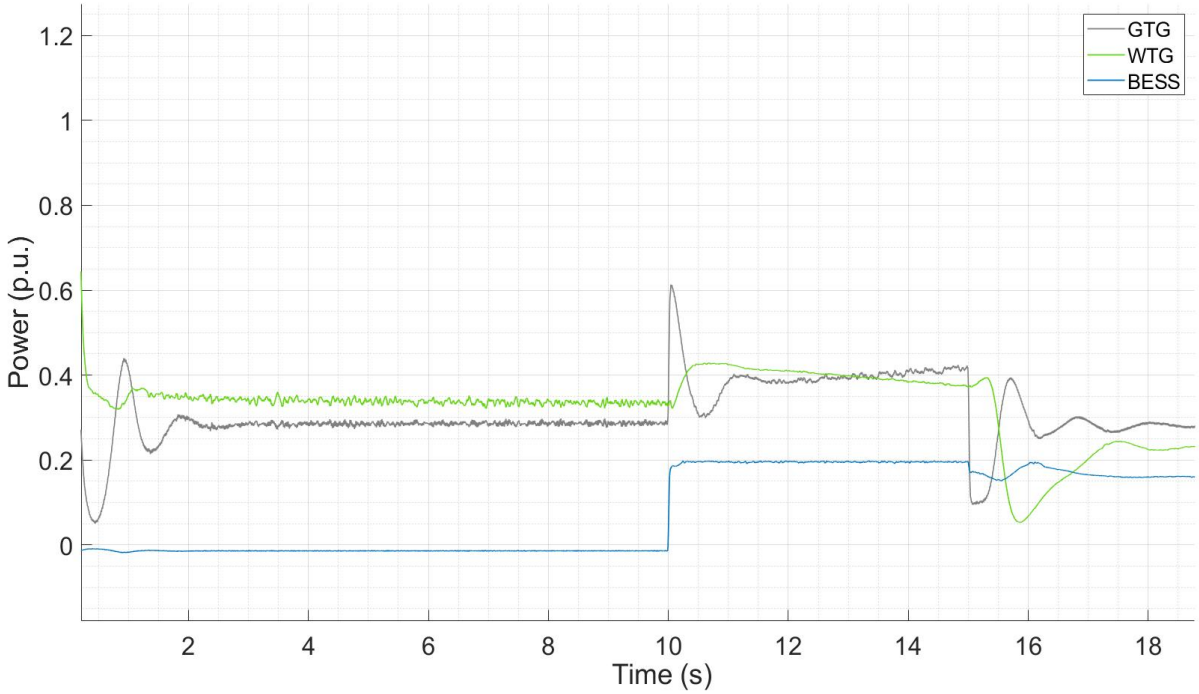

Figure 6.9: Individual power generation profiles from PSEMS.

It has been shown in the power flow analysis in Figure 6.9 that PSEMS is capable of meeting the total load consumption of the fixed and flexible loads. In the event of a drop in wind speed, it is possible to maintain output power to the fixed loads with the BESS. In order to study the transient stability results, the same simulation is conducted for our proposed system with no EMS. The results are shown in Figure 6.10.

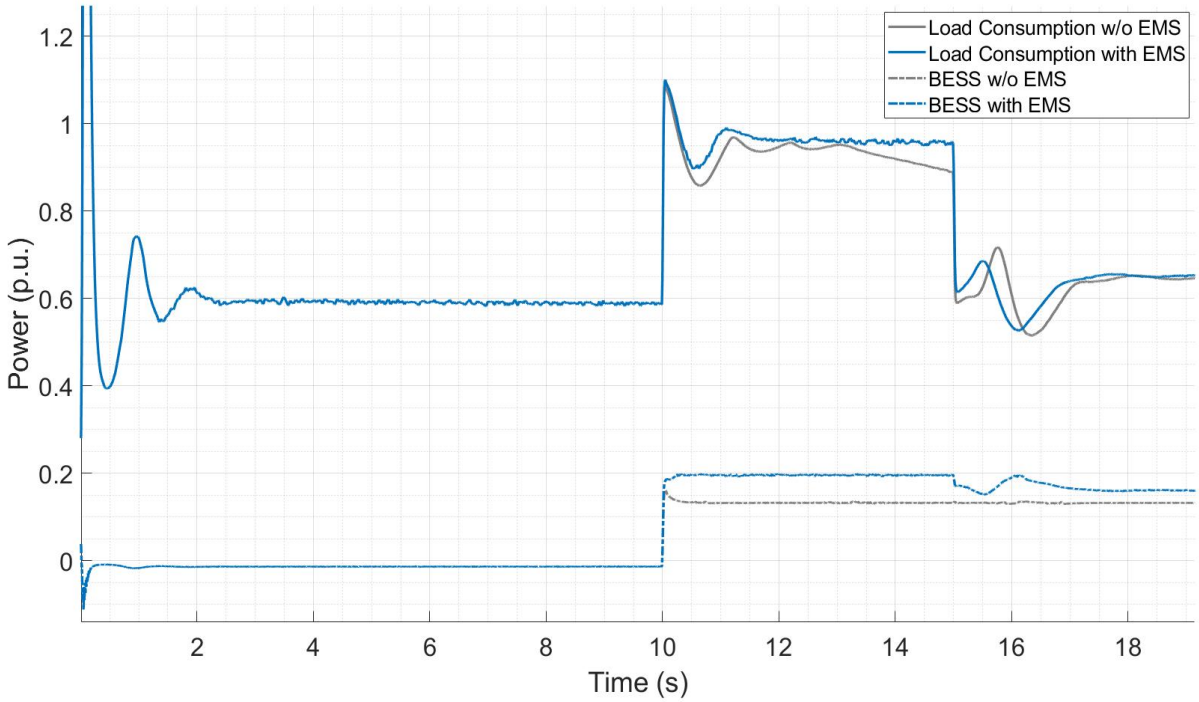

Figure 6.10: Load consumption is based on proposed system either with EMS or no EMS during Event 1 is switched to Event 2.

At $t = 10\ s$, Event 1 is switched to Event 2. The load consumption with EMS surges to 1.1 $p.u.$, followed by a dip of 0.9 $p.u.$ before settling down to 0.95 $p.u.$ at 12 s. In contrast to the load consumption without EMS, a similar surge of 1.1 $p.u.$ is observed, followed by a bigger dip of about 0.85 $p.u.$ before oscillating at 0.95 $p.u.$ at 12 s and a gradual decline to 0.9 $p.u.$ at 14.5 s. It is demonstrated that the load consumption without EMS has a higher continuous deviation of 0.1 $p.u.$, compared to that in PSEMS of 0.05 $p.u.$. It can also be observed that the BESS without EMS is supplying an output power of approximately 0.14 $p.u.$, as compared to the BESS embedded with EMS, which is capable of maintaining 0.2 $p.u.$ in output power. At $t = 15\ s$, a lower wind speed of 8 m/s is simulated. As such, the flexible load is disconnected, leaving the fixed load with the primary power generation and BESS. It is observed that the load consumption without EMS reacted slower with a dip of 0.51 $p.u.$ at 16.4 s before reaching a steady state at 18 s. The PSEMS has a faster response during the transient period with a dip of 0.51 $p.u.$ at 16.1 s before settling down at 18 s.

Figure 6.11 presents the simulation results of the voltage at PCC for the proposed system embedded with EMS and without EMS. The voltage deviation is compared to the IEC standards given in Section 2.5. At the start of Event 1, a voltage oscillation with a surge of 1.11 $p.u.$ followed by a dip of 0.95 $p.u.$ from 0 to 2.5 s is observed before the voltage stabilised to steady state. This is due to the starting up of the individual power generations in the GTG and WTG.

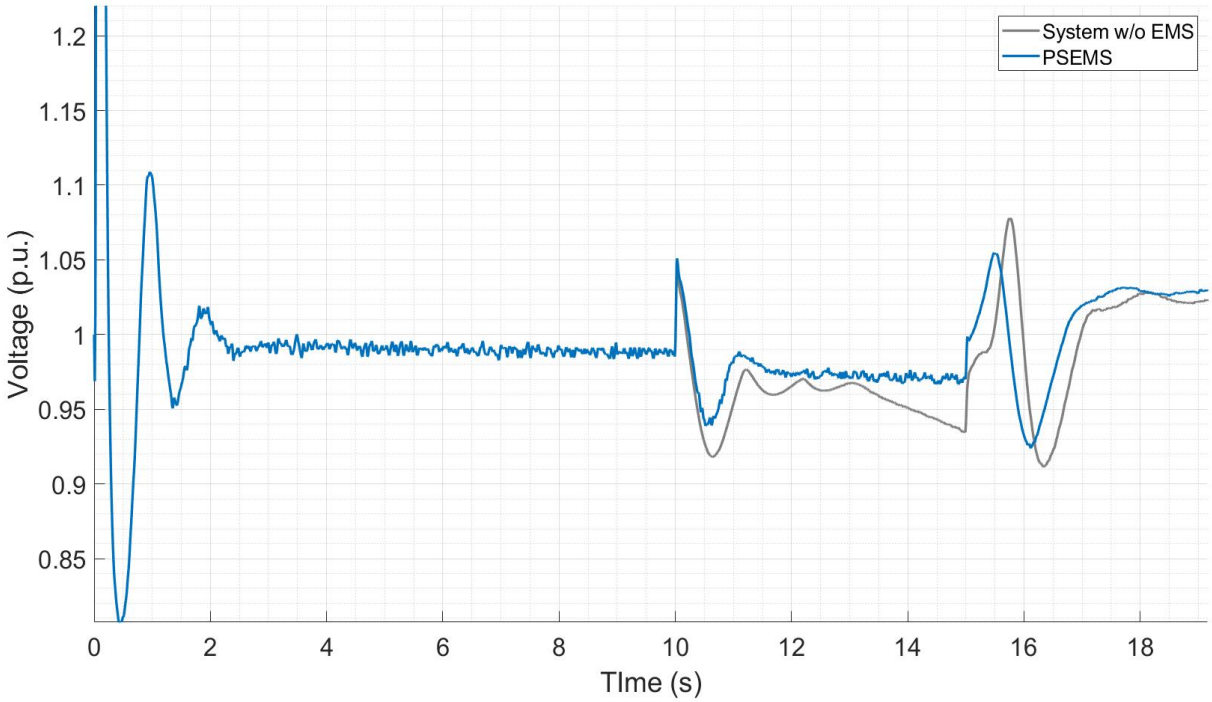

Figure 6.11: Output voltage (p.u.) is based on proposed system either with EMS (PSEMS) or no EMS when Event 1 is switched to Event 2.

As shown in the figure, the rated voltage flows to the fixed load is at 0.99 $p.u.$ with a -1 % in continuous voltage deviation for both systems.

When Event 1 is switched to Event 2 at $t = 10$ s, both systems have a similar surge of 1.05 $p.u.$ followed by a dip range between 0.92 to 0.94 $p.u.$. It is observed that PSEMS has a maximum voltage deviation of 5/-6 % and a transient period of 2 s whereas proposed system without EMS has a maximum voltage deviation of 5/-8 % before oscillating at 11 s and showing a gradual decline in voltage. Subsequently, PSEMS is maintaining output voltage at 0.97 $p.u.$, with a -3 % in continuous voltage deviation. On the other hand, the system without EMS oscillated in the output voltage and showed a gradual decline to approximately 0.93 $p.u.$, which is -7% in voltage deviation. At $t = 15$ s, a lower wind speed of 8 m/s is simulated. As such, the flexible load is disconnected, leaving the fixed load with the primary power generation and BESS. It is shown that PSEMS has a maximum voltage deviation of 5.5/-7.5 %, whereas the system without EMS has a maximum voltage deviation of 8/-9 %. The PSEMS sustained at a continuous voltage deviation of 3 % with voltage flow of 1.03 $p.u.$ at 17.2 s while the system without EMS shows an oscillating voltage of around 1.03 $p.u.$ at $t = 18$ s. It is shown that the PSEMS meets the IEC standards 61892-1 for maximum and continuous voltage deviation.

Figure 6.12 presents the frequency deviation results for PSEMS and the system without

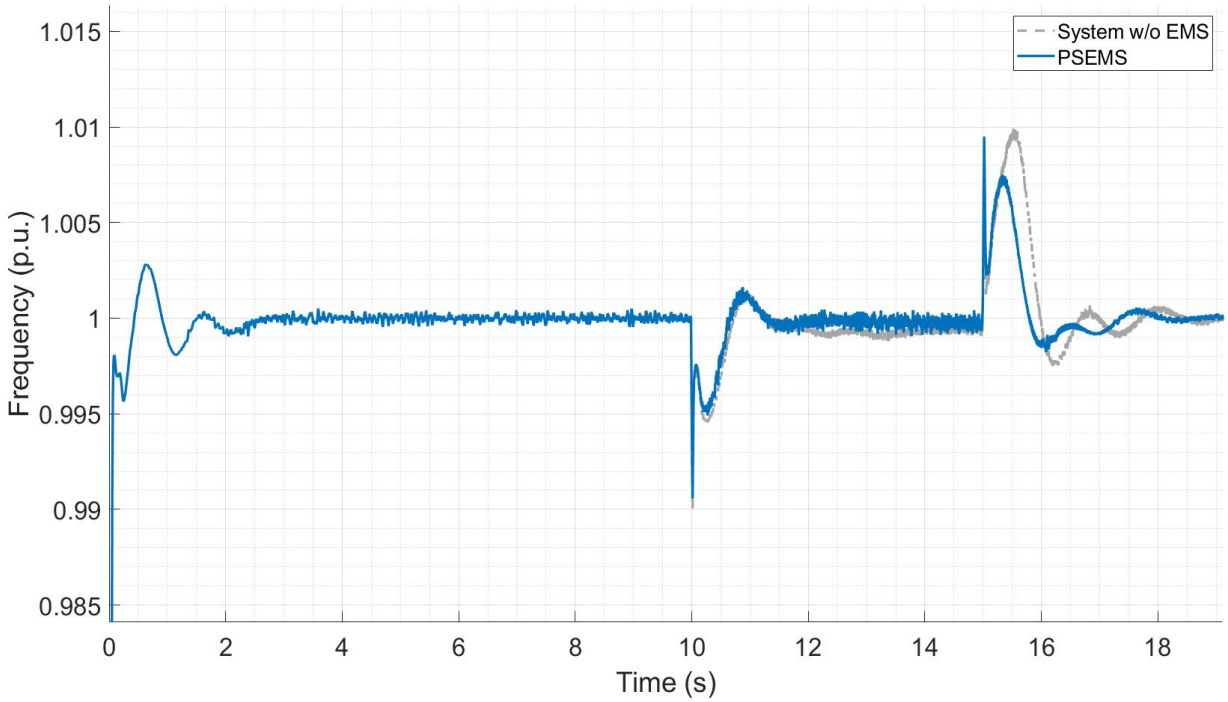

Figure 6.12: Output frequency (p.u.) is based on proposed system either with EMS (PSEMS) or no EMS when Event 1 is switched to Event 2.

EMS. At the start of Event 1, the output frequency at PCC has a surge of 1.005 $p.u.$ followed by a dip to 0.998 $p.u.$ before reaching steady state of 1 $p.u.$ at 2.5 s. At $t = 10$ s, the PSEMS dipped to 0.9905 $p.u.$, followed by a surge of 1.001 $p.u.$ before reaching steady state of 1 $p.u.$ in 11.5 s. This reflects 0.1/-0.95 % in maximum frequency deviation with 0 % in continuous frequency deviation for PSEMS. The system without EMS dipped at 0.99 $p.u.$, followed by a surge of 1.001 $p.u.$ before reaching steady state of 0.999 $p.u.$ in 11.5 s. Hence, this reflects 0.1/-1 % in maximum frequency deviation and 0.1 % in continuous frequency deviation. At $t = 15$ s, a lower wind speed of 8 m/s is simulated. As such, the flexible load is disconnected, leaving the fixed load with the primary power generation and BESS. The PSEMS has a surge of 1.0095 $p.u.$ followed by dip at 0.9985 $p.u.$ and the system without EMS has a surge of 1.01 $p.u.$ followed by dip at about 0.9975 $p.u.$. Thus, the PSEMS demonstrates a 0.95/-0.15 % in maximum frequency deviation, whereas the system without EMS shows a 1/-0.25 % in maximum frequency deviation. Following this, both systems reached a steady state at 1 $p.u.$ in 18 s with 0 % in continuous frequency deviation.

In summary, the voltage deviation and frequency deviation results for Case 1 are shown in Table 6.3. The system without EMS is abbreviated as "System w/o EMS". In term of voltage deviation, there is an improvement in PSEMS with 5/-6 % and 5.5/-7.5 % as compared to the system without EMS with 5/-8 % and 8/-9 %. A similar outcome in frequency deviation is

observed where PSEMS has a 0.1/-0.95 % and 0.95/-0.15 % in frequency deviation, which are better than the system without EMS with 0.1/-1 % and 1/-0.25 % in frequency deviation.

Table 6.3: Results of voltage and frequency deviation in Case 1

Event	Voltage Deviation (%)		Frequency Deviation (%)	
	System w/o EMS	PSEMS	System w/o EMS	PSEMS
Flexible load is turned on with BESS	5/-8	5/-6	0.1/-1	0.1/-0.95
Flexible load is disconnected with a lower wind speed	8/-9	5.5/-7.5	1/-0.25	0.95/-0.15

6.5.2 Case 2: Event 1 is switched to Event 3

In the previous section, it has been shown that PSEMS has a lower voltage and frequency deviation, which meets the IEC standards, as compared to the system without EMS. As such, the PSEMS will be compared against the current state of the art in [11] with an identical test scenario. The exact range of the wind profile is not discussed in [11] and hence, it is assumed that the wind speed varies between 6 m/s to 10 m/s for the PSEMS simulation. In the state of the art, the BESS is also used to alleviate the stochasticity in wind and addition of flexible loads, which is simulated as a change from Event 1 to Event 3.

The simulation results of the voltage at PCC for the PSEMS is shown in Figure 6.13 when Event 1 is switched to Event 3. At the start of Event 1, the output voltage of PSEMS is at 0.99 $p.u.$ to fixed load, which results in -1 % in continuous voltage deviation. When Event 3 starts at $t = 10$ s, the output voltage has a high surge of 1.051 $p.u.$, followed by a dip of 0.939 $p.u.$ at approximately 10.6 s before retracting to 0.99 $p.u.$ slightly after 11 s. This results in a 5.1/-6.1 % in maximum voltage deviation, which is compared against the U_{MAX} and U_{MIN} of 1.086 and 0.91 respectively in [11]. As such, the Previous U_{MAX} and Previous U_{MIN} in the state of the art generate 8.6/-9 % in maximum voltage deviation, which are 3.5/-2.9 % more than PSEMS. It is also observed in Figure 6.13 that the output voltage starts to oscillate between 0.955 $p.u.$ and 0.975 $p.u.$ at 11 s due to inconsistent output power from the WTG. The GTG is not able to react instantaneously to fluctuations in the wind power output and BESS is providing support to the output voltage to maintain the output power quality. On average, the PSEMS provides -4.5 % in continuous voltage deviation, which meets the IEC standards for both maximum and continuous voltage deviation.

The simulation results of the frequency at PCC for the PSEMS is shown in Figure 6.14. At the start of Event 1, output frequency is at 1 $p.u.$ up until $t = 10$ s. Once Event 3 starts at $t =$

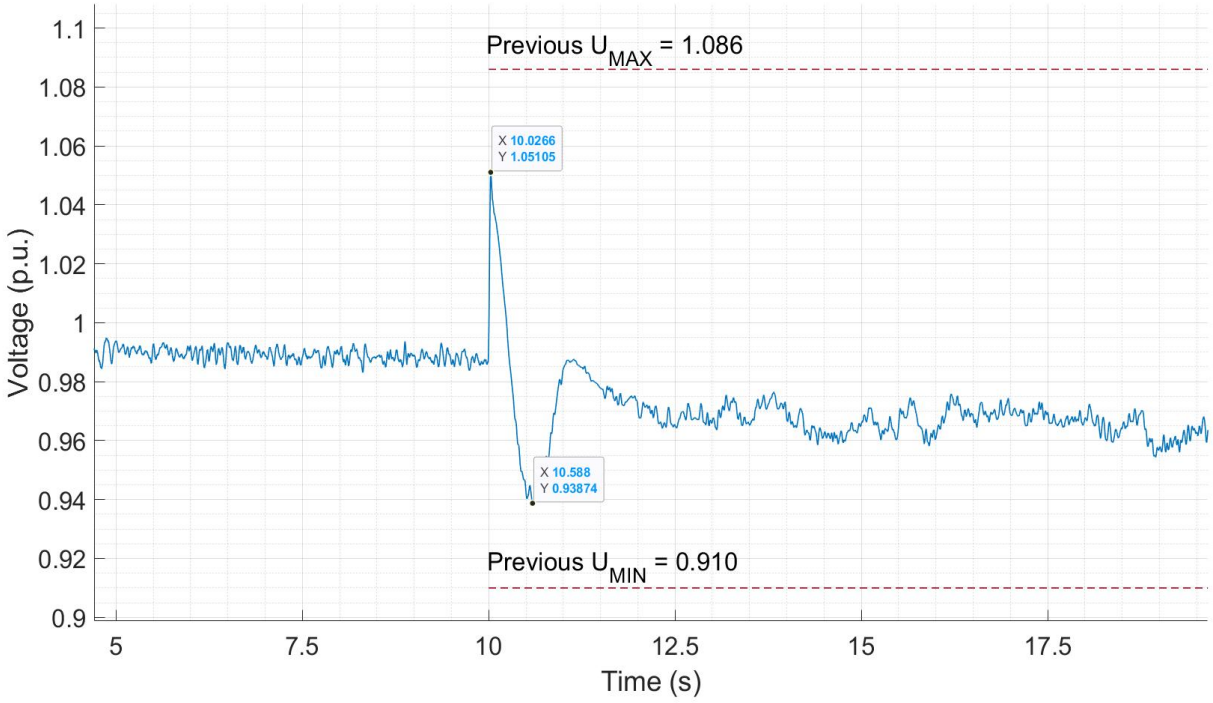

Figure 6.13: PSEMS of output voltage when Event 1 is switched to Event 3.

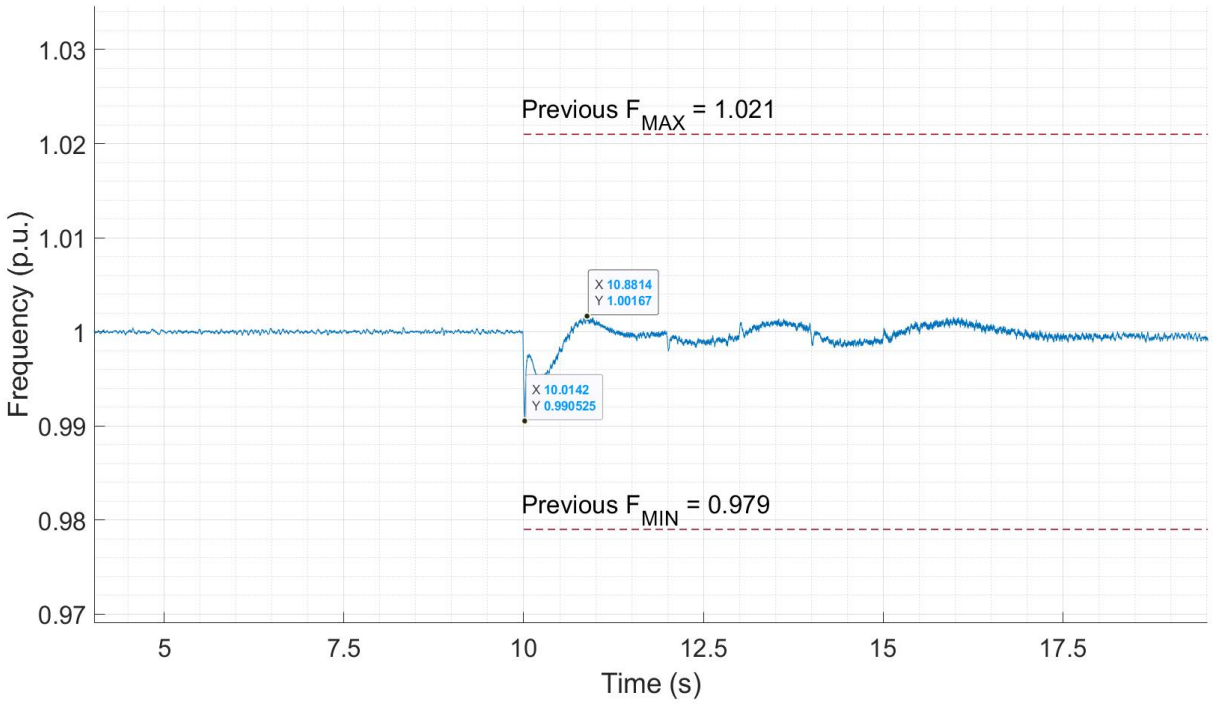

Figure 6.14: PSEMS of output frequency when Event 1 is switched to Event 3.

10 s, there is a dip to 0.9905 $p.u.$, followed a low surge of 1.0016 $p.u.$ in output frequency. This transient period with a time duration of nearly 1 s reflects 0.16/-0.95 % in maximum frequency deviation. The F_{MAX} and F_{MIN} in the state of the art have 1.021 $p.u.$ and 0.979 $p.u.$ respectively that generate 2.1/-2.1 % in maximum frequency deviation [11]. Thus, the previous F_{MAX} and previous F_{MIN} are 1.94/-1.15 % higher in maximum frequency deviation, as compared to the PSEMS. It is also observed in Figure 6.14 after $t = 11$ s that the PSEMS output frequency oscillates between 1.0016 $p.u.$ and 0.9984 $p.u.$, which represents 0.16/-0.16 % in continuous frequency deviation. As such, the PSEMS meet the IEC standards for both maximum and continuous frequency deviation.

In summary, both voltage deviation and frequency deviation for Case 2 are shown in Table 6.4. The proposed system with EMS is abbreviated as PSEMS while results from state of art is found in [11]. When fixed load is switched to flexible load followed by stochastic wind speed, there is an improvement in the voltage deviation in PSEMS with 5.1/-6.1 % as compared with result from state of art having 8.6/-9 %. Likewise, there is a significant reduction of 3.5/-2.9 % improvement in voltage deviation when our designed EMS is compared with the current state of art. For frequency deviation, the outcome is similar as the PSEMS demonstrates 0.1/-0.95 % in frequency deviation, which is smaller than that of the state of art at 2.1/-2.1 %. Hence, there is a significant reduction of 1/-1.15 % improvement in frequency deviation when our designed EMS is compared against the current state of the art.

Table 6.4: Results of voltage and frequency deviation in case 2

Event	Voltage Deviation (%)		Frequency Deviation (%)	
	PSEMS	State of Art	PSEMS	State of Art
Flexible load is turned on with BESS	5.1/-6.1	8.6/-9	0.16/-0.95	2.1/-2.1

The transient values obtained from the simulation result in PSEMS are compared against the metrics from the current state of the art [11], as shown in Table 6.5. In term of frequency analysis during transient period, PSEMS shows results of 1.0016 $p.u.$ in F_{max} and 0.9905 $p.u.$ in F_{min}, which are better than the state of the art of 1.021 $p.u.$ in F_{max} and 0.979 $p.u.$ in F_{min}. For voltage analysis, PSEMS achieved 0.9905 $p.u.$ in U_{max} and and 0.938 $p.u.$ in U_{min}, which are also better than the state of the art of 1.086 $p.u.$ in U_{max} and 0.910 $p.u.$ in U_{min}. F_{RMSD} and U_{RMSD} are derived from the root mean square deviation, $RMSD$, which is calculated in Equation 6.7:

$$RMSD = \sqrt{\frac{\sum_1^N (X-1)^2}{N}}, \tag{6.7}$$

where X relates to measured voltage or measured frequency and N is the number of the samples taken. In terms of F_{RMSD}, PSEMS has the values of 0.0068 $p.u.$ which is lesser, as compared with state of the art of 0.021 $p.u.$. For U_{RMSD}, PSEMS has the values of 0.057 $p.u.$ which is lesser, as compared with state of the art of 0.088 $p.u.$. Hence, there is an improvement in PSEMS with 67.6% on F_{RMSE} and 35.2% on U_{RMSE}.

Table 6.5: Results of voltage and frequency deviation in PSEMS and state of the art

Metrics	PSEMS ($p.u.$)	State of Art ($p.u.$)	PSEMS Improvement (%)
F_{max}	1.0016	1.021	1.9
F_{min}	0.9905	0.979	1.2
F_{RMSD}	0.0068	0.021	67.6
U_{max}	1.051	1.086	3.2
U_{min}	0.938	0.910	3.1
U_{RMSD}	0.057	0.088	35.2
U / F_{max}	0.990	1.086	7
U / F_{min}	1.051	0.910	4.3

6.5.3 Case 3: Event 1 is switched to Event 4

This section is a study of the future test stated in [11] to demonstrate that excess output power in PCC can be used to charge the BESS. As such, BESS is simulated in a charging scenario where Event 1 is switched to Event 4. The load flow analysis of individual power generation, comprising of GTG, WTG and BESS is presented in Figure 6.15. At the start of Event 1 with a constant wind speed of 9.6 m/s, the GTG and WTG are generating an output power of 0.28 $p.u.$ and 0.33 $p.u.$ respectively to balance the fixed load consumption of 0.6 $p.u.$ without any excess power. At $t = 10$ s, Event 1 is switched to Event 4, in which a BESS with a SOC of 50% is connected with no change in load and a constant wind speed of 9.6 m/s. It is shown in Figure 6.15 that there is an increase of output power from GTG that caused a surge from 0.28 $p.u.$ to approximately 5.9 $p.u.$. During this transient period which ended at 10.5 s, the WTG has gradually injected more output power, which provided the excess output power to charge the BESS. This resulted in a power surge to -0.27 $p.u.$ to charge the BESS during the transient period. Following this, BESS charges at 0.18 $p.u.$ consistently till $t = 15$ s. This excess output power of 0.18 $p.u.$ is gained from the GTG, which generated an output power from 0.38 $p.u.$ at about 11 s to 0.42 $p.u.$ at 15 s while the WTG generated an output power from 0.42 $p.u.$ at about 11 s to 0.38 $p.u.$ at 15 s.

The output voltage and frequency analysis for PSEMS when Event 1 is switched to Event 4 is presented in Figure 6.16. At the start of Event 1, PSEMS has an output voltage of 0.99 $p.u.$ till $t = 10$ s before Event 4 starts. Thereupon, there is an immediate surge of 1.024 $p.u.$ followed by 0.937 $p.u.$ in output voltage during transient period of 1 s. This has resulted in a maximum

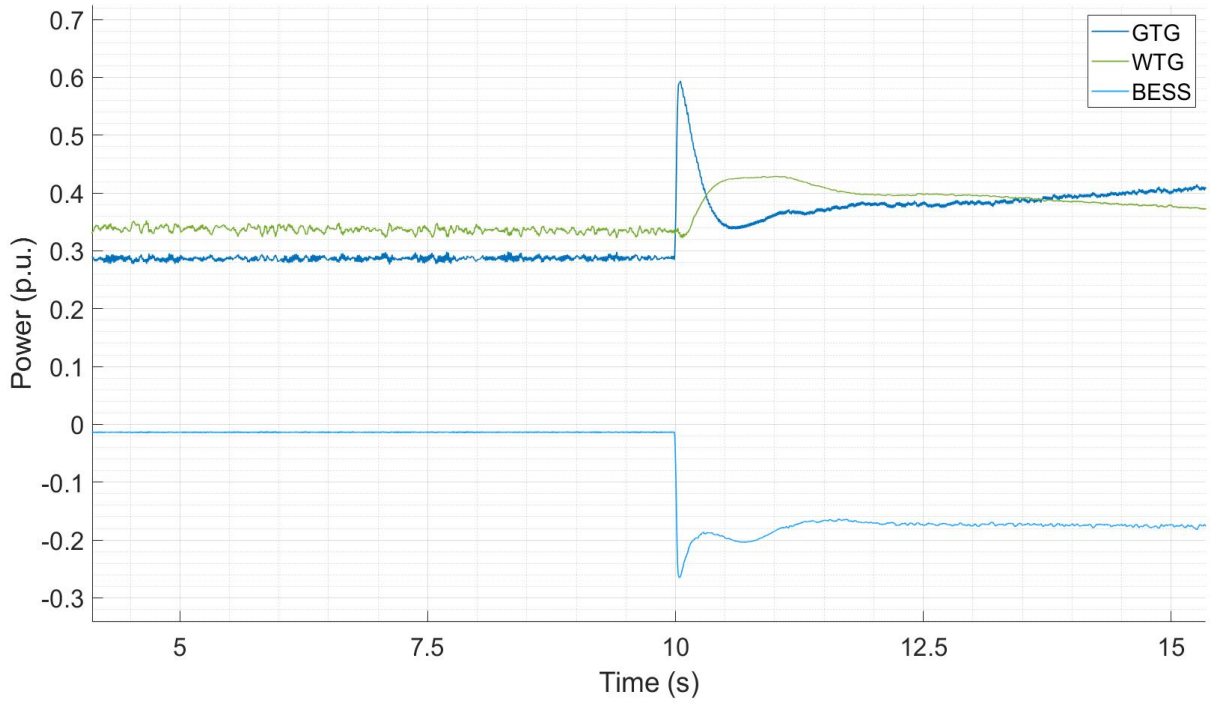

Figure 6.15: PSEMS of individual power generation when Event 1 is switched to Event 4.

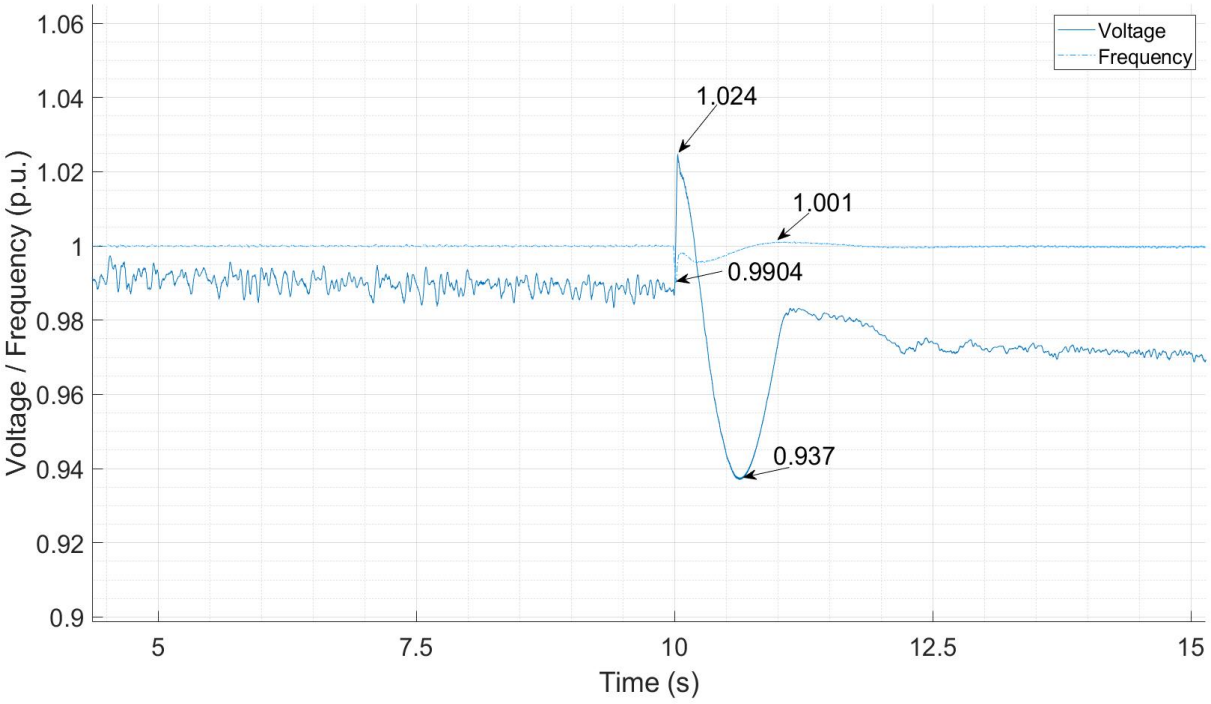

Figure 6.16: PSEMS of output voltage and output frequency when Event 1 is switched to Event 4.

voltage deviation of 2.4/-6.3 % when BESS is switched on to charge the excess output power from the PCC. Beyond $t = 11\ s$, the output voltage has fallen to 0.97 $p.u.$, which represents 3 % in continuous voltage deviation. The output frequency is at 1 $p.u.$ at the start of Event 1 till $t = 10\ s$. Once Event 4 starts at $t = 10\ s$, there is a dip of 0.9904 $p.u.$, followed by a surge of 1.001 $p.u.$ before reaching its steady state of 1 $p.u.$ at 12 s. This represents 0.1/-0.96 % in maximum frequency deviation with no continuous frequency deviation. Likewise, all voltage and frequency deviation have met the IEC standards 61892-1, which is shown in Table 2.5. As this test was not conducted in the state of the art, there is no result available for comparison.

6.6 Evaluation of Cost and Carbon Reduction

In Section 6.5, the load flow analysis and transient stability results of the PSEMS have been compared to the state of the art. It has been shown that the PSEMS is technically viable, meets the IEC standards and demonstrates an improved performance in Table 6.5. Hence, a cost analysis and the carbon reduction benefits with the PSEMS will be examined in this section.

Considering the system architecture, the PSEMS comprise of one set of GTG, one set of WTG with 2 MW of BESS. Its cost is compared against that of the typical O &G system in Figure 5.8, which comprises of two sets of GTG with no additional WTG and BESS. For the sake of comparison, the GTGs and WTG are rated at 10 MW and 6 MW respectively. In the cost analysis that includes CAPEX and OPEX, the cost estimation of the GTG is retrieved from [76] and the cost estimation of the WTG and BESS are referenced from [77]. The cost of the emergency GTG, which is usually installed in the typical system will be excluded as it will inflate the cost of the typical system.

The cost of individual power generation from GTG, WTG and BESS is discussed in Chapter 4.6 where the CAPEX and OPEX of GTG, WTG and BESS are presented in Equations 4.1 to 4.6. Figure 6.17 presents the cost comparison between the typical and proposed system. At the start of first year, the typical system comprising of two sets of GTG shows a lower, cost as compared with proposed system that comprises of one GTG, one WTG and a BESS. As shown in Figure 6.17, the proposed system is about 0.46 $p.u.$ higher than the base cost, which is the typical system at the end of the first year at 1 $p.u.$. At the end of the second year, the gap between proposed system of 1.6 $p.u.$ and the typical system of 1.31 $p.u.$, starts to narrow. At the end of the third year, the cost of the proposed system at 1.74 $p.u.$ closed up to that of the conventional system at 1.62 $p.u.$. At 3.75 years, the proposed system has reached the breakeven point, which is the cost of the typical system at that point. Subsequently in the fourth year, the proposed system is of a lower cost at 1.88 $p.u.$ while conventional system is of a higher cost at

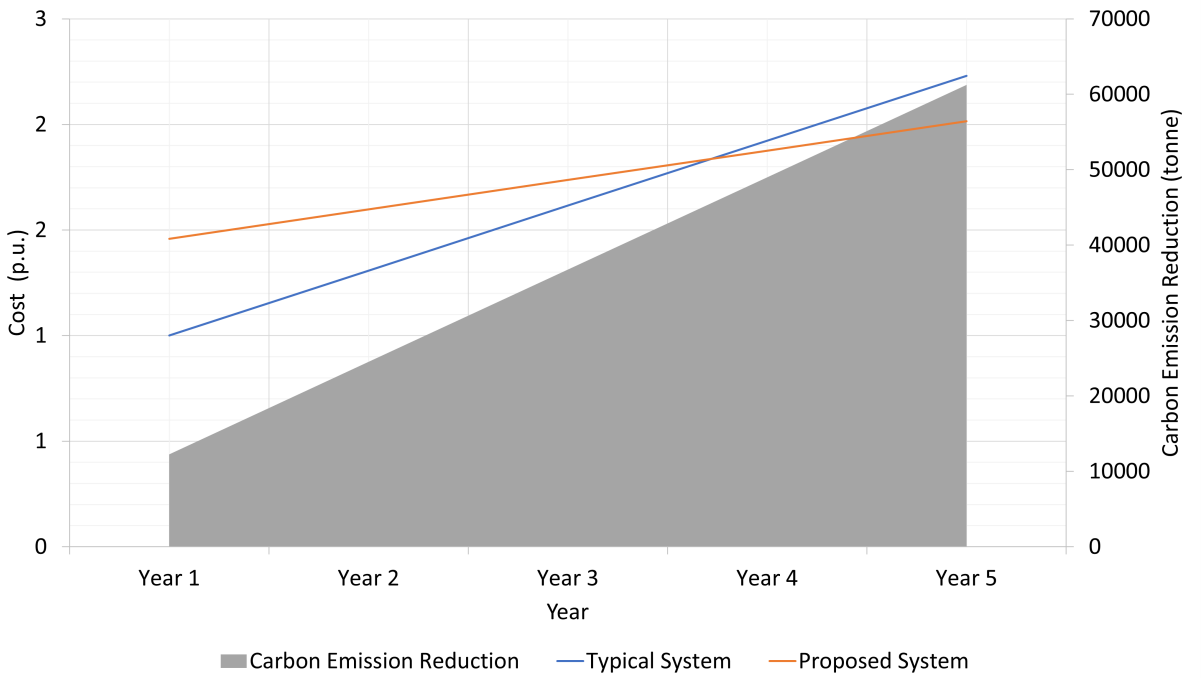

Figure 6.17: Conventional and proposed system: ROI with carbon emission reduction in 5 years' time.

1.92 $p.u.$. At the fifth year, the proposed system cost at 2.02 $p.u.$ while conventional system is at 2.23 $p.u.$.

It is observed in Figure 6.17 that the cost of PSEMS will breakeven with that of the typical system in less than four years. Although the PSEMS has a higher intial cost due to the offshore WTG, the return on investment (ROI) can be achieved at 3.75 years. This is due to cost of the gas consumption, which contributes to an increasing yearly cost of the typical system. In addition, the proposed system provides carbon emission reduction, which is calculated from carbon emission, C_E as follows:

$$C_E = P_{out} \times t \times CO_{2,em} \tag{6.8}$$

where P_{out} relates to output power rating in kW, t is in hours and $CO_{2,em}$ is the emission rate measured in metric tons CO_2/kWh.

The carbon emission reference is found in [78] showing 117,000 pounds per Billion BTU of energy input for natural gas. Hence, at the start of first year, carbon emission reduction is at 1 $p.u.$ which is approximately 12248.48 tonne per year. At the end of the fifth year, this gradually increases to approximately 61242.43 tonnes by the end of the fifth year.This is equivalent to approximately 13313 cars driving on road in one year, taking into consideration that one car emits

4.6 tonnes of carbon emission in a year [80]. The U.S. national weighted average CO2 marginal emission rate in 2019 is at 7.09 × 10-4 metric tons CO_2/kWh [79]. With a capacity factor of 35 % in the offshore WTG indicated in [3], carbon reduction per year is 12864 tons. At the end of the fifth year, this gradually increases to approximately 64320.48 tonnes.

6.7 Summary

In this chapter, our PSEMS has been developed. It has been demonstrated that PSEMS has the ability to improve transient stability in offshore O&G platforms application without having to increase the capacity of BESS. The proposed system entails an EMS and comprises of one set of GTG, one set of WTG and 2 *MW* of BESS. A load flow analysis was conducted to evaluate the ability of the PSEMS to provide high quality output power to the fixed and flexible loads. The study has shown that due to load variation, PSEMS has a 5.5/-8 % in maximum voltage deviation, which is lower than the system without EMS with 8/-9 % in maximum voltage deviation. Both systems achieved the same maximum frequency deviation.

A test scenario similar to that in the current state of the art was developed and simulated with a stochastic wind profile and load variation. The PSEMS has 5.1/-6.1 % and 0.16/-0.95 % respectively in maximum voltage and frequency deviation, which is significantly better than that of the state of the art at 8.6/-9 % and 2.1/-2.1 % respectively. A final test scenario was developed for the charging of BESS, which was mentioned as future work in the state of the art. It was observed that the PSEMS has 2.4/-6.3 % and 0.1/-0.96 % respectively in maximum voltage and frequency deviation. All of the test cases have shown that PSEMS has an improved output power quality, as compared to the other systems, and meets the IEC standards 61892-1.

While much attention has been focused on the transient stability enhancement from PSEMS, the techno-economic feasibility and the carbon reduction benefits in the PSEMS is crucial to evaluate its business potential. Although the PSEMS provides carbon emission reduction due to offshore WTG, its overall cost is higher than typical system by 0.5 times. The ROI can be achieved only at 3.75 years later due to greater consumption of gas contributing to overall cost in the typical system. At the end of five years, the PSEMS has a lower cost, as compared with the typical system. In addition, the integration of offshore WTG to the O&G platforms eliminates approximately 183773 tonnes of carbon emission. This is equivalent to approximately 39950 cars driving on road in one year, taking into consideration that one car emits 4.6 tonne of carbon emission in a year [80]. As such, the PSEMS is techno-economically feasible and capable of improving transient stability in offshore O&G platforms, in the presence of stochastic wind and load variations.

Chapter 7

Conclusions and Future Directions

7.1 Conclusion

This thesis contributes to the development and analysis of a hybrid energy system for offshore O&G rigs in the following areas:

1. Study of a proposed system comprising of a BESS integrated with offshore WTG and O&G platforms, which is validated with ETAP for transient stability analysis improvement [51].

2. Transient stability enhancement in proposed system to meet NORSOKS and IEC standards 61892-1, considering intermittency of power generation profiles [61].

3. Optimisation of BESS for optimal improvement solution in transient stability of proposed system, with CAPEX and OPEX analysis [61], [62].

4. Development of an EMS to improve transient stability, in the presence of dynamic loads and stochastic wind speeds.

5. Decarbonisation in the development of a techno-economic solution for the proposed system under heavy power consumption on offshore O&G platforms [51], [61].

In this thesis, the development and analysis of a hybrid energy system for offshore O&G rigs has been carried out. It has been discussed in Chapter 2 that the establishment of world's first offshore wind power for offshore O&G is constructed in the Norwegian North Sea, which will be completed in 2022. This is the essential industry proof of concept for our proposed system, which shows that the work in this thesis is heading in the right direction. Our proposed system has been incorporated with an EMS, which has been shown to improve transient stability in offshore O&G platforms. This proposed system has proven to be techno-economically feasible in improving transient stability with a significant reduction in overall carbon emission, while

meeting the IEC standards 61892-1 for mobile and fixed offshore units. A summary of our results is listed as follows:

- In Chapter 3, a detailed study of the integration of O&G production platforms with offshore WTG and BESS is first conducted in MATLAB/Simulink for load flow and power stability analysis [51].

- In Chapter 4, transient stability analysis is conducted for voltage and frequency with variations in BESS sizing, using a commercial software, ETAP. In the event of a power fault in the primary power generation in either the GTG or WTG, it has been demonstrated that the proposed O&G platforms integrated with WTG and BESS improves transient stability and meets the IEC standards 61892-1 for O&G industry [61].

- In Chapter 4, a power quality optimisation study is conducted in the scenario where the capacity for BESS can potentially be doubled by removing an additional EG [62]. The studies presented, not only determine the system configuration that meets the IEC standards 61892-1, but also illustrate that increasing capacity in BESS will decrease both voltage deviation and frequency deviation in output power to load. A commercial software application, ETAP, is used to generate transient stability results that were compared with the IEC standards for both conventional and proposed systems. It has also been reviewed that cost analysis is vital for the development of the business case for the proposed system. It is expected that there will be an increase in CAPEX and OPEX, which will rise due to additional secondary power generation from WTG and support from BESS.

- In Chapter 5, load flow analysis is carried out for the system configuration where only one EG is kept, and BESS till four times its initial capacity is installed. The faults in the secondary power generation of the WTG are studied to investigate if the BESS is able to provide the secondary response to the system. It has been shown that the primary response from GTG is limited and slower, as compared to that of the BESS. Similar to Chapter 4, variations in the BESS sizing has been considered, along with the associated cost of increasing the BESS capacity. Based on the cost analysis data given in Chapter 4.6, a detailed techno-economic analysis with increased capacity of BESS is presented in Section 5.5. To the best of our understanding, no research has been carried out to size on-board BESS for transient stability enhancement, which is addressed in this chapter.

- Uncertainties such as the intermittency of wind and perturbations from dynamic loads might result in large output power oscillation to load and high transient voltage and frequency deviation in real world scenarios. Hence, an energy management strategy is developed in Chapter 6 of this thesis. Our proposed system with EMS has shown to be effective in improving transient stability and has achieved a significant improvement in transient voltage/frequency deviation, besides meeting IEC standards 61892-1. The designed EMS

is also able to charge excess output power that is injected in the power grid to BESS while meeting IEC standards, which has not been studied in the state of the art, to the best of our knowledge.

- In term of techno-economic analysis, it has been shown that the BESS has the lowest CAPEX and OPEX in Chapter 4, as compared to the WTG and GTG. It has been demonstrated that the proposed system can achieve optimum transient stability by replacing two sets of GTGs with BESS, which significantly reduces the CAPEX and OPEX, as presented in Chapter 5. Notwithstanding that offshore WTG has a higher overall cost, as compared to the typical O&G platforms, it is computed and analysed that the return of investment (ROI) for the proposed system can be achieved in fourth year, as shown in Chapter 6.6.
- Intangible benefit is achieved in the reduction of carbon emissions for offshore O&G platform as the WTG and BESS reduces the amount of fossil fuel used by the GTG in meeting the load requirements. The integration of offshore WTG to the O&G platforms eliminates approximately 12248.48 tonnes of carbon emission annually. This is equivalent to approximately 13313 cars driving on road in one year, taking into consideration that one car emits 4.6 tonne of carbon emission in a year [80].

7.2 Suggestion for Future Work

This thesis has taken to full route from the development of ideas, modelling and simulation to techno-economic analysis. New results have been obtained but some topics are still open and recommended for future work as follows.

A typical system for an offshore O&G platform consists of three GTGs onboard, including a conventional system comprising of offshore O&G platform and nearby offshore WTG, which is integrated with BESS and incorporated with our designed EMS that is modelled in MATLAB Simulink. Simscape in MATLAB has the ability to create custom component models to design and build an EMS, which can close up the gap in the enhancement of output power quality. There will be technical challenge of improving transient stability faces during the development of offshore wind power for offshore O&G as commercial software ETAP is always used in the industry for transient stability analysis. This thesis has shown that our proposed EMS provides improved results, as compared to the state of art in the same system configuration and similar test conditions. In real life operations, the site conditions could vary according to geographical location. Wind speed fluctuation, shear and gust could lead to shut down and yaw out situations. Hence, an in-depth study on the load flow and transient stability, in the event of such perturbations and disturbances is required. In addition, more advanced control algorithms have to be developed in the EMS to maintain the output power at PCC and improve transient stability.

The first integration of offshore wind for electrification with nearby O&G platforms is expected to complete in 2022. This is only the beginning of such developments and more is expected to come, in our strive towards lower carbon emissions. For a sustainable long term future, future work should focus on developing better control algorithms to enable enhanced decarbonisation, such that the offshore WTG can be used to power multiple O&G platforms. There are potential benefits in which the CAPEX and OPEX can be reduced with improved control, power scheduling and dispatch. However, offshore WTG does not generate power when wind speed either falls below 4 m/s or rise above 25 m/s, which pose technical challenges in transient stability. With multiple offshore O&G platforms that are interconnected, the uncertainty in load demand will require a sophisticated control algorithm for output power quality enhancement and transient stability.

Despite the fact that BESS can replace a GTG onboard with similar footprint area, other energy storage technologies should also be explored. A recent industrial project in [81] mentioned the production of hydrogen from an electrolyser onboard the O&G platform. Given that hydrogen has a higher energy storage density than BESS, future work can involve an assessment to improve transient stability on site, using hydrogen as the energy storage technology. This should be evaluated on a case-by-case basis. If the wind speed profile at a particular geographical location is unfavourable, it might be advantageous to explore energy storage technologies of a higher energy density.

Bibliography

[1] Sanchez, S., Tedeschi, E., Silva, J., Jafar, M. and Marichalar, A. (2017). *Smart load management of water injection systems in offshore oil and gas platforms integrating wind power*. IET Renewable Power Generation.

[2] He, W., Jacobsen, G., Anderson, T., Olsen, F., Hanson, T.D., Korpås, M., Toftevaag, T., Eek, J., Uhlen, K. and Johansson, E. (2010). *The potential of integrating wind power with offshore oil and gas platforms*. Wind Engineering.

[3] Årdal, A.R., Sharifabadi, K., Bergvoll, Ø. and Berge, V. (2014). *Challenges with integration and operation of offshore oil & gas platforms connected to an offshore wind power plant*. 2014 Petroleum and Chemical Industry Conference Europe.

[4] De Alegria, I.M., Martín, J.L., Kortabarria, I., Andreu, J. and Ereño, P.I. (2009). *Transmission alternatives for offshore electrical power*. Renewable and sustainable energy reviews.

[5] Vrana, T.K. and Härtel, P. (2018). *Estimation of investment model cost parameters for VSC HVDC transmission infrastructure*. Renewable and sustainable energy reviews.

[6] Tveiten, Å.S. and Tangerås, B.T. (2018). *Hywind Tampen, project NPV calculation with and without subsidies*. University of Stavanger, Norway.

[7] Legorburu, I., Johnson, K.R. and Kerr, S.A. (2018). *Multi-use maritime platforms-North Sea oil and offshore wind: Opportunity and risk*. Ocean & Coastal Management.

[8] Korpås, M., Warland, L., He, W. and Tande, J.O.G.(2012). *A case-study on offshore wind power supply to oil and gas rigs*. Energy Procedia.

[9] Riboldi, L., Alves, E.F., Pilarczyk, M., Tedeschi, E. and Nord, L.O. (2020). *Innovative hybrid energy system for stable power and heat supply in offshore oil & gas installation (HES-OFF): System design and grid stability*. Computer Aided Chemical Engineering.

[10] Årdal, A.R., Undeland, T. and Sharifabadi, K. (2012). *Voltage and frequency control in offshore wind turbines connected to isolated oil platform power systems*. Energy Procedia.

[11] Alves, E., Sanchez, S., Brandao, D. and Tedeschi, E. (2019). *Smart load management with energy storage for power quality enhancement in wind-powered oil and gas applications*. Energies.

[12] Chapaloglou, S., Brandao, D.I. and Tedeschi, E (2021). *Dynamic Converter Capacity Allocation for Multifunctional Energy Storage Systems in Oil and Gas Applications*. In 2021 Sixteenth International Conference on Ecological Vehicles and Renewable Energies.

[13] International Electrotechnical Commission. (2019). *IEC 61892-1:2019*. https://webstore.iec.ch/publication/28085.

[14] MacAngus-Gerrard, G.(2017). *Offshore Electrical Engineering Manual*. Gulf Professional Publishing.

[15] Røkke, N.A., Hustad, J.E. and Berg, S.(1993). *Pollutant emissions from gas fired turbine engines in offshore practice: measurements and scaling*. Turbo Expo: Power for Land, Sea, and Air.

[16] Walsh, P.P. and Fletcher, P.(2004). *Gas turbine performance*. John Wiley & Sons.

[17] Anaya-Lara, O., Campos-Gaona, D., Moreno-Goytia, E. and Adam, G.(2014). *offshore wind energy generation: control, protection, and integration to electrical systems*. John Wiley & Sons.

[18] Korkoren K., Manyonge A. W., Rading J. O. (2014) *Mathematical Model of Variable Speed Pitch Regulated Turbine in a Wind Energy Conversion System*. American Journal of Mathematical Science and Applications. vol. 2, pp.33-39.

[19] Council for the Curriculum and Assessments (2013) *GCE LEVEL, Environmental Technology*. https://ccea.org.uk/downloads/docs/Support/Fact

[20] Gouws, R. and Dobzhanskyi, O.(2015). *Efficiency analysis of a three-phase power transformer*. Crown Publications.

[21] Zhong, Q.C. and Hornik, T.(2012). *Control of power inverters in renewable energy and smart grid integration*. John Wiley & Sons.

[22] Burns, J.C., Kassam, A., Sinha, N.N., Downie, L.E., Solnickova, L., Way, B.M. and Dahn, J.R.(2013). *Predicting and extending the lifetime of Li-ion batteries*. Journal of The Electrochemical Society.

[23] Sjøtun, S.G.(2019). *A ferry making waves: A demonstration project 'doing'institutional work in a greening maritime industry*. Norsk Geografisk Tidsskrift-Norwegian Journal of Geography.

[24] Sampaio, M.R., Rosa, L.P. and Márcio de Almeida, D. (2007). *Ethanol electric propulsion as a sustainable technological alternative for urban buses in Brazil*. Elsevier.

[25] Fischer, M., Werber, M. and Schwartz, P.V.(2009). *Batteries: Higher energy density than gasoline?*. Elsevier.

[26] Luo, F., Meng, K., Dong, Z.Y., Zheng, Y., Chen, Y. and Wong, K.P.(2015). *Coordinated operational planning for wind farm with battery energy storage system*. IEEE Transactions on Sustainable Energy.

[27] J. Himelic, F. Novachek.(2010). *Sodium Sulfur Battery Energy Storage And Its Potential To Enable Further Integration of Wind*. Smart.grid.gov.

[28] Xu, X., Bishop, M., Oikarinen, D.G. and Hao, C.(2016). *Coordinated operational planning for wind farm with battery energy storage system*. CSEE Journal of Power and Energy Systems.

[29] Opedal, J.F. (2017). *Electrical Grid Study of Using Offshore Wind Power for Oil & Gas Offshore Installations*. NTNU.

[30] Standards Norway (2018). *NORSOK Standards*. Standards Norway.

[31] He, W., Uhlen, K., Hadiya, M., Chen, Z., Shi, G. and del Rio, E. (2013). *Case study of integrating an offshore wind farm with offshore oil and gas platforms and with an onshore electrical grid*. Journal of Renewable Energy.

[32] Kolstad, M.L., Sharifabadi, K., Årdal, A.R. and Undeland, T.M. (2013). *Grid integration of offshore wind power and multiple oil and gas platforms*. 2013 MTS/IEEE OCEANS-Bergen.

[33] Marvik, J.I., Øyslebø, E.V. and Korpås, M. (2013). *Electrification of offshore petroleum installations with offshore wind integration*. Renewable energy.

[34] Haileselassie, T.M., Molinas, M. and Undeland, T. (2008). *Electrification of offshore petroleum installations with offshore wind integration*. Nordic Workshop on Power and Industrial Electronics (NORPIE/2008), June 9-11, 2008, Espoo, Finland.

[35] Leiding, T., Bastigkeit, I., Bégué, F., Gates, L., Herklotz, K., Müller, S., Neumann, T., Schwenk, P., Senet, C., Tinz, B. and Wilts, F. (2015). *Standardization of Meteorological Data from FINO Offshore Platforms*. EGU General Assembly Conference Abstracts.

[36] Elgenedy, M., Ahmed, K., Burt, G., Rogerson, G. and Jones, G. (2021). *Unlocking the UK Continental Shelf electrification potential for offshore oil and gas installations: a power grid architecture perspective*. Energies.

[37] Comer, B., Chen, C. and Rutherford, D. (2018). *Relating short-term measures to IMO's minimum 2050 emissions reduction target*. unpublished, presented at the international council on clean transportation.

[38] Gavenas, E., Rosendahl, K.E. and Skjerpen, T. (2015). *CO2-emissions from Norwegian oil and gas extraction*. Energy, Elsevier.

[39] Shahriari, S., Edalat, P. and Salehi, G. (2018). *Cost-benefit investigation of offshore wind power generation for soroush offshore complex*. International Journal of Maritime Technology.

[40] Haces-Fernandez, F., Li, H. and Ramirez, D. (2018). *Cost-benefit investigation of offshore wind power generation for soroush offshore complex*. Energies.

[41] Oliveira-Pinto, S., Rosa-Santos, P. and Taveira-Pinto, F. (2019). *Electricity supply to offshore oil and gas platforms from renewable ocean wave energy: Overview and case study analysis*. Energy Conversion and Management, Elsevier.

[42] Andersson, U., Jubert, D.C. and Evers, T. (2011). *Developing and installing substations for oil and gas facilities in very cold and remote locations*. IEEE Transactions on Industry Applications.

[43] Nguyen, T.V., Voldsund, M., Breuhaus, P. and Elmegaard, B. (2016). *Energy efficiency measures for offshore oil and gas platforms*. Energy, Elsevier.

[44] Voldsund, M., Ertesvåg, I.S., He, W. and Kjelstrup, S. (2013). *Exergy analysis of the oil and gas processing on a North Sea oil platform a real production day*. Energy, Elsevier.

[45] Bothamley, M. (2004). *Offshore processing options for oil platforms*. SPE Annual Technical Conference and Exhibition.

[46] Equinor (Statoil) (2019). *Hywind Pilot Park, Aberdeenshire*. https://www.power-technology.com/projects/hywind-pilot-park-aberdeenshire/.

[47] Nilsson, D. and Westin, A. (2014). *Floating wind power in Norway-Analysis of opportunities and challenges*. CODEN: LUTEDX/TEIE.

[48] Campos-Gaona, D., Madariaga, A., Zafar, J., Anaya-Lara, O. and Burt, G. (2018). *Techno-economic analysis of energy storage system for wind farms: the UK perspective*. 2018 International Conference on Smart Energy Systems and Technologies (SEST).

[49] Bak, Y., Lee, J.S. and Lee, K.B. (2018). *Low-voltage ride-through control strategy for a grid-connected energy storage system*. Applied Sciences.

[50] Tesvolt GmbH. *Tesvolt The Energy Storage Experts*. Tesvolt GmbH.

[51] Tee, J.Z., Tan, K.H., Lim, I.L.H., Zhou, K. and Anaya-Lara, O. (2019). *Integration of Offshore Wind with O&G Platforms with an Energy Storage System*. 2019 IEEE PES Innovative Smart Grid Technologies Europe (ISGT-Europe).

[52] Tee, J.Z., Chia, E.Z.D., Tan, K.H., Lim, L.H.I., Zhou, K. and Anaya-Lara, O. (2019). *Techno-economic analysis and battery storage placement in grid-connected photovoltaic (pv) system*. PVSEC 2019.

[53] Zhang, C., Wei, Y.L., Cao, P.F. and Lin, M.C. (2018). *Energy storage system: Current studies on batteries and power condition system*. Renewable and Sustainable Energy Reviews.

[54] Vimmerstedt, L., Akar, S., Augustine, C., Beiter, P., Cole, W., Feldman, D., Kurup, P., Lantz, E., Margolis, R., Oladosu, D. and Stehly, T. (2019). *2019 Annual Technology Baseline ATB Cost and Performance Data for Electricity Generation Technologies*. National Renewable Energy Lab.(NREL), Golden, CO (United States).

[55] Stehly, T., Beiter, P. and Duffy, P. (2019). *2019 Cost of Wind Energy Review*. National Renewable Energy Lab.(NREL), Golden, CO (United States).

[56] Cole, W.J. and Frazier, A. (2019). *Cost projections for utility-scale battery storage*. National Renewable Energy Lab.(NREL), Golden, CO (United States).

[57] U.S. Energy Information Administration. (2017). *Distributed Generation and Combined Heat & Power System Characteristics and Costs in the Buildings Sector*. US Energy Information Administration.

[58] Musial, WD and Beiter, PC and Spitsen, P and Nunemaker, J and Gevorgian, V). (2018). *Offshore Wind Technologies Market Report (No. NREL/TP-5000-74278; DOE/GO-102019-5192)*. National Renewable Energy Lab (NREL), Golden, CO, USA.

[59] Stehly, TJ and Beiter, PC). (2018). *2018 Cost of Wind Energy Review (No. NREL/TP-5000-74598)*. National Renewable Energy Lab (NREL).

[60] Mongird, K., Viswanathan, V.V., Balducci, P.J., Alam, M.J.E., Fotedar, V., Koritarov, V.S. and Hadjerioua, B. (2019). *Energy storage technology and cost characterization report*. National Renewable Energy Lab (NREL).

[61] Tee, J.Z., Lim, I.L.H., Zhou, K. and Anaya-Lara, O. (2020). *Transient Stability Analysis of Offshore Wind With O&G Platforms and an Energy Storage System*. 2020 IEEE Power & Energy Society General Meeting (PESGM).

[62] Tee, J.Z., Lim, I.L.H., Yang, J., Choo, C.T., Anaya-Lara, O. and Chui, C.K. (2020). *Power System Stability of Offshore Wind with an Energy Storage to Electrify O&G Platform*. 2020 IEEE REGION 10 CONFERENCE (TENCON).

[63] Kawabe, K. and Yokoyama, A. (2014). *Improvement of Transient Stability and Short-Term Voltage Stability by Rapid Control of Batteries on EHV Network in Power Systems*. Electrical Engineering in Japan.

[64] Datta, U., Kalam, A. and Shi, J. (2018). *Battery energy storage system to stabilize transient voltage and frequency and enhance power export capability*. IEEE Transactions on Power Systems.

[65] Xie, X., Zhong, J., Sun, Y., Wang, J. and Wei, C, (2018). *Online Optimal Power Control of an Offshore Oil-Platform Power System*. 2021 Sixteenth International Conference on Ecological Vehicles and Technology and Economics of Smart Grids and Sustainable Energy.

[66] Olatomiwa, L., Mekhilef, S., Ismail, M.S. and Moghavvemi, M. (2016). *Energy management strategies in hybrid renewable energy systems: A review*. Renewable and Sustainable Energy Reviews.

[67] Alves, E.F., Mota, D.D.S. and Tedeschi, E. (2021). *Sizing of Hybrid Energy Storage Systems for Inertial and Primary Frequency Control*. Frontiers in Energy Research.

[68] Technical specifications (2019). *SWT-6.0-154 Offshore wind turbine*. SIEMENS GAMESA.

[69] Alhejaj, S.M. and Gonzalez-Longatt, F.M. (2016). *Sizing of Hybrid Energy Storage Systems for Inertial and Primary Frequency Control*. 2016 International Conference for Students on Applied Engineering (ICSAE).

[70] Rancilio, G., Lucas, A., Kotsakis, E., Fulli, G., Merlo, M., Delfanti, M. and Masera, M. (2019). *Modeling a large-scale battery energy storage system for power grid application analysis*. Energies.

[71] Wood III, D.L., Li, J. and Daniel, C. (2015). *Prospects for reducing the processing cost of lithium ion batteries*. Journal of Power Sources, Elsevier.

[72] Li, J., Du, Z., Ruther, R.E., An, S.J., David, L.A., Hays, K., Wood, M., Phillip, N.D., Sheng, Y., Mao, C. and Kalnaus, S. (2017). *Toward low-cost, high-energy density, and high-power density lithium-ion batteries*. Jom, Springer.

[73] Li, K., Wei, F., Tseng, K.J. and Soong, B.H. (2017). *A practical lithium-ion battery model for state of energy and voltage responses prediction incorporating temperature and ageing effects*. IEEE Transactions on Industrial Electronics.

[74] Fusero, M., Tuckey, A., Rosini, A., Serra, P., Procopio, R. and Bonfiglio, A. (2019). *A comprehensive inverter-BESS primary control for AC microgrids*. Energies.

[75] Ernst, B., Oakleaf, B., Ahlstrom, M.L., Lange, M., Moehrlen, C., Lange, B., Focken, U. and Rohrig, K. (2007). *Predicting the wind*. IEEE power and energy magazine.

[76] Cost, C. (2020). *Performance Characteristic Estimates for Utility Scale Electric Power Generating Technologies*. US Energy Information Administration, Sargent and Lundy.

[77] Taylor, M., Ralon, P., Anuta, H. and Al-Zoghoul, S. (2020). *IRENA Renewable Power Generation Costs in 2019*. International Renewable Energy Agency: Abu Dhabi, UAE.

[78] keyhani (2016) *Design of smart power grid renewable energy systems*. John Wiley & Sons

[79] EPA (2020) *AVERT, U.S. national weighted average CO2 marginal emission rate, year 2019 data*. U.S. Environmental Protection Agency, Washington, DC

[80] United States Environmental Protection Agency (2021). *Greenhouse Gas Emissions from a Typical Passenger Vehicle*. Green Vehicle Guide.

[81] Neptune Energy (2021). *World's first offshore green hydrogen project on an oil platform gets go-ahead*. Rechargenews.